Proceedings of the Mini-Workshop

Few-Quark States
and the Continuum

Bled, Slovenia, September 15–22, 2008

Edited by

Bojan Golli

Mitja Rosina

Simon Širca

University of Ljubljana and Jožef Stefan Institute

The Mini-Workshop *Few-Quark States and the Continuum*

List of participants

Patrick Achenbach, Mainz, `patrick@kph.uni-mainz.de`
Marko Bračko, Ljubljana, `marko.bracko@ijs.si`
Fabien Buisseret, Mons-Hainaut, `fabien.buisseret@umh.ac.be`
Veljko Dmitrašinović, Belgrade, `dmitrasin@yahoo.com`
Dietmar Ebert, Berlin, `debert@physik.hu-berlin.de`
Svjetlana Fajfer, Ljubljana, `svjetlana.fajfer@ijs.si`
Yoshikazu Fujiwara, Kyoto, `yfujiwar@scphys.kyoto-u.ac.jp`
Bojan Golli, Ljubljana, `bojan.golli@ijs.si`
Dubravko Klabučar, Zagreb, `klabucar@phy.hr`
William Klink, Iowa, `william-klink@uiowa.edu`
Nejc Košnik, Ljubljana, `nejc.kosnik@ijs.si`
Felipe Llanes-Estrada, Madrid, `fllanes@fis.ucm.es`
Milan Potokar, Ljubljana, `Milan.Potokar@ijs.si`
Saša Prelovšek, Ljubljana, `Sasa.Prelovsek@ijs.si`
Mitja Rosina, Ljubljana, `mitja.rosina@ijs.si`
Ica Stancu, Liege, `fstancu@ulg.ac.be`
Simon Širca, Ljubljana, `simon.sirca@fmf.uni-lj.si`
Sachiko Takeuchi, Tokio, `sachi-ta@hoffman.cc.sophia.ac.jp`
Eef Van Beveren, Coimbra, `eef@teor.fis.uc.pt`

Contents

Preface

We were happy to host already the tenth Mini-Workshop on hadronic physics at Bled and to see that the enthusiasm for this type of encounters has not waned. We intend to continue with this series of meetings emphasising broad discussions beyond the time constraints of usual conferences. The beautiful environent of Lake Bled also helped to more relaxed discussions and to strengthening the friendly links during the hours of leisure.

An important issue is the description of hadronic resonances as decaying states and obtaining correct hadronic decay widths. Another one is the understanding of new resonances in the charmonium spectrum; are they tetraquarks, or just threshold- or open-channel effects? Even the low-energy scalar mesons seem to be too numerous and excite the imagination of theorists: are they tetraquarks, exotics, or just analytic continuations of the resonance pole in the second Riemann sheet? These considerations of quark states and their coupling to the continuum matched well the central topic of our meeting.

There were also excellent experimental reviews. Measurements at Mainz and Jefferson Lab reveal numerous puzzles in the Roper resonance. A theoretical explanation of some of them was presented, assuming a two-step process via the Δ resonance or via σ meson. The twelve new resonances in charmonium spectrum are further documented at Belle and excite several theoretical speculations. The interest in double-strange hypernuclei has been revived at MAMI with the prospect to see Ξ hypernuclei in near future; the Ξ-N interaction would be an interesting test of quark-model calculations presented at this Workshop.

The idea that the Y-shaped effective potential in the 3q-system dominates was further developed using new methods for baryon spectra. Oher methods for baryon spectra include the $1/N_c$ expansion with spectrum-generating algebra.

Tetraquarks continue to excite. How to distinguish them from hybrids and from threshold effects? Does one distinguish them in recent Lattice QCD calculations? Can tetraquarks be described as two-diquark systems? Related questions for systems with pentaquark configurations abounded as well.

New lessons on relativity served as a reminder to nonrelativistic participants.

Ljubljana, November 2008

M. Rosina
B. Golli
S. Širca

Workshops organized at Bled

▷ *What Comes beyond the Standard Model* (June 29–July 9, 1998), Vol. **0** (1999) No. 1
▷ *Hadrons as Solitons* (July 6–17, 1999)
▷ *What Comes beyond the Standard Model* (July 22–31, 1999)
▷ *Few-Quark Problems* (July 8–15, 2000), Vol. **1** (2000) No. 1
▷ *What Comes beyond the Standard Model* (July 17–31, 2000)
▷ *Statistical Mechanics of Complex Systems* (August 27–September 2, 2000)
▷ *Selected Few-Body Problems in Hadronic and Atomic Physics* (July 7–14, 2001), Vol. **2** (2001) No. 1
▷ *What Comes beyond the Standard Model* (July 17–27, 2001), Vol. **2** (2001) No. 2
▷ *Studies of Elementary Steps of Radical Reactions in Atmospheric Chemistry*
▷ *Quarks and Hadrons* (July 6–13, 2002), Vol. **3** (2002) No. 3
▷ *What Comes beyond the Standard Model* (July 15–25, 2002), Vol. **3** (2002) No. 4
▷ *Effective Quark-Quark Interaction* (July 7–14, 2003), Vol. **4** (2003) No. 1
▷ *What Comes beyond the Standard Model* (July 17–27, 2003), Vol. **4** (2003) Nos. 2-3
▷ *Quark Dynamics* (July 12–19, 2004), Vol. **5** (2004) No. 1
▷ *What Comes beyond the Standard Model* (July 19–29, 2004), Vol. **5** (2004) No. 2
▷ *Exciting Hadrons* (July 11–18, 2005), Vol. **6** (2005) No. 1
▷ *What Comes beyond the Standard Model* (July 18–28, 2005), Vol. **6** (2005) No. 2
▷ *Progress in Quark Models* (July 10–17, 2006), Vol. **7** (2006) No. 1
▷ *What Comes beyond the Standard Model* (September 16–29, 2006), Vol. **7** (2006) No. 2
▷ *Hadron Structure and Lattice QCD* (July 9–16, 2007), Vol. **8** (2007) No. 1
▷ *What Comes beyond the Standard Model* (July 18–28, 2007), Vol. **8** (2007) No. 2
▷ *Few-Quark States and the Continuum* (September 15–22, 2008), Vol. **9** (2008) No. 1
▷ *What Comes beyond the Standard Model* (July 15–25, 2008), Vol. **9** (2008) No. 2

Also published in this series

▷ Book of Abstracts, *XVIII European Conference on Few-Body Problems in Physics*, Bled, Slovenia, September 8–14, 2002, Edited by Rajmund Krivec, Bojan Golli, Mitja Rosina, and Simon Širca, Vol. **3** (2002) No. 1–2

Hypernuclear physics as seen by an experimenter

P. Achenbach

Institut für Kernphysik, Joh. Gutenberg-Universität, Mainz, Germany

In the new millennium hypernuclear physics is undergoing a renewed interest, both theoretically and experimentally.

Hadrons and nuclei are understood as many-body systems made of quarks and gluons, bound by the strong force. Information on baryon-baryon interactions is mainly obtained from nuclear experiments with projectiles and targets out of nucleons, addressing interactions in flavour SU(2) only. The difficulties to study hyperon-nucleon (YN) and hyperon-hyperon (YY) interactions by reaction experiments are related to the practical problems in the preparation of low energy hyperon beams and the impossibility of hyperon targets due to the short ($\sim$200 ps) life-times of hyperons. The investigation of a hypernucleus, where one or more nucleons have been replaced by one or more hyperons, allows addressing a rich spectrum of physics topics ranging from genuine nuclear physics to particle physics. Although fifty years have already passed since the discovery of the first hypernuclear events, studies of hypernuclei are still at the forefront of nuclear physics. The presence of the hyperon can induce several effects on the host nucleus, like changes of both size and shape, modification of cluster structure, manifestation on new symmetries or changes of nucleon collective motions. One of the most spectacular effects, observed so far in what is called impurity nuclear physics, is the shrinking of the nucleus core. Such a behaviour can be considered a precursor of matter condensation induced by strange particles.

Only recently, it has already been demonstrated that hypernuclei can be used as a micro-laboratory to study YN and YY interactions. In the case of ΛN interaction, the spin-orbit term has been found to be smaller than that for the nucleon. In a recent experiment at BNL the spacing of the $(5/2^+, 3/2^+)$ doublet in $^9_\Lambda$Be was measured to be (43 ± 5) keV [1]. Although these small spin splittings can only be observed using gamma spectroscopy, reaction spectra are equally important because they provide the complete spectrum of excitations. In addition, experimental data on medium to heavy single Λ hypernuclei have shown a much larger spin-orbit splitting than observed in light hypernuclei [2].

Hypernuclei physics, born and developed mainly in Europe, has seen a renaissance at the turn of the century. Until now, experimental information has mainly come from meson-induced reactions and most recently from coincident γ-ray spectroscopy of hypernuclei. Even though a number of new experimental techniques have been developed for the hypernuclear spectroscopy in the last decade, our knowledge is still limited to a small number of hypernuclei. The large

variety of novel experimental approaches to hypernuclei will provide a wide basis for a comprehensive understanding of strange hadrons in cold nuclear systems. The spectroscopy of single Λ- and double ΛΛ-hypernuclei will remain one of the most valuable tools for the experimental investigation of strangeness nuclear physics in the near future.

1   The hypernuclear programme at MAMI

At the Institut für Kernphysik in Mainz, Germany, the microtron MAMI has been upgraded to 1.5 GeV electron beam energy and can now be used to study strange hadronic systems [3].

Electron beams have excellent spatial and energy definitions, and targets can be physically small and thin ($10 - 50\,\text{mg/cm}^2$) allowing studies of almost any isotope. The cross-section for the reaction, $\sigma \sim 140\,\text{nb/sr}$ on a ^{12}C target as first measured at Jefferson Laboratory in Experiment E89-009 [4], is small compared to strangeness exchange $n(K^-, \pi^-)\Lambda$ or associated production $n(\pi^+, K^+)\Lambda$. This smallness can be well compensated in electro-production by the available large electron beam intensities, but often the resulting electromagnetic background is limiting the reaction rates.
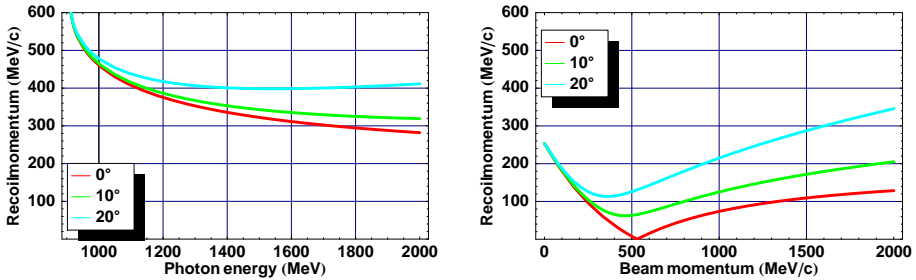
Fig. 1. Recoil momentum for strangeness electro-production (left) and strangeness exchange (right) reactions at three different kaon angles are shown as a function of the energy of the virtual photon, respectively the beam momentum. Reaction cross-sections and transition amplitudes to individual states depend strongly on the recoil momentum.

In order to produce a hypernucleus, the hyperon emerging from the reaction has to be bound in the nucleus. Reaction cross-sections and transition amplitudes to individual states depend strongly on the transferred momentum to the hyperon. If the momentum transfer is large compared with typical nuclear Fermi momenta, the hyperon will preferentially leave the nucleus. The (K^-, π^-) reaction is characterised by the existence of a "magic momentum" where the recoil momentum of the hyperon becomes zero as is shown Fig. 1. It populates, consequently, substitutional states in which a nucleon is converted to a Λ in the same state. The $(e, e'K^+)$ reaction, on the other hand, produces neutron-richer Λ hypernuclei converting a proton to a Λ hyperon and transfers a large recoil

momentum to a hypernucleus. This reaction is preferable when high-spin hypernuclear states are studied. In addition, this reaction has the unique characteristic of providing large amplitudes for the population of spin-flip hypernuclear states with unnatural parities [5], such as $(_\nu p_{3/2}^{-1},_\Lambda s_{1/2})2^-$, where the spin quantum number, $J^P = 2^-$, of the nucleon-hole Λ-particle state has maximum $J =_\nu l +_\Lambda l + 1 = 1 + 0 + 1 = 2$.

KAOS is a very compact magnetic spectrometer suitable especially for the detection of kaons, that was used before at GSI in a single-arm configuration [6]. During the last years it was installed at the Mainz microtron MAMI in the existing spectrometer facility operated by the A1 collaboration [7]. In the very near future the spectrometer will be set-up for the first time with tracking detectors arranged in two arms, to either side of the main dipole. The special kinematics for electroproduction of hypernuclei requires the detection of both, the associated kaon and the scattered electron, at forward laboratory angles. The KAOS spectrometer will cover simultaneously electron scattering angles close to $0°$ and kaon scattering angles around $5°$ up to $15°$ in order to extract dynamical information from the K^+ angular distribution [8].
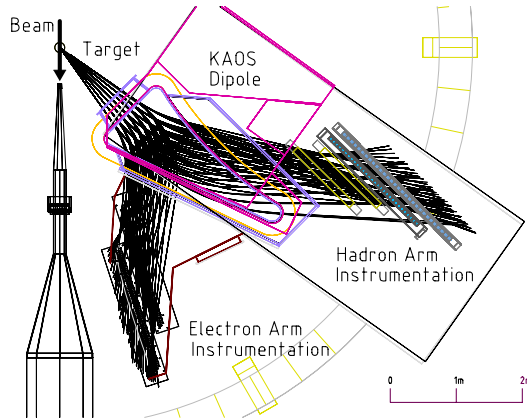
Fig. 2. Overview of the KAOS spectrometer of the A1 collaboration at the Mainz microtron MAMI: electrons and hadrons are detected simultaneously under small scattering angles. Charged particle trajectories through the spectrometer are shown by full lines. The electron arm tracking detector will be located close to the electron beam. High radiation levels are expected at that position.

The KAOS spectrometer's electron arm detectors will operate close to zero degrees scattering angle and in close proximity to the electron beam. Fig. 2 shows a schematic drawing of the set-up in the spectrometer hall. The magnet bends the central trajectory on both sides by ~45 degrees with a momentum dispersion of 2.2 cm/%. The first-order focusing is realized as seen in Fig. 2. In addition to a broad neutron spectrum high electromagnetic background levels are expected at the detector locations. It is consequently imperative to operate radiation hard and intrinsically fast detectors.

While the instrumentation of the hadron arm is operational, a new coordinate detector of the spectrometer's electron arm is under development [9,10]. It will consist of two vertical planes of fibre arrays (x and θ), covering an active area of $L \times H \sim 2000 \times 300 \, mm^2$, supplemented by one or two horizontal planes (y and φ). The 18,432 fibres of the vertical tracking detectors will be connected to 4,608 electronics channels with logic signals fed into the level-1 trigger. The track information will be used to reconstruct the target coordinates and particle momentum, and the time information used to determine the time-of-flight of the particle from target to the detection planes. New front-end electronics has been developed for the fast signals of more than 4,000 MaPMT channels of the fibre detector in the KAOS spectrometer's electron arm.
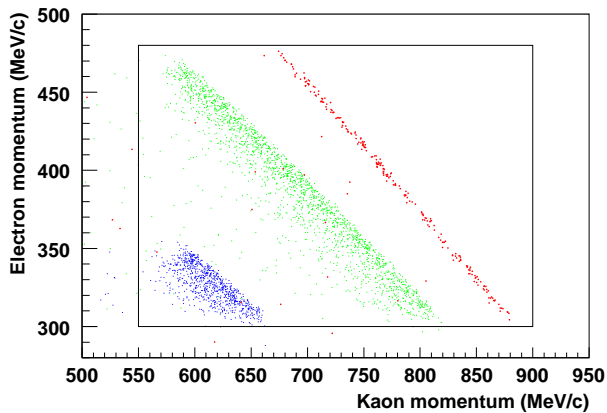
Fig. 3. (color online) Simulated correlation between electron and kaon momenta, where Σ (blue, left) and Λ (green, centre) hyperons have been generated for the elementary production off the proton and the $^{12}_{\Lambda}$B hypernuclei (red, right) have been generated for a carbon target. The rectangular box indicates the simultaneous momentum acceptance of the KAOS spectrometer in its two-arm configuration.

In Fig. 3 the simulated correlation in electro-production between the electron momentum and the kaon momentum is plotted, where Λ and Σ hyperons have been generated for the elementary production off the proton and the $^{12}_{\Lambda}$B hypernuclei have been generated for a carbon target. The events have been generated randomly in phase-space and weighted by a factor for the virtual photon flux and the modelled transition form factor. In the Monte Carlo, the production probability was assumed to drop exponentially with the relative momentum between Λ hyperon and core nucleus and typical values of $\sigma_p = 100 \, MeV/c$ and $k_F = 200 \, MeV/c$ were assumed. The rectangular box in Fig. 3 indicates the simultaneous momentum acceptance of the KAOS spectrometer. Its large momentum acceptance covers the quasi-free process as well as the hypernuclear production reaction. In practice, this fact will simplify the identification of the hypernuclear events in the data sample.

It is currently planned to perform a first experiment with two complete vertical planes of the fibre detector in the KAOS spectrometer's electron arm in 2009.

The hypernuclear programme will follow as soon as the two-arm configuration of the spectrometer is operational and the magnet optics is determined in such a way that sub-MeV mass resolution is possible. The latter situation is assumed to be reached in late 2009 or early 2010.

2   The HypHI experiment

Until recently hypernuclear spectroscopy has been restricted to the investigation of hypernuclei close to the valley of beta-decay stability as in most experiments targets made of stable nuclei are used with meson and electron beams. The recently proposed HypHI project (Hypernuclear spectroscopy with stable heavy ion beams and rare-isotope beams) is dedicated to hypernuclear spectroscopy with stable heavy ion beams and rare isotope beams at GSI, Germany, and FAIR, the Facility for Antiproton and Ion Research [11]. This approach has some advantages: firstly, it is possible to investigate a number of hypernuclei simultaneously in a single experiment and secondly the hypernuclei are created at extreme isospins. The observation of the Λ-hypernucleus decay modes offers the unique opportunity to look at the four-baryon, strangeness-changing, weak vertex. The determination of the relative weights of the different decay channels represents a long-standing puzzle. The HypHi project is divided into four phases. To study the feasibility of hypernuclear spectroscopy with heavy ion beams the phase 0 experiment was proposed [12], aiming at the identification of the π^- decay channels of $^3_\Lambda$H, $^4_\Lambda$H and $^5_\Lambda$He produced by ^{6}Li 2 AGeV beams impinging on a ^{12}C target of $8\,g/cm^2$ mass.

Hypernuclear production via heavy ion collisions is described by the participant-spectator model and was first studied theoretically by Kerman and Weiss [13]. In the collisions hyperons are produced in the participant region with a wide rapidity distribution centered around mid-rapidity. Hypernuclei can be formed in coalescence of hyperon(s) in the projectile fragments, with the velocity of hypernuclei close to the projectile velocity with $\beta > 0.9$. Decays of hypernuclei can be studied in-flight, and most of their decay vertices are a few tens of a centimetre behind the target at which hypernuclei are produced.

The experimental set-up, which will consist of an analysing dipole magnet as well as time-of-flight (TOF) and tracking detectors, was designed to measure the invariant mass of particles decaying behind the target. The TOF branch will consist of a start detector and two position-sensitive TOF walls for positive and negative charged particles, placed behind the dipole. In addition, the scintillators will provide energy deposit information for the charge identification of the registered particles. Three tracking detectors made of scintillating fibres will be positioned between target and magnet and will be used to trigger readout system on events which contain a decay vertex behind the target. The fibre detector will also become crucial in distinguishing the hypernuclei $^4_\Lambda$H and $^3_\Lambda$H from the background containing α and Λ particles produced at the target.

A further advantage of this approach is that hypernuclei are produced as projectile fragments at beam rapidity that will open a way to direct measurements of hypernuclear magnetic moments. In meson and electron beam induced

experiments, recoil momenta of produced hypernuclei are small. Therefore, it has been impossible so far to conduct direct measurement on hypernuclear magnetic moments by means of spin precession in strong magnetic fields. This is one of the goals of the final project phase.

3   The hypernuclear programme at PANDA

The single hypernuclei research programme will be complemented by experiments on multi-strange systems with $\overline{\text{P}}$ANDA at the planned FAIR facility. The $\overline{\text{P}}$ANDA hypernuclear programme shall reveal the $\Lambda\Lambda$ strong interaction strength, not feasible with direct scattering experiments [14,15]. In the anti-proton storage ring HESR relatively low momentum Ξ^- will be produced in $\overline{\text{p}}\text{p} \to \Xi^-\overline{\Xi}^+$ or $\Xi^-\overline{\Xi}^0$ reactions. The associated $\overline{\Xi}$ will scatter or annihilate inside the residual nucleus. The annihilation products contain at least two anti-kaons that can be used as a tag for the reaction. Due to the large yield of hyperon-antihyperon pairs produced a high production rate of single and double hypernuclei in an active secondary target under unique experimental conditions will be feasible. High resolution γ-ray spectroscopy based on high-purity germanium (HPGe) detectors represents one of the most powerful means of investigation in nuclear physics: the introduction of this technique determined a significant progress in the knowledge of the nuclear structure. Consequently, for the high resolution spectroscopy of excited hypernuclear states an efficient, position sensitive HPGe array is foreseen. To maximise the detection efficiency the detectors must be located as close as possible to the target. Hereby the main limitation is the load of particles from background reactions. Most of the produced charged particles are emitted into the forward region. Since the γ-rays from the slowly moving hypernuclei are emitted rather isotropically the HPGe detectors will be arranged at backward axial angles $\theta \geq 100°$. A full simulation of the hypernuclei detector's geometry has been completed.
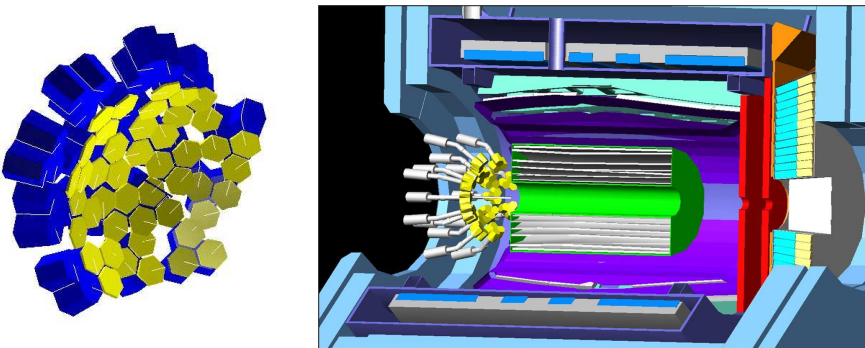

Fig. 4. Simulated set-up with HPGe cluster detectors (left) situated at backward angles for hypernuclei experiments at $\overline{\text{P}}$ANDA (right). The beam enters from left.

Fig. 4 shows the simulated γ-ray spectroscopy set-up with several HPGe cluster detectors (each comprising 3 crystals). A small fibre barrel read-out by silicon photomultiplier has been discussed as an option for a time-of-flight start detector to identify hypernuclear reactions. For this sub-detector system the achievable time resolution at minimum detector mass is a main issue.

The hypernuclear physics addressed by this experiment is currently discussed in the upcoming „$\overline{\text{P}}$ANDA Physics Book". In the planned set-up there exist many experimental challenges and several European research groups are working on the realisation of the detectors. A detailed design will be available in the mid-term future. When reflecting upon the state of the preparations for this set-up, one should be aware that the construction of the anti-proton storage ring and the $\overline{\text{P}}$ANDA experiment has not yet started.

Acknowledgements

References

1. H. Tamura, et al., γ-ray spectroscopy in Λ hypernuclei, Nucl. Phys. A 754 (2005) 58c–69c.
2. T. Nagae, et al., Structure of a Λ-hypernucleus $^{89}_{\Lambda}$Y measured with the SKS spectrometer, Nucl. Phys. A 670 (1–4) (2000) 269c–272c.
3. K.-H. Kaiser, et al., The 1.5 GeV harmonic double-sided microtron at Mainz University, Nucl. Instr. and Meth. in Phys. Res. A 573 (3) (2008) 159–170.
4. T. Miyoshi, et al., High resolution spectroscopy of the $^{12}_{\Lambda}$B hypernucleus produced by the $(e, e'K^{+})$ reaction, Phys. Rev. Lett. 90 (23) (2000) 232502.
5. T. Motoba, M. Sotona, K. Itonaga, Photoproduction of polarized hypernuclei, Prog. Theor. Phys. Suppl. 117 (1994) 123–133.
6. P. Senger, et al., The kaon spectrometer at SIS, Nucl. Instr. and Meth. in Phys. Res. A 327 (1993) 393–411.
7. K. I. Blomqvist, et al., The three-spectrometer facility at the Mainz microtron MAMI, Nucl. Instr. and Meth. in Phys. Res. A 403 (3) (1998) 263–301.
8. P. Achenbach, Probing hypernuclei at $\overline{\text{P}}$ANDA and at MAMI-C, in: J. Pochodzalla, Th. Walcher (Eds.), Proceedings of the IX International Conference on Hypernuclear and Strange Particle Physics, Johannes Gutenberg-Universität, Mainz, 10–14 October 2006, Springer, Berlin, 2007, pp. 79–84.
9. P. Achenbach, et al., New detectors for the kaon and hypernuclear experiments with KAOS at MAMI and with $\overline{\text{P}}$ANDA at GSI, in: V. Luth (Ed.), Proceedings of the IX International Symposium on Detectors for Particle, Astroparticle and Synchrotron Radiation Experiments, SLAC, 3–6 April 2006, eConf C0604032, 2006, p. 144.
10. P. Achenbach, et al., In-beam tests of scintillating fibre detectors at MAMI and at GSI, Nucl. Instr. and Meth. in Phys. Res. A 593 (2008) 353–360.

11. T. R. Saito, et al., The HypHI project at GSI and FAIR, in: J. Pochodzalla, Th. Walcher (Eds.), Proceedings of the IX. International Conference on Hypernuclear and Strange Particle Physics, Joh. Gutenberg-Universität, Mainz, 10–14 October 2006, Springer, Berlin, 2007, pp. 171–176.
12. T. R. Saito, et al., Proposal of the HypHI Phase 0 experiment, accepted by EA 33, GSI (2006).
13. A. K. Kerman, M. S. Weiss, Phys. Rev. C **8** (1973) 408.
14. J. Pochodzalla, Future experiments on hypernuclei and hyperatoms, Nucl. Instr. and Meth. in Phys. Res. B 214 (2004) 149–152.
15. $\overline{\text{P}}$ANDA Collabaration, Strong interaction studies with antiprotons, Technical Progress Report, GSI, Darmstadt (2005).

Light and heavy baryon masses: the $1/N_c$ expansion and the quark model[*]

F. Buisseret[a], C. Semay[a], F. Stancu[b], N. Matagne[c]

[a]Groupe de Physique Nucléaire Théorique, Université de Mons-Hainaut, Place du Parc 20, B-7000 Mons, Belgium
[b]University of Liège, Institute of Physics B5, Sart Tilman, B-4000 Liège 1, Belgium
[c]Institut für Theoretische Physik, Universität Giessen, D-35392 Giessen, Germany

Abstract. We establish a connection between the quark model and the $1/N_c$ expansion mass formulas used in the description of baryon resonances. We show that a remarkable compatibility exists between the two methods in the light and heavy baryon sectors. In particular, the band number used to classify baryons in the $1/N_c$ expansion is explained by the quark model and the mass formulas for both approaches are consistent.

1 Introduction

Since pioneering work [1] in the field, the standard approach for baryon spectroscopy is the constituent quark model. The Hamiltonian typically contains a spin independent part formed of the kinetic plus the confinement energies and a spin dependent part given by a hyperfine interaction. The quark model results are *de facto* model dependent; it is therefore very important to develop model independent methods that can help in alternatively understanding baryon spectroscopy and support (or not) quark model assumptions. Apart from promising lattice QCD calculations [2], large N_c QCD, or alternatively the $1/N_c$ expansion, offers such a method. In 1974 't Hooft generalized QCD from SU(3) to an arbitrary number of colors SU(N_c) [3] and suggested a perturbative expansion in $1/N_c$, applicable to all QCD regimes. Witten has then applied the approach to baryons [4] and this has led to a systematic and predictive $1/N_c$ expansion method to study static properties of baryons. The method is based on the discovery that, in the limit $N_c \to \infty$, QCD possesses an exact contracted SU($2N_f$) symmetry [5] where N_f is the number of flavors. This symmetry is approximate for finite N_c so that corrections have to be added in powers of $1/N_c$. Notice that a baryon is a bound state of N_c quarks in the large N_c formalism.

The $1/N_c$ expansion has successfully been applied to ground state baryons, either light [6,7] or heavy [8,9]. Its applicability to excited states is a subject of current investigations. The classification scheme used in the $1/N_c$ expansion for excited states is based on the standard SU(6) classification as in a constituent quark

---

[*] Based on talks presented by F. Buisseret and F. Stancu

model. Baryons are grouped into excitation bands $N = 0, 1, 2,\ldots$, each band containing at least one SU(6) multiplet, the band number N being the total number of excitation quanta in a harmonic oscillator picture.

The purpose of the present paper is to show that there is a compatibility between the quark model and the $1/N_c$ expansion methods. It is organized as follows. We first give a summary of the $1/N_c$ expansion method in Sec. 2. Then we present a relativistic quark model in Sec. 3 and derive analytic mass formulas from its Hamiltonian in Sec. 4. The comparison between the quark model and the $1/N_c$ mass formulas is discussed in Sec. 5 and conclusions are drawn in Sec. 6. We point out that the results summarized hereafter have been previously presented in Refs. [10,11] for the light baryons and [12] for the heavy baryons. This work aims at being a pedagogical overview of these last three references.

2   Baryons in large N_c QCD

2.1   Light nonstrange quarks

We begin with a summary of the $1/N_c$ expansion in the case $N_f = 2$, but the arguments are similar for any N_f. The contracted $SU(2N_f)$ symmetry is here the group SU(4) which has 15 generators: The spin and isospin subgroup generators S_i and T_a and operators acting on both spin and isospin degrees of freedom denoted by G_{ia} $(i, a = 1, 2, 3)$.

The SU(4) algebra is

$$[S_i, T_a] = 0, \quad [S_i, G_{ja}] = i\varepsilon_{ijk}G_{ka}, \quad [T_a, G_{ib}] = i\varepsilon_{abc}G_{ic},$$

$$[S_i, S_j] = i\varepsilon_{ijk}S_k, \quad [T_a, T_b] = i\varepsilon_{abc}T_c, \quad [G_{ia}, G_{jb}] = \frac{i}{4}\delta_{ij}\varepsilon_{abc}T_c + \frac{i}{4}\delta_{ab}\varepsilon_{ijk}S_k.$$

In the limit $N_c \to \infty$ one has $[G_{ia}, G_{jb}] \to 0$ which implies the existence of a contracted algebra. These SU(4) generators form the building blocks of the mass operator, at least in the ground state band ($N = 0$). For orbitally excited states the generators ℓ^i of SO(3), as well as the tensor operator $\ell^{(2)ij}$ also appear since the symmetry under consideration is extended to $SU(4) \otimes SO(3)$.

In the $1/N_c$ expansion the mass operator M has the general form

$$M = \sum_i c_i O_i, \tag{1}$$

where the coefficients c_i encode the QCD dynamics and have to be determined from a fit to the existing data, and where the operators O_i are $SU(4) \otimes SO(3)$ scalars of the form

$$O_i = \frac{1}{N_c^{n-1}} O_\ell^{(k)} \cdot O_{SF}^{(k)}. \tag{2}$$

Here $O_\ell^{(k)}$ is a k-rank tensor in SO(3) and $O_{SF}^{(k)}$ a k-rank tensor in SU(2)-spin, but invariant in SU(2)-flavor. The lower index i in the left hand side represents a specific combination. Each n-body operator is multiplied by an explicit factor of $1/N_c^{n-1}$ resulting from the power counting rules [4], where n represents the

minimum of gluon exchanges to generate the operator. For the ground state, one has $k = 0$. For excited states the $k = 2$ tensor is important. In practical applications, it is customary to include terms up to $1/N_c$ and drop higher order corrections of order $1/N_c^2$.

As an example, we show the operators used in the calculation of the masses of the $[\mathbf{70}, 1^-]$ multiplet up to order $1/N_c$ included [13] (the sum over repeated indices is implicit)

$$O_1 = N_c\,\mathbf{1}, \quad O_2 = \frac{1}{N_c}\ell^i S^i, \quad O_3 = \frac{1}{N_c}T^a T^a, \quad O_4 = \frac{1}{N_c}S^i S^i,$$

$$O_5 = \frac{15}{N_c^2}\ell^{(2)ij} G^{ia} G^{ja}, \quad O_6 = \frac{3}{N_c^2}\ell^i T^a G^{ia}. \tag{3}$$

Note that although O_5 and O_6 carry a factor of $1/N_c^2$ their matrix elements are of order $1/N_c$ because they contain the coherent operator G^{ia} which brings an extra factor N_c. $O_1 = N_c\,\mathbf{1}$ is the trivial operator, proportional to N_c and the only one surviving when $N_c \to \infty$ [4]. The operators O_2 (spin-orbit), O_5 and O_6 are relevant for orbitally excited states only. All the SU(4) quadratic invariants $S^i S^i$, $T^a T^a$ and $G^{ia} G^{ia}$ should enter the mass formula but they are related to each other by the operator identity [7]

$$\{S^i, S^i\} + \{T^a, T^a\} + 4\{G^{ia}, G^{ia}\} = \frac{1}{2}N_c(3N_c + 4), \tag{4}$$

so one can express $G^{ia} G^{ia}$ in terms of $S^i S^i$ and $T^a T^a$.

Assuming an exact SU(2)-flavor symmetry, the mass formula for the ground state band up to order $1/N_c$ takes the following simple form [7]

$$M = c_1 N_c + c_4 \frac{1}{N_c}S^2 + \mathcal{O}\left(\frac{1}{N_c^3}\right), \tag{5}$$

which means that for $N = 0$ only the operators O_1 and O_4 (spin-spin) contribute to the mass.

Among the excited states, those belonging to the $N = 1$ band, or equivalently to the $[\mathbf{70}, 1^-]$ multiplet, have been most extensively studied, either for $N_f = 2$ (see *e.g.* Refs. [14–18]) or for $N_f = 3$ [19]. The $N = 2$ band contains the $[\mathbf{56}', 0^+]$, $[\mathbf{56}, 2^+]$, $[\mathbf{70}, \ell^+]$ $(\ell = 0, 2)$, and $[\mathbf{20}, 1^+]$ multiplets. There are no physical resonances associated to $[\mathbf{20}, 1^+]$. The few studies related to the $N = 2$ band concern the $[\mathbf{56}', 0^+]$ for $N_f = 2$ [20], $[\mathbf{56}, 2^+]$ for $N_f = 3$ [21], and $[\mathbf{70}, \ell^+]$ for $N_f = 2$ [22], later extended to $N_f = 3$ [23]. The method has also been applied [24] to highly excited non-strange and strange baryons belonging to $[\mathbf{56}, 4^+]$, the lowest multiplet of the $N = 4$ band [25].

The group theoretical similarity of excited symmetric states and the ground state makes the analysis of these states simple [21,24]. For mixed symmetric states, the situation is more complex. There is a standard procedure which reduces the study of mixed symmetric states to that of symmetric states. This is achieved by the decoupling of the baryon into an excited quark and a symmetric core of $N_c - 1$ quarks. This procedure has been applied to the $[\mathbf{70}, 1^-]$ multiplet [14–19] and to

the $[\mathbf{70}, \ell^+]$ (ℓ = 0, 2) multiplets [22,23]. But it has recently been shown that the decoupling is not necessary [13], provided one knows the matrix elements of the $SU(2N_f)$ generators between mixed symmetric states. The derivation of these matrix elements is not trivial. For SU(4) they have been derived by Hecht and Pang [26] in the context of nuclear physics and adapted to quark physics in Ref. [13], where it has been shown that the isospin-isospin term becomes as dominant in Δ as the spin-spin term in N resonances.

The derivation of SU(6) matrix elements between mixed symmetric states $[N_c - 1, 1]$ is underway [27].

A detailed description of the problems raised by the standard procedure [17] of the separation of a system of mixed spin-flavour symmetry $[N_c - 1, 1]$ into a symmetric core of $N_c - 1$ quarks and an excited quark has been given in Refs. [28,29].

2.2   Inclusion of strangeness

For light strange baryons ($N_f = 3$) the mass operator in the $1/N_c$ expansion has the general form

$$M = \sum_{i=1} c_i O_i + \sum_{i=1} d_i B_i, \qquad (6)$$

where the operators O_i are invariants under SU(6) transformations and the operators B_i explicitly break SU(3)-flavor symmetry. In the case of nonstrange baryons, only the operators O_i contribute, see Eq. (1). Therefore B_i are defined such as their expectation values are zero for nonstrange baryons. The coefficients d_i are determined from the experimental data including strange baryons. In Eq. (6) the sum over i is finite and in practice it contains the most dominant operators. Examples of O_i and B_i can be found in Refs. [21,23,24].

Assuming that each strange quark brings the same contribution ΔM_s to the SU(3)-flavor breaking terms in the mass formula, we define the total contribution of strange quarks as [11]

$$n_s \, \Delta M_s = \sum_{i=1} d_i B_i, \qquad (7)$$

where $n_s = -\mathcal{S}$ is the number of strange quarks in a baryon, $\mathcal{S}$ being its strangeness.

2.3   Heavy quarks

The approximate spin-flavor symmetry for large N_c baryons containing light $q = \{u, d, s\}$ and heavy $Q = \{c, b\}$ quarks is SU(6)$\times$ SU(2)$_c$ $\times$ SU(2)$_b$, *i.e.* there is a separate spin symmetry for each heavy flavor. Over a decade ago the $1/N_c$ expansion has been generalized to include an expansion in $1/m_Q$ and light quark flavor symmetry breaking [8]. The majority of the currently available experimental data concerning heavy baryons is related to ground state baryons made of one heavy and two light quarks [30]. Such heavy baryons, denoted as qqQ baryons, have been recently reanalyzed within the combined $1/N_c$ and $1/m_Q$ expansion [9], and masses in good agreement with experiment have been obtained.

A first attempt to extend this framework to excited heavy baryons can be found in Refs. [31] but much work remains to be done in this field. That is why we focus here on the $N = 0$ band for qqQ baryons only.

Let us first consider that SU(3)-flavor symmetry is exact. In this case the mass operator $M^{(1)}$ is a flavor singlet and in the combined $1/m_Q$ and $1/N_c$ expansion to order $1/m_Q^2$ it takes the following form

$$M^{(1)} = m_Q \mathbf{1} + \Lambda_{qq} + \lambda_Q + \lambda_{qqQ}. \tag{8}$$

The leading order term is m_Q at all orders in the $1/N_c$ expansion. Next we have

$$\Lambda_{qq} = c_0 \, N_c \, \mathbf{1} + \frac{c_2}{N_c} J_{qq}^2, \quad \text{and} \quad \lambda_Q = N_Q \frac{1}{2m_Q} \left(c_0' \mathbf{1} + \frac{c_2'}{N_c^2} J_{qq}^2 \right), \tag{9}$$

where J_{qq} is identical to the total spin S_{qq} of the light quark pair when one deals with the $N = 0$ band. Note that Λ_{qq} contains the dynamical contribution of the light quarks and is independent of m_Q while λ_Q gives $1/m_Q$ corrections. The last term, λ_{qqQ}, contains the heavy-quark spin-symmetry violating operator which reads

$$\lambda_{qqQ} = 2\frac{c_2''}{N_c m_Q} J_{qq} \cdot J_Q, \tag{10}$$

where J_Q is identical to the spin S_Q of the heavy quark.

The unknown coefficients c_0, c_2, c_0', c_2', and c_2'' are functions of $1/N_c$ and of a QCD scale parameter Λ. Each coefficient has an expansion in $1/N_c$ where the leading term (in dimensionless units) is of order unity and does not depend on $1/m_Q$. Thus, without loss of generality, by including dimensions, one can set $c_0 \equiv \Lambda$. The quantity Λ, as well as the other coefficients, have to be fitted to the available experimental data. In agreement with Ref. [8], we take

$$c_0 = \Lambda, \quad c_2 \sim \Lambda, \quad c_0' \sim c_2' \sim c_2'' \sim \Lambda^2. \tag{11}$$

The inclusion of SU(3)-flavor breaking leads to an expansion of the mass operator in the SU(3)-violating parameter ϵ which contains the singlet $M^{(1)}$, an octet $M^{(8)}$, and a 27-plet $M^{(27)}$. The last term brings contributions proportional to ϵ^2 and we neglect it. For $M^{(8)}$ we retain its dominant contribution T^8 to order N_c^0. Then the mass formula becomes

$$M = M^{(1)} + \epsilon T^8. \tag{12}$$

The flavor breaking parameter ϵ is governed by the mass difference $m_s - m$ (where m is the average of the m_u and m_d masses) and therefore is $\epsilon \sim 0.2\text{-}0.3$. It is measured in units of the chiral symmetry breaking scale parameter $\Lambda_\chi \sim 1$ GeV.

3   Quark model for baryons

3.1   Main Hamiltonian

The quark model used here to describe baryons aims at capturing the main physical features of a three-quark system while keeping the formalism as simple as

possible in order to get analytical mass formulas. It contains: Relativistic kinetic energy for the quarks, Y-junction confining potential, one-gluon exchange potential and quark self-energy contribution added as perturbative terms. Let us now shortly describe all these ingredients.

A baryon, seen as a bound state of three valence quarks, can be described, at the dominant order, by the spinless Salpeter Hamiltonian $H = \sum_{i=1}^{3} \sqrt{\mathbf{p}_i^2 + m_i^2} + V_Y$, where m_i is the bare mass of the quark i and where V_Y is the confining interaction potential. We use the bare mass of the quarks in the relativistic kinetic energy term as suggested by the field correlator method [32], but other approaches, like Coulomb gauge QCD, rather favor a running constituent quark mass [33]. Although very interesting conceptually, the influence of this choice on the mass spectra should not be so dramatic than it could have been expected at the first glance: First, the bare and constituent heavy quark masses are nearly identical. Second, the constituent light quark masses quickly decrease at large momentum and become similar to the bare masses; a common limit is reached for the excited states. The situation is thus mainly different for low-lying nnn baryons (u and d quarks are commonly denoted as n), where the bare mass m_n can be set equal to 0, but where the constituent mass is about 300 MeV [33]. However, the strength of additional interactions like one-gluon exchange (see next section) can be tuned in both cases and lead to final mass spectra which are quite similar.

Both the flux tube model [34] and lattice QCD [35] support the Y-junction picture for the confining potential: A flux tube starts from each quark and the three tubes meet at the Torricelli (or Steiner or Fermat) point of the triangle formed by the three quarks, let us say the ABC triangle. This point T, located at $\mathbf{x}_T$, minimizes the sum of the flux tube lengths and leads to the following confining potential $V_Y = a \sum_{i=1}^{3} |\mathbf{x}_i - \mathbf{x}_T|$, where the position of quark i is denoted by $\mathbf{x}_i$ and where a is the energy density of the flux tubes. If all the angles of ABC are less than 120°, then the Toricelli point is such that the angles $\widehat{ATB}$, $\widehat{BTC}$, and $\widehat{ATC}$ are all equal to 120°. If the angle corresponding to an apex is greater than 120°, the Toricelli point is precisely at this apex.

As $\mathbf{x}_T$ is a complicated three-body function, it is interesting to approximate the confining potential by a more tractable form. In the following, we shall use

$$H_R = \sum_{i=1}^{3} \sqrt{\mathbf{p}_i^2 + m_i^2} + V_R, \tag{13}$$

$$V_R = k\,a \sum_{i=1}^{3} |\mathbf{x}_i - \mathbf{R}|, \tag{14}$$

where $\mathbf{R}$ is the position of the center of mass and k is a corrective factor [36]. The accuracy of the replacement (14) has been checked to be very satisfactory (better than 5%) in this last reference provided that the appropriate scaling factor is used: $k_0 = 0.952$ for qqq baryons and $k_1 = 0.930$ for qqQ baryons. For highly excited states, the contribution of the configurations in which the Toricelli point is located on one of the quarks becomes more and more important, and one could think that the center of mass approximation (14) is then wrong. But in such cases

the angle made by the Toricelli point and the other two quarks is larger than 120° and the center of mass is consequently still close to the true Toricelli point. The approximation (14), although being less accurate for highly excited states, remains however relevant.

3.2 Perturbative terms

Besides the Hamiltonian (13), other contributions are necessary to reproduce the baryon masses. We shall add them as perturbations to the dominant Hamiltonian (13). The most widespread correction is a Coulomb interaction term of the form

$$\Delta H_{oge} = -\frac{2}{3} \sum_{i<j} \frac{\alpha_{S,ij}}{|\mathbf{x}_i - \mathbf{x}_j|}, \tag{15}$$

arising from one-gluon exchange processes, where $\alpha_{S,ij}$ is the strong coupling constant between the quarks i and j. Actually, one should deal with a running form $\alpha_S(r)$, but it would considerably increase the difficulty of the computations. Typically, we need two values: $\alpha_0 = \alpha_{S,qq}$ for a qq pair and $\alpha_1 = \alpha_{S,qQ}$ for a qQ pair, in the spirit of what has been done in a previous study describing mesons in the relativistic flux tube model [37]. There it was found that $\alpha_1/\alpha_0 \approx 0.7$ describes rather well the experimental data of $q\bar{q}$ and $Q\bar{q}$ mesons.

Another perturbative contribution to the mass is the quark self-energy. This is due to the color magnetic moment of a quark propagating through the QCD vacuum. It adds a negative contribution to the hadron masses [38]. The quark self-energy contribution for a baryon is given by

$$\Delta H_{qse} = -\frac{fa}{2\pi} \sum_i \frac{\eta(m_i/\delta)}{\mu_i}, \tag{16}$$

where μ_i is the kinetic energy of the quark i, that is $\mu_i = \left\langle \sqrt{\mathbf{p}_i^2 + m_i^2} \right\rangle$, the average being computed with the wave function of the unperturbed spinless Salpeter Hamiltonian (13). The factors f and δ have been computed in quenched and unquenched lattice QCD studies; it seems well established that $3 \leq f \leq 4$ and $(1.0 \leq \delta \leq 1.3)$ GeV [39]. The function $\eta(\epsilon)$ is analytically known; we refer the reader to Ref. [38] for an explicit formula. It can accurately be fitted by

$$\eta(\epsilon) \approx 1 - \beta\epsilon^2 \quad \text{with} \quad \beta = 2.85 \quad \text{for} \quad 0 \leq \epsilon \leq 0.3,$$
$$\approx \frac{\gamma}{\epsilon^2} \qquad \text{with} \quad \gamma = 0.79 \quad \text{for} \quad 1.0 \leq \epsilon \leq 6.0. \tag{17}$$

Let us note that the corrections depending on the parameter γ appear at order $1/m_Q^3$ in the mass formula, so they are not considered in this work.

We finally point out that the quark model we developed in this section is spin independent. This neglect of the fermionic nature of the quarks is the reason why such a model is often called "semirelativistic": The implicit covariance is preserved, but spin effects are absent. Spin dependent contributions (spin-spin, spin-orbit, etc.) typically come from relativistic corrections to the one-gluon exchange

potential. It is useful to mention that in our formalism such potential terms between the quarks i and j should be of the form [32]

$$V_{ij} \propto (\mu_i \mu_j)^{-1}. \tag{18}$$

4 Mass formulas

4.1 The auxiliary field method

The comparison between the quark model and large N_c mass formulas would be more straightforward if we could obtain analytical expressions. To this aim, the auxiliary field method is used in order to transform the Hamiltonian (13) into an analytically solvable one [40]. With $\lambda = k a$, we obtain

$$H(\mu_i, \nu_j) = \sum_{j=1}^{3} \left[\frac{\mathbf{p}_j^2 + m_j^2}{2\mu_j} + \frac{\mu_j}{2} \right] + \sum_{j=1}^{3} \left[\frac{\lambda^2 (\mathbf{x}_j - \mathbf{R})^2}{2\nu_j} + \frac{\nu_j}{2} \right]. \tag{19}$$

The auxiliary fields, denoted as μ_i and ν_j, are operators, and $H(\mu_i, \nu_j)$ is equivalent to H up to their elimination thanks to the constraints

$$\delta_{\mu_i} H(\mu_i, \nu_j)|_{\mu_i = \hat{\mu}_i} = 0 \;\Rightarrow\; \hat{\mu}_i = \sqrt{\mathbf{p}_i^2 + m_i^2},$$
$$\delta_{\nu_j} H(\mu_i, \nu_j)|_{\nu_j = \hat{\nu}_j} = 0 \;\Rightarrow\; \hat{\nu}_j = \lambda |\mathbf{x}_j - \mathbf{R}|. \tag{20}$$

$\langle \hat{\mu}_i \rangle$ is the quark kinetic energy, and $\langle \hat{\nu}_i \rangle$ is the energy of one flux tube, the average being computed with the wave function of the unperturbed spinless Salpeter Hamiltonian (13). The equivalence relation between Hamiltonians (13) and (19) is $H(\hat{\mu}_i, \hat{\nu}_j) = H$.

Although the auxiliary fields are operators, the calculations are considerably simplified if one considers them as variational parameters. They have then to be eliminated by a minimization of the masses, and their extremal values $\mu_{i,0}$ and $\nu_{j,0}$ are logically close to $\langle \hat{\mu}_i \rangle$ and $\langle \hat{\nu}_j \rangle$ respectively [40]. This technique can give approximate results very close to the exact ones [41]. If the auxiliary fields are assumed to be real numbers, the Hamiltonian (19) reduces formally to a non-relativistic three-body harmonic oscillator, for which analytical solutions can be found. A first step is to replace the quark coordinates $\mathbf{x}_i = \{\mathbf{x}_1, \mathbf{x}_2, \mathbf{x}_3\}$ by the Jacobi coordinates $\mathbf{x}_k' = \{\mathbf{R}, \boldsymbol{\xi}, \boldsymbol{\eta}\}$ defined as [42]

$$\mathbf{R} = (\mu_1 \mathbf{x}_1 + \mu_2 \mathbf{x}_2 + \mu_3 \mathbf{x}_3)/\mu_t, \quad \text{with} \quad \mu_t = \mu_1 + \mu_2 + \mu_3, \tag{21}$$

and $\boldsymbol{\xi} \propto \mathbf{x}_1 - \mathbf{x}_2$, $\boldsymbol{\eta} \propto (\mu_1 \mathbf{x}_1 + \mu_2 \mathbf{x}_2)/(\mu_1 + \mu_2) - \mathbf{x}_3$.

In the case of two quarks with mass m and another with mass m_3, the mass spectrum of the Hamiltonian (19) is given by ($\mu_1 = \mu_2 = \mu$, $\nu_1 = \nu_2 = \nu$ by symmetry)

$$M(\mu, \mu_3, \nu, \nu_3) = \omega_\xi (N_\xi + 3/2) + \omega_\eta (N_\eta + 3/2) + \mu + \nu + \frac{\mu_3 + \nu_3}{2} + \frac{m^2}{\mu} + \frac{m_3^2}{2\mu_3}, \tag{22}$$

$$\text{where} \quad \omega_\xi = \frac{\lambda}{\sqrt{\mu\nu}}, \quad \omega_\eta = \frac{\lambda}{\sqrt{2\mu+\mu_3}}\sqrt{\frac{\mu_3}{\mu\nu}+\frac{2\mu}{\mu_3\nu_3}}. \tag{23}$$

The integers $N_{\xi/\eta}$ are given by $2n_{\xi/\eta} + \ell_{\xi/\eta}$, where $n_{\xi/\eta}$ and $\ell_{\xi/\eta}$ are the radial and orbital quantum numbers relative to the variable ξ/η respectively. Moreover, $\langle \xi^2 \rangle$ and $\langle \eta^2 \rangle$ are analytically known. This eventually allows to compute $\langle (x_1 - x_3)^2 \rangle$ and $\langle (x_2 - x_3)^2 \rangle$, which are needed to know the one-gluon exchange contribution.

The four auxiliary fields appearing in the mass formula (22) have to be eliminated by solving simultaneously the four constraints

$$\partial_\mu M(\mu,\mu_3,\nu,\nu_3) = 0, \quad \partial_{\mu_3} M(\mu,\mu_3,\nu,\nu_3) = 0,$$
$$\partial_\nu M(\mu,\mu_3,\nu,\nu_3) = 0, \quad \partial_{\nu_3} M(\mu,\mu_3,\nu,\nu_3) = 0. \tag{24}$$

This task cannot be analytically performed in general, but solutions can fortunately be found in the case of light and heavy baryons.

4.2 Light baryons

Since we do not distinguish between the u and d quarks in our quark model and commonly denote them as n, there are only four possible configurations: nnn, sss, nss and snn, that can all be described by the mass formula (22). Important simplifications occur by setting $m_n = 0$, which is a good approximation of the u and d quark bare masses. However, the non vanishing value for m_s causes Eqs. (24) to have no analytical solution unless a power expansion in m_s is performed. This is justified *a priori* since the strange quark is still a light one. After such a power expansion, the final mass formula reads [10]

$$M_{qqq} = M_0 + n_s \, \Delta M_{0s} \qquad (n_s = 0,1,2,3),$$

$$M_0 = 6\mu_0 - \frac{2k_0 a\alpha_0}{\sqrt{3}\mu_0} - \frac{3fa}{2\pi\mu_0}, \quad \Delta M_{0s} = \frac{m_s^2}{\mu_0}\left[\frac{1}{2} - \frac{k_0 a\alpha_0}{6\sqrt{3}\mu_0^2} + \frac{fa}{2\pi}\left(\frac{3}{4\mu_0^2} + \frac{\beta}{\delta^2}\right)\right],$$

$$\mu_0 = \sqrt{\frac{k_0 a(N+3)}{3}}. \tag{25}$$

The mass formula M_{qqq} depends only on $N = N_\xi + N_\eta$. The contribution of terms proportional to $N_\xi - N_\eta$, vanishing for $n_s = 0$ and 3, was found to be very weak in the other cases by a numerical resolution of Eqs. (24).

An important feature of the above mass formula has to be stressed: It only depends on N the total number of excitation quanta of the system. But, this integer is precisely the band number introduced in large N_c QCD to classify the baryon states in a harmonic oscillator picture. Indeed the spinless Salpeter Hamiltonian (13) has been transformed into a harmonic oscillator by the auxiliary field method and it is thus natural that a such band number appears. The great advantage of the auxiliary field method is that it allows to obtain analytical mass formulas for a relativistic Hamiltonian while making explicitly the band number used in the large N_c classification scheme to appear. The origin of N is thus explained by the dynamics of the three-quark system and the comparison with the $1/N_c$ mass formulas is therefore possible.

4.3   Heavy baryons

A mass formula for qqQ baryons can also be found from Eq. (22). An expansion in m_s is still needed to get analytical expressions, but an expansion in $1/m_Q$ can also be done since we deal with one heavy quark. One obtains [12]

$$M_{qqQ} = m_Q + M_1 + n_s \, \Delta M_{1s} + \Delta M_Q \qquad (n_s = 0, 1, 2),$$

$$M_1 = 4\mu_1 - \frac{2}{3}\left(\alpha_0 \sqrt{\frac{k_1 a}{2N_\xi + 3}} + 2\alpha_1 \sqrt{\frac{2k_1 a}{N + 3}}\right) - \frac{fa}{\pi\mu_1},$$

$$\Delta M_{1s} = \frac{m_s^2}{\mu_1}\left[\frac{1}{2} - \frac{1}{12\mu_1}\left(\alpha_0\sqrt{\frac{k_1 a}{2N_\xi + 3}} + 2\alpha_1\sqrt{\frac{2k_1 a}{N + 3}}\right) + \frac{fa}{2\pi}\left(\frac{3}{4\mu_1^2} + \frac{\beta}{\delta^2}\right)\right],$$

$$\Delta M_Q = \frac{k_1 a}{2m_Q}\left[\left(1 - \frac{fa}{2\pi\mu_1^2}\right)G(N, N_\eta) - \frac{\alpha_0}{6}\sqrt{\frac{2N_\eta + 3}{2N_\xi + 3}}\left(\sqrt{\frac{2(2N_\eta + 3)}{N + 3}} - 1\right)\right.$$
$$\left. + \frac{4\alpha_1}{3}\frac{2N_\eta + 3}{N + 3}\right],$$

$$\mu_1 = \sqrt{\frac{k_1 a(N + 3)}{2}}, \quad G(N, N_\eta) = \sqrt{2N_\eta + 3}\left(\sqrt{2(N + 3)} - \sqrt{2N_\eta + 3}\right).$$
$$\tag{26}$$

At the lowest order in m_s and $1/m_Q$, this mass formula depends only on N. However, when corrections are added, the mass formula is no longer symmetric in N_η and N_ξ. Is it still possible to find a single quantum number? The answer is yes, provided we make the reasonable assumption that an excited heavy baryon will mainly "choose" the configuration that minimizes its mass.

   The dominant correction of order $1/m_Q$ is the term that depends on the function $G(N, N_\eta)$. The baryon mass is lowered when $G(N, N_\eta)$ is minimal, that is to say for $N_\eta = N$. The analysis of the dominant part of the Coulomb term shows that the baryon mass is also lowered in this case. So it is natural to assume that the favored configuration, minimizing the baryon energy, is $N_\eta = N$ and $N_\xi = 0$. It is also possible to reach the same conclusion by checking that an excitation of type N_η will keep the baryon smaller in average than the corresponding excitation in N_ξ. This is favored because of the particular shape of the potential, having for consequence that the more the system is small, the more it is light.

   As for light baryons, the quark model shows that heavy baryons can be labeled by a single band number N in a harmonic oscillator picture. A light diquark-heavy quark structure is then favored since the light quark pair will tend to remain in its ground state. Note that the diquark picture combined with a detailed relativistic quark model of heavy baryons leads to mass spectra in very good agreement with the experimental data [43].

4.4   Regge trajectories

The band number N emerges from the quark model as a good classification number for baryons. It is now interesting to focus on the behavior of the baryon

masses at large values of N, *i.e.* for highly excited states. In this limit, the formula (25) gives

$$M^2_{qqq} \approx 12\,ak_0(N+3) - \frac{24}{\sqrt{3}}ak_0\alpha_0 - \frac{16fak_0}{\pi} + 6\left[1 + \frac{fak_0\beta}{\pi\delta^2}\right]n_s m_s^2. \quad (27)$$

Our quark model thus states that light baryons should follow Regge trajectories, that is a linear relation $M^2 \propto N$, with a common slope, irrespective of the strangeness of the baryons. The Regge slope of strange and nonstrange baryons is also predicted to be independent of the strangeness in the $1/N_c$ expansion method [44]. Too few experimental data are unfortunately available to check this result. In the heavy baryon sector, the mass formula (26) with $N_\xi = 0$ and $N_\eta = N$ becomes at the dominant order

$$(M - m_Q)^2 = 8a\frac{k_1}{k_0}(N+3). \quad (28)$$

This model predicts Regge trajectories for heavy baryons, with a slope of $8ak_1/k_0 \approx 7.8a$ instead of $12ak_0 \approx 11.4\,a$ for light baryons.

The Regge slope for light baryons is here given by $12ak_0$. However, from experiment we know that the Regge slopes for light baryons and light mesons are approximately equal. For light mesons, the exact value obtained in the framework of the flux tube model is $2\pi a$, a lower value than the one obtained from formula (27). This is due to the auxiliary field method that has been shown to overestimate the masses [45]. What can be it done to remove this problem is to rescale a. Let us define σ such that $12ak_0 = 2\pi\sigma$; then the formula (27) is able to reproduce the light baryon Regge slope for a physical value σ of the flux tube energy density. The scaling $a = \pi\sigma/(6k_0)$ will consequently be assumed in the rest of this paper.

5   Large N_c QCD versus Quark Model results

5.1   Light nonstrange baryons

The coefficients c_i appearing in the $1/N_c$ mass operator can be obtained from a fit to experimental data. For example, the case $N = 0$ is particularly simple. Equation (5) can be applied to N and Δ baryons. Taking $N_c = 3$ together with $M_N = 940$ MeV for $S = 1/2$, and $M_\Delta = 1232$ MeV for $S = 3/2$, we get

$$c_1^{(N=0)} = 289 \text{ MeV}, \quad c_4^{(N=0)} = 292 \text{ MeV}. \quad (29)$$

Since the spin-orbit contribution vanishes for $N = 0$, no information can be obtained for c_2. We refer the reader to Refs. [19,21,22,24] for the determination of c_i at $N > 0$.

In the $1/N_c$ expansion method, the dominant term $c_1 N_c$ in the mass formula (1) contains the spin-independent contribution to the baryon mass, which in a quark model language represents the confinement and the kinetic energy. So,
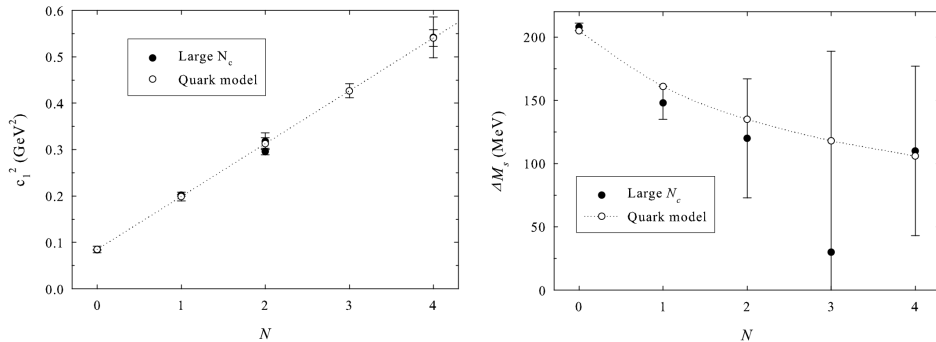
Fig. 1. Plot of c_1^2 (left) and ΔM_s (right) versus the band number N. The values computed in the $1/N_c$ expansion (full circles) from a fit to experimental data are compared with the quark model results with $\sigma = 0.163$ GeV^2, $\alpha_0 = 0.4$, $f = 3.6$, and $m_s = 0.240$ GeV (empty circles and dotted line to guide the eyes). No data is available for $N = 3$ in large N_c studies. The large N_c data are nearly indistinguishable from the quark model prediction in the left plot.

it is natural to identify this term with the mass given by the formula (25). Then, for $N_c = 3$ we have

$$c_1^2 = \frac{M_{qqq}^2}{9} = \frac{2\pi}{9}\sigma(N+3) - \frac{4\pi}{9\sqrt{3}}\sigma\alpha_0 - \frac{f\sigma}{3}. \qquad (30)$$

Figure 1 shows a comparison between the values of c_1^2 obtained in the $1/N_c$ expansion method and those derived from Eq. (30) for various values of N. From this comparison one can see that the results of large N_c QCD are entirely compatible with the formula (30) provided $\sigma = 0.163$ GeV^2, a rather low but still acceptable value according to usual potential models, $\alpha_0 = 0.4$, and $f = 3.6$: These are very standard values.

Equation (18) implies that c_2 and $c_4 \propto \mu_0^{-2}$. Therefore we expect the dependence of N of these coefficients to be of the form

$$c_2 = \frac{c_2^0}{N+3}, \quad c_4 = \frac{c_4^0}{N+3}. \qquad (31)$$

We see that such a behavior is consistent with the large N_c results in Fig. 2. We chose $c_2^0 = 208 \pm 60$ MeV so that the point with $N = 1$, for which the uncertainty is minimal, is exactly reproduced. Let us recall that the spin-orbit term is vanishing for $N = 0$, so no large N_c result is available in this case. To compute the parameter c_4^0 a fit was performed on all the large N_c results. In this way we have obtained $c_4^0 = 1062 \pm 198$ MeV. Note that $c_4^0 \gg c_2^0$. This shows that the spin-spin contribution is much larger than the spin-orbit contribution, which justifies the neglect of the spin-orbit one in quark model studies.
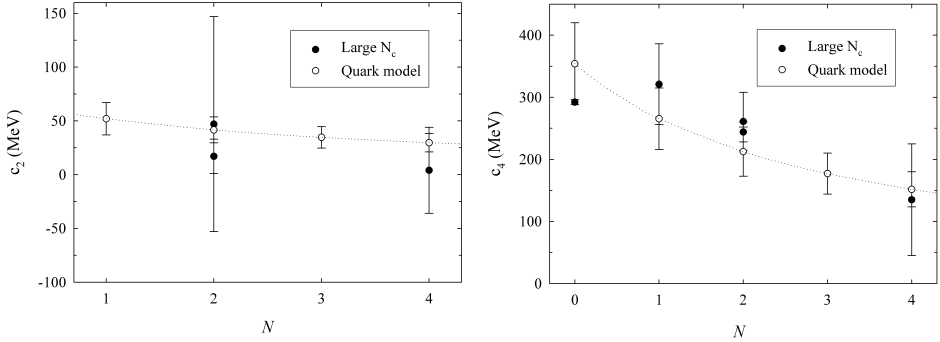
Fig. 2. Values of c_2 (left) and c_4 (right) versus the band number N. The values computed in the $1/N_c$ expansion (full circles) from a fit to experimental data are compared with results from formula (31) (empty circles and dotted line to guide the eyes). No data is available for N = 3 in large N_c studies.

5.2   Light strange baryons

We have first to find out the values of ΔM_s coming from the $1/N_c$ expansion. For N = 0, 1, and 3, they can be found in Ref. [44], and the case N = 4 is available in Ref. [24]. The situation is slightly more complicated in the N = 2 band due to a larger number of available results. We refer the reader to Ref. [11] for a detailed discussion about the computation of ΔM_s in this case.

The mass shift due to strange quarks is given in the quark model formalism by ΔM_{0s} in Eq. (25). A comparison of this term with its large N_c counterpart is given in Fig. 1, where we used the same parameters as for light nonstrange baryons. The only new parameter is the strange quark mass, that we set equal to 240 MeV, a higher mass than the PDG value but rather common in quark model studies. One can see that the quark model predictions are always located within the error bars of the large N_c results. Except for N = 3, whose large N_c value would actually require further investigations, the central values of ΔM_s in the large N_c approach are close to the quark model results and they decrease slowly and monotonously with increasing N. Thus, in both approaches, one predicts a mass correction term due to SU(3)-flavor breaking which decreases with the excitation energy (or N).

5.3   Heavy baryons

As mentioned previously, our present study is restricted to ground state heavy baryons made of one heavy and two light quarks. In the $1/N_c$, $1/m_Q$ expansion the parameters to be fitted are Λ, m_Q and $\epsilon \Lambda_\chi$. At the dominant order, the value of Λ can be extracted from the mass combinations [8]

$$\Lambda_Q = m_Q + N_c \Lambda, \quad \frac{1}{3}(\Sigma_Q + 2\Sigma_Q^*) - \Lambda_Q = 2\frac{\Lambda}{N_c}, \quad \Sigma_Q^* - \Sigma_Q = \frac{3}{2}\left(\frac{2\Lambda^2}{N_c m_Q}\right), \quad (32)$$

resulting from the mass formula (8). Here and below the particle label represents its mass. A slightly more complicated mass combination, involving light baryons as well as heavy ones, directly leads to m_Q, that is [9]

$$\frac{1}{3}(\Lambda_Q + 2\Xi_Q) - \frac{1}{4}\left[\frac{5}{8}(2N + 3\Sigma + \Lambda + 2\Xi) - \frac{1}{10}(4\Delta + 3\Sigma^* + 2\Xi^* + \Omega)\right] = m_Q.$$
(33)

This mass combination gives

$$m_c = 1315.1 \pm 0.2 \text{ MeV}, \quad m_b = 4641.9 \pm 2.1 \text{ MeV}, \tag{34a}$$

while the value

$$\Lambda \approx 324 \text{ MeV} \tag{34b}$$

ensures that the mass combinations (32) are optimally compatible with the experimental values for $Q = c$ and b. A measure of the SU(3)-flavor breaking factor is given by [8]

$$\Xi_Q - \Lambda_Q = \frac{\sqrt{3}}{2}(\epsilon\Lambda_\chi). \tag{35}$$

The value $(\epsilon\Lambda_\chi) = 206$ MeV leads to $\Xi_Q - \Lambda_Q = 178$ MeV, which is the average value of the corresponding experimental data.

The new parameters appearing in the quark model are m_c, m_b, $k_1 = 0.930$, and α_1. For the other parameters we keep the values fitted in the light baryon sector. We take $\alpha_1 = 0.7\alpha_0$ from the quark model study of Ref. [37]. The heavy quark masses can be fitted to the experimental data as follows. The quark model mass formula (26) is spin independent; it should thus be suitable to reproduce the masses of heavy baryons for which $J^2_{qq} = 0$. Namely, one expects that

$$M_{nnc}|_{N=0} = \Lambda_c = 2286.46 \pm 0.14 \text{ MeV}, \quad M_{nnb}|_{N=0} = \Lambda_b = 5620.2 \pm 1.6 \text{ MeV}.$$
(36)

These values are reproduced by formula (26) with $m_c = 1.252$ GeV and $m_b = 4.612$ GeV. It is worth mentioning that we predict $M_{nsc}|_{N=0} = 2433$ MeV and $M_{nsb}|_{N=0} = 5767$ MeV with these parameters. These values are very close to the experimental Ξ_c and Ξ_b masses respectively.

We can now compare the quark model and the $1/N_c$, $1/m_Q$ mass formulas. On the one hand the mass combination (33) leads to $m_c = 1315$ MeV and $m_b = 4642$ MeV. On the other hand, the quark model mass formula (26) is compatible with the experimental data provided that $m_c = 1252$ MeV and $m_b = 4612$ MeV. Both approaches lead to quark masses that differ by less than 5%. Thus they agree at the dominant order, where only m_Q is present.

The other parameter involved in the large N_c mass formula is Λ. A comparison of the spin independent part of the mass formulas (8) and (26) leads to the following identification for $N_c = 3$

$$c_0 = \frac{1}{3} M_1|_{N=0} = \frac{4}{3}\mu_1 - \frac{2}{27}\sqrt{\frac{k_1\pi\sigma}{2k_0}}(\alpha_0 + 2\sqrt{2}\alpha_1) - \frac{f\sigma}{18k_0\mu_1}, \tag{37}$$

with $\mu_1 = \sqrt{k_1 \pi \sigma / 4 k_0}$. According to Eqs. (11) and (34b) one has $c_0 = \Lambda \simeq 0.324$ GeV. The quark model gives 0.333 GeV for the expression after the second equality sign in Eq. (37), which means a very good agreement for the QCD scale Λ. The terms of order $1/m_Q$ lead to the identity

$$
\begin{aligned}
c_0' &= 2m_Q \, \Delta M_Q|_{N=0} \\
&= \frac{k_1 \pi \sigma}{6 k_0} \left[3 \left(\sqrt{2} - 1 \right) \left(1 - \frac{f\sigma}{12 k_0 \mu_1^2} \right) - \frac{\alpha_0}{6} \left(\sqrt{2} - 1 \right) + \frac{4\alpha_1}{3} \right].
\end{aligned}
\tag{38}
$$

Note that to test this relation the value of m_Q is not needed, like for the identity (37). The large N_c parameter, $\Lambda = 0.324$ GeV, gives for the left hand side of (38) $c_0' \sim \Lambda^2 = 0.096$ GeV^2 and the quark model gives for the right hand side 0.091 GeV^2, which is again a good agreement. Finally, the SU(3)-flavor breaking term is proportional to $\epsilon \Lambda_\chi \sim m_s - m \sim m_s$ in the mass formula (12). Equations (12), (26), and (35) lead to

$$
\begin{aligned}
\frac{\sqrt{3}}{2} \epsilon \Lambda_\chi &= \Delta M_{1s}|_{N=0} \\
&= \frac{m_s^2}{\mu_1} \left[\frac{1}{2} - \frac{1}{36 \mu_1} \sqrt{\frac{k_1 \pi \sigma}{2 k_0}} \left(\alpha_0 + 2\sqrt{2} \alpha_1 \right) + \frac{f\sigma}{12 k_0} \left(\frac{3}{4\mu_1^2} + \frac{\beta}{\delta^2} \right) \right].
\end{aligned}
\tag{39}
$$

The large N_c value $\epsilon \Lambda_\chi = 0.206$ GeV and the quark model estimate 0.170 GeV also compare satisfactorily. We point out that, except for m_c and m_b, all the model parameters are determined from theoretical arguments combined with phenomenology, or are fitted on light baryon masses. The comparison of our results with the $1/N_c$ expansion coefficients c_0, c_0' and $\epsilon \Lambda_\chi$ are independent of the m_Q values. So we can say that this analysis is parameter free.

An evaluation of the coefficients c_2, c_2', and c_2'' through a computation of the spin dependent effects is out of the scope of the present approach. But at the dominant order, one expects from Eq. (18) that $c_2 \propto \mu_1^{-2}$ and $c_2'' \propto \mu_1^{-1}$. The ratio c_2''/c_2 should thus be of order $\mu_1 = 356$ MeV, which is roughly in agreement with Eq. (11) stating that $c_2''/c_2 \sim \Lambda$. This gives an indication that the quark model and the $1/N_c$ expansion method would remain compatible if the spin-dependent effects were included.

6   Conclusions

We have established a connection between the quark model and the $1/N_c$ expansion both for light baryons and for heavy baryons containing a heavy quark. In the latter case the $1/N_c$ expansion is supplemented by an $1/m_Q$ expansion due to the heavy quark. A clear correspondence between the various terms appearing in the $1/N_c$ and quark model mass formulas is observed, and the fitted coefficients of the $1/N_c$ mass formulas can be quantitatively reproduced by the quark model.

These results bring reliable QCD-based support in favor of the constituent quark model assumptions and lead to a better insight into the coefficients c_i encoding the QCD dynamics in the $1/N_c$ mass operator. In particular, the dynamical

origin of the band number labeling the baryons in large N_c QCD is explained by the quark model.

As an outlook, we mention two important studies that we hope to make in the future. First, the $N = 1$ baryons of qqQ type are poorly known in the $1/N_c$, $1/m_Q$ expansion. They should be reconsidered and compared to the quark model. Second, the ground state baryons made of two heavy quarks and a light quark could be studied in a combined $1/N_c$, $1/m_Q$ expansion-quark model approach, leading to predictions for the mass spectrum of these baryons.

References

1. N. Isgur and G. Karl, Phys. Rev. D **18**, 4187 (1978); Phys. Rev. D **19**, 2653 (1979); Phys. Rev. D **20**, 1191 (1979).
2. S. Aoki *et al.* [PACS-CS Collaboration], arXiv:0807.1661 [hep-lat].
3. G. 't Hooft, Nucl. Phys. **72**, 461 (1974).
4. E. Witten, Nucl. Phys. B **160**, 57 (1979).
5. J. L. Gervais and B. Sakita, Phys. Rev. Lett. **52**, 87 (1984); Phys. Rev. D **30**, 1795 (1984); R. Dashen and A. V. Manohar, Phys. Lett. B **315**, 425 (1993); 438 (1993).
6. R. Dashen, E. Jenkins, and A. V. Manohar, Phys. Rev. D **49**, 4713 (1994); **51**, 2489 (1995);**51**, 3697 (1995).
7. E. Jenkins, Ann. Rev. Nucl. Part. Sci. **48**, 81 (1998).
8. E. E. Jenkins, Phys. Rev. D **54**, 4515 (1996).
9. E. E. Jenkins, Phys. Rev. D **77**, 034012 (2008).
10. C. Semay, F. Buisseret, N. Matagne, and Fl. Stancu, Phys. Rev. D **75**, 096001 (2007).
11. C. Semay, F. Buisseret, and Fl. Stancu, Phys. Rev. D **76**, 116005 (2007).
12. C. Semay, F. Buisseret, and Fl. Stancu, Phys. Rev. D **78**, 076003 (2008).
13. N. Matagne and F. Stancu, Nucl. Phys. A **811**, 291 (2008).
14. C. D. Carone *et al.*, Phys. Rev. D **50**, 5793 (1994).
15. J. L. Goity, Phys. Lett. B **414**, 140 (1997).
16. D. Pirjol and T. M. Yan, Phys. Rev. D **57**, 1449 (1998) ; **57**, 5434 (1998).
17. C. E. Carlson, C. D. Carone, J. L. Goity, and R. F. Lebed, Phys. Lett. B **438**, 327 (1998); Phys. Rev. D **59**, 114008 (1999).
18. T. D. Cohen and R. F. Lebed, Phys. Rev. D **67**, 096008 (2003).
19. C. L. Schat, J. L. Goity, and N. N. Scoccola, Phys. Rev. Lett. **88**, 102002 (2002);J. L. Goity, C. L. Schat, and N. N. Scoccola, Phys. Rev. D **66**, 114014 (2002).
20. C. E. Carlson and C. D. Carone, Phys. Lett. B **484**, 260 (2000).
21. J. L. Goity, C. L. Schat, and N. N. Scoccola, Phys. Lett. B **564**, 83 (2003).
22. N. Matagne and Fl. Stancu, Phys. Lett. B **631**, 7 (2005).
23. N. Matagne and Fl. Stancu, Phys. Rev. D **74**, 034014 (2006).
24. N. Matagne and Fl. Stancu, Phys. Rev. D **71**, 014010 (2005).
25. P. Stassart and Fl. Stancu, Z. Phys. A **359**, 321 (1997).
26. K. T. Hecht and S. C. Pang, J. Math. Phys. **10** (1969) 1571.
27. N. Matagne and Fl. Stancu, *in preparation*.
28. N. Matagne and Fl. Stancu, Phys. Rev. D **77**, 054026 (2008)
29. N. Matagne and Fl. Stancu, AIP Conf. Proc. **1038**, 278 (2008), arXiv:0805.4368 [hep-ph].
30. C. Amsler *et al.* [Particle Data Group], Phys. Lett. B **667**, 1 (2008).

31. J.-P. Lee, C. Liu, and H. S. Song, Phys. Rev. D **59**, 034002 (1998); **62**, 096001 (2000).
32. Yu. A. Simonov, hep-ph/9911237; A. Yu. Dubin, A. B. Kaidalov, and Yu. A. Simonov, Phys. Atom. Nucl **56**, 1745 (1993).
33. F. J. Llanes-Estrada and S. R. Cotanch, Phys. Rev. Lett. **84**, 1102 (2000); Phys. Lett. B **504**, 15 (2001).
34. J. Carlson, J. Kogut, and V. R. Pandharipande, Phys. Rev. D **27**, 233 (1983).
35. Y. Koma *et al.*, Phys. Rev. D **64**, 014015 (2001); F. Bissey *et al.*, Phys. Rev. D **76**, 114512 (2007).
36. B. Silvestre-Brac *et al.*, Eur. Phys. J. C **32**, 385 (2004).
37. C. Semay and B. Silvestre-Brac, Phys. Rev. D **52**, 6553 (1995).
38. Yu. A. Simonov, Phys. Lett. B **515**, 137 (2001).
39. A. Di Giacomo and H. Panagopoulos, Phys. Lett. B **285**, 133 (1992); A. Di Giacomo and Yu. A. Simonov, Phys. Lett. B **595**, 368 (2004).
40. C. Semay, B. Silvestre-Brac, and I. M. Narodetskii, Phys. Rev. D **69**, 014003 (2004).
41. I. M. Narodetskii, C. Semay, and A. I. Veselov, Eur. Phys. J C **55**, 403 (2008).
42. F. Buisseret and C. Semay, Phys. Rev. D **73**, 114011 (2006).
43. D. Ebert, R. N. Faustov and V. O. Galkin, Phys. Rev. D **72**, 034026 (2005).
44. J. L. Goity and N. Matagne, Phys. Lett. B **655**, 223 (2007).
45. F. Buisseret and V. Mathieu, Eur. Phys. J. A **29**, 343 (2006).

The spectrum of charmonium in the Resonance-Spectrum Expansion⋆

Eef van Beveren[a] and George Rupp[b]

[a]Centro de Física Computacional, Departamento de Física, Universidade de Coimbra,
P-3004-516 Coimbra, Portugal
[b]Centro de Física das Interacções Fundamentais, Instituto Superior Técnico,
Universidade Técnica de Lisboa, Edifício Ciência, P-1049-001 Lisboa, Portugal

Abstract. We argue that the resonance-like structures Y(4260) [1,2], Y(4360), Y(4660) [3] and Y(4635) [4], which were recently reported to have been observed in experiment, are non-resonant manifestations of the Regge zeros that appear in the production amplitude of the Resonance-Spectrum Expansion. Charmonium $c\bar{c}$ states are visible on the slopes of these enhancements.

In the Resonance-Spectrum Expansion (RSE) [5], which is based on the model of Ref. [6], the meson-meson scattering amplitude is given by an expression of the form (here restricted to the one-channel case)

$$T(E) = \left\{ -2\lambda^2 \mu p j_\ell^2 (pr_0) \sum_{n=0}^{\infty} \frac{|g_{nL(\ell)}|^2}{E - E_{nL(\ell)}} \right\} \Pi(E) \quad , \tag{1}$$

where p is the center-of-mass (CM) linear momentum, $E = E(p)$ is the total invariant two-meson mass, j_ℓ and $h_\ell^{(1)}$ are the spherical Bessel function and Hankel function of the first kind, respectively, μ is the reduced two-meson mass, and r_0 is a parameter with dimension mass^{-1}, which can be interpreted as the average string-breaking distance. The coupling constants g_{NL}, as well as the relation between ℓ and $L = L(\ell)$, were determined in Ref. [7]. The overall coupling constant λ, which can be formulated in a flavor-independent manner, represents the probability of quark-pair creation. The dressed partial-wave RSE propagator for strong interactions is given by

$$\Pi_\ell(E) = \left\{ 1 - 2i\lambda^2 \mu p j_\ell (pr_0) h_\ell^{(1)} (pr_0) \sum_{n=0}^{\infty} \frac{|g_{NL}|^2}{E - E_{NL}} \right\}^{-1} \quad . \tag{2}$$

⋆ Talk delivered by Eef van Beveren

This propagator has the very intriguing property that it vanishes for $E \to E_{NL}$. We will show in the following that this phenomenon can be, and has indeed been, observed in experiment, but not in scattering processes, as one easily verifies that the RSE amplitude for strong scattering (1) does not vanish in the limit $E \to E_{NL}$. However, for strong production processes, we derived in Ref. [8], following a procedure similar to the one by Roca, Palomar, Oset, and Chiang [9], a relation between the production amplitude **P** and the scattering amplitude **T**, reading

$$\mathbf{P}_\ell = j_\ell(pr_0) + i\,\mathbf{T}_\ell h_\ell^{(1)}(pr_0) \quad , \tag{3}$$

which, using Eqs. (2) and (1), can also be written as

$$\mathbf{P}_\ell = j_\ell(pr_0)\,\mathbf{\Pi}_\ell(E) \quad . \tag{4}$$

From this expression we find, by the use of Eq. (2), that the production amplitude tends to zero when $E \to E_{NL}$. This effect must be visible in experimental strong production cross sections.

Actually, in Ref. [8] we found, for the complete production amplitude in the case of multi-channel processes, that Eq. (4) represents the leading term, and that the remainder is expressed in terms of the inelastic components of the scattering amplitude. The latter terms do not vanish in the limit $E \to E_{NL}$, as we have seen above. Hence, the production amplitude only vanishes *approximately* in this limit, in case inelasticity is suppressed.

The reaction of electron-positron annihilation into multi-hadron final states takes basically place via one photon, hence with $J^{PC} = 1^{--}$ quantum numbers. Consequently, when the photon materializes into a pair of current quarks, which couple via the $q\bar{q}$ propagator to the final multi-hadron state, we may assume that the intermediate propagator carries the quantum numbers of the photon. Moreover, alternative processes are suppressed.

We may thus conclude that, if we want to discover whether the propagator really vanishes at $E \to E_{NL}$, then the ideal touchstone is e^+e^- annihilation into multi-hadron states. Furthermore, there also exist predictions for the values of E_{NL}, with $L = 0$ or $L = 2$, given by the parameter set of Ref. [10]. For $c\bar{c}$ one finds in the latter paper $E_{0,0} = 3.409$ GeV and $\omega = 0.19$ GeV, which results for the higher $c\bar{c}$ confinement states in the spectrum $E_{1,0} = E_{0,2} = 3.789$ GeV, $E_{2,0} = E_{1,2} = 4.169$ GeV, $E_{3,0} = E_{2,2} = 4.549$ GeV, ...

The latter two levels of the $c\bar{c}$ confinement spectrum can indeed be clearly observed in experiment. For example, the non-resonant signal in $e^+e^- \to \pi^+\pi^-\psi(2S)$ (see Fig. 5 of Ref. [3]) is divided into two substructures [11–13], since the full $c\bar{c}$ propagator (2), dressed with meson loops, vanishes at $E_3 = 4.55$ GeV [10]. In the same set of data, one may observe a lower-lying zero at $E_2 = 4.17$ GeV [10], more distinctly visible in the data on $e^+e^- \to \pi^+\pi^- J/\psi$ (see Fig. 3 of Ref. [2]). The true $c\bar{c}$ resonances can be found on the slopes of the above-mentioned non-resonant structures, unfortunately with little statistical significance, if any.

In fact, in Ref. [1], where the BaBar Collaboration announced the observation of the Y(4260) structure in $e^+e^- \to \pi^+\pi^- J/\psi$, one reads: "*no other structures are evident at the masses of the quantum number $J^{PC} = 1^{--}$ charmonium states, i.e.,*

the $\psi(4040)$, $\psi(4160)$, *and* $\psi(4415)$". However, in Ref. [14], we demonstrated that the BaBar data at about 4.15 GeV are consistent with the mass and width of the $\psi(4160)$. Here, we will show that also the $\psi(4415)$ is clearly visible in the BaBar data, possibly even with enough statistical significance.

So we indeed observe minima in production processes, which confirm vanishing $q\bar{q}$ propagators. Moreover, the $q\bar{q}$ confinement spectrum predicted 25 years ago in Ref. [10] seems to agree well with experimental observations for vector mesons. Accordingly, we expect vector-meson $q\bar{q}$ resonances associated with each of the Regge states: one ground state, dominantly in a $q\bar{q}$ S-wave, and two resonances for each of the higher excited Regge states, viz. one dominantly in an S-wave, and the other mostly in a D-wave. In Ref. [15], we reported on indications for four, possibly five, new $c\bar{c}$ vector states, in the $e^+e^- \to \Lambda_c^+\Lambda_c^-$ amplitudes of the Belle Collaboration [4]. Here, we will just concentrate on the $\psi(4S)$.

A full description of the $\pi^+\pi^- J/\psi$ involves a three-body calculation. In the present work, however, we will limit us to an effective two-body calculation for $(\pi^+\pi^-) J/\psi$, assuming for the $\pi^+\pi^-$ effective mass just a fraction of the available phase space. Furthermore, we assume an S-wave for the relative orbital angular momentum of the $\pi^+\pi^-$-J/ψ system. Under these assumptions, we obtain for the amplitude the result depicted in Fig. 1a, for the case that the propagator of Eq. (2) is substituted by a structureless vertex.

As expected, we observe no resonances in the amplitude of Fig. 1a. Next, we suppress the effect of the resonance poles in the propagator of Eq. (2), such that the zeros at $E = E_{NL}$ dominate production (see Eq. (4)). The resulting amplitudes are shown in Figs. 1b and 1c. We observe that now our theoretical amplitude is in rather good agreement with the data. There is an excess of data for energies below 4.0 GeV, stemming from the tail of the $\psi(3685)$ resonance, which dominates the amplitude at lower masses and which is not accounted for in our amplitude. Furthermore, in Ref. [14] we discussed the $\psi(4160)$ resonance, which, since not accounted for here, leads to an overestimate of the BaBar data by our theoretical amplitude.

However, there is a rather large overestimate visible in Fig. 1c at the mass of the $\psi(4415)$. In Fig. 1d, we show that the difference between data and our non-resonant amplitude can be perfectly explained by accounting for a $c\bar{c}$ resonance with mass and width consistent with the $\psi(4415)$. Moreover, the experimental error bars indicate that sufficient statistics is available to include this resonance in a data analysis for the non-resonant Y structures.

Summarizing, we have shown that the $c\bar{c}$ confinement spectrum, which underlies scattering and production of multi-meson systems containing charmonium $q\bar{q}$ pairs, can be observed in production amplitudes. Moremore, we have shown that the $c\bar{c}$ resonance poles are present in the $e^-e^+ \to J/\psi\pi^+\pi^-$ amplitude.
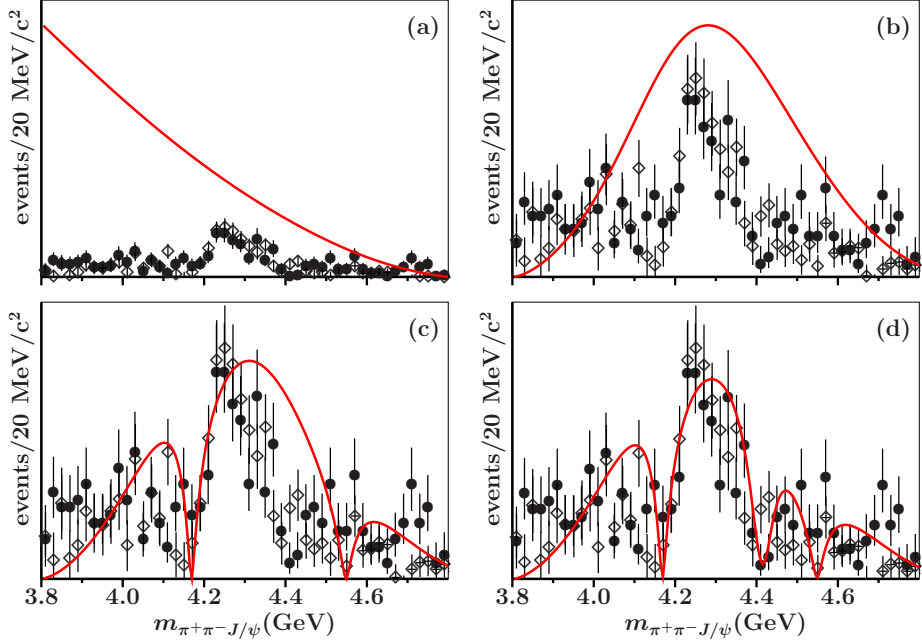
Fig.1. The $J/\psi(\pi^+\pi^-)$ invariant-mass distributions for the reaction $e^-e^+ \rightarrow J/\psi\pi^+\pi^-$. Data are taken from Ref. [1] ($\bullet$) and Ref. [2] ($\diamond$). The theoretical results (solid lines) are also discussed in the text: (a) shows the distribution for a non-resonant structureless $c\bar{c}$ propagator; (b) and (c) show the effect of Regge zeros in the $c\bar{c}$ vector propagator, thereby suppressing the contributions of its $c\bar{c}$ poles; (b) for just the Regge zero at 3.79 GeV; (c) for the zeros at 4.17 and 4.55 GeV as well; (d) shows the additional effect of the $c\bar{c}$ resonance pole in the propagator at $4.415 - i0.036$ GeV [16].

References

1. B. Aubert *et al.* [BABAR Collaboration], Phys. Rev. Lett. **95**, 142001 (2005).
2. C. Z. Yuan *et al.* [Belle Collaboration], Phys. Rev. Lett. **99**, 182004 (2007).
3. X. L. Wang *et al.* [Belle Collaboration], Phys. Rev. Lett. **99**, 142002 (2007).
4. G. Pakhlova *et al.* [Belle Collaboration], arXiv:0807.4458 [hep-ex].
5. E. van Beveren and G. Rupp, Int. J. Theor. Phys. Group Theor. Nonlin. Opt. **11**, 179 (2006).
6. E. van Beveren, C. Dullemond, and G. Rupp, Phys. Rev. D **21**, 772 (1980) [Erratum-ibid. D **22**, 787 (1980)].
7. E. van Beveren, Z. Phys. C **21**, 291 (1984).
8. E. van Beveren and G. Rupp, Ann. Phys. **323**, 1215 (2008).
9. L. Roca, J. E. Palomar, E. Oset and H. C. Chiang, Nucl. Phys. A **744**, 127 (2004).
10. E. van Beveren, G. Rupp, T. A. Rijken, and C. Dullemond, Phys. Rev. D **27**, 1527 (1983).
11. G. J. Ding, J. J. Zhu and M. L. Yan, Phys. Rev. D **77**, 014033 (2008).
12. Z. Q. Liu, X. S. Qin and C. Z. Yuan, Phys. Rev. D **78**, 014032 (2008).
13. F. K. Guo, C. Hanhart and U. G. Meissner, Phys. Lett. B **665**, 26 (2008).
14. E. van Beveren and G. Rupp, arXiv:hep-ph/0605317.
15. E. van Beveren, X. Liu, R. Coimbra, and G. Rupp, arXiv:0809.1151 [hep-ph].
16. C. Amsler *et al.* [Particle Data Group Collaboration], Phys. Lett. B **667**, 1 (2008).

Low-lying states in the Y-string three-quark potential[*]

V. Dmitrašinović[a], T. Sato[b], M. Šuvakov[c]

[a] Vinča Institute of Nuclear Sciences, lab 010, P.O. Box 522, 11001 Beograd, Serbia
[b] Dept. of Physics, Graduate School of Science, Osaka University, Toyonaka 560-0043,
Japan
[c] Institut J. Stefan, Dept. of Theoretical Physics F-1, Jamova 39, 1000 Ljubljana, Slovenia

Abstract. We give a brief summary of our study of low-lying states in the Y-string three-quark potential [1], currently under review. We study the masses of various three-quark SU(6) multiplets in the N=0,1,2 shells, confined by the Y-string three-quark potential, at four levels of approximation with increasing accuracy. We show the general trend of convergence of these four approximations.

1 Introduction

The so-called Y-junction string three-quark potential, defined by

$$V_Y = \sigma \min_{\mathbf{x_0}} \sum_{i=1}^{3} |\mathbf{x_i} - \mathbf{x_0}|. \tag{1}$$

has long been advertised [2–7] as a natural description of the flux tube confinement mechanism, that is allegedly active in QCD. Lattice investigations, Refs. [8–10] contradict each other, however, in their attempts to distinguish between the Y-string, Fig. 1, and the Δ-string potential, see Fig. 2, which is indistinguishable from the sum of three linear two-body potentials. One may therefore view the present lattice results as inconclusive and await the next generation of calculations. Yet, one would wish to resolve this dilemma on a purely theoretical basis: do these two kinds of string potentials predict sufficiently different baryon spectra that can be differentiated by experiment? At this time one must use the quark model in order to try and resolve this dilemma.

$$V_\Delta = \sigma \sum_{i<j=1}^{3} |\mathbf{x_i} - \mathbf{x_j}|, \tag{2}$$

Over the past 25 years, the Y-string potential has been used in several studies of baryons in the (constituent) quark model with various hyperfine interactions [4–6,11], and yet some of the most basic predictions of this potential, such as its influence on the splitting of the low-lying three-quark states have remained widely

---

[*] Talk presented by V. Dmitrašinović
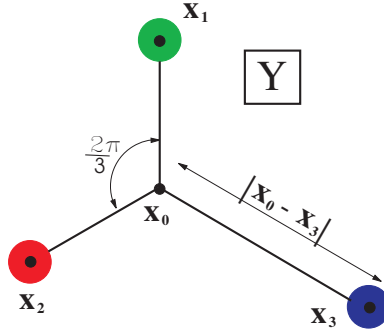
Fig.1. Three-quark Y-junction string potential.
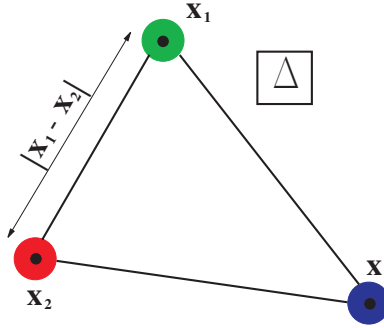
Fig.2. Three-quark Δ-shape string potential.

unknown. That has to do with the technical complications in the implementation of the potential Eq. (1), that can best be seen when expressed in terms of the three-body Jacobi coordinates $\boldsymbol{\rho}, \boldsymbol{\lambda}$

$$\boldsymbol{\rho} = \frac{1}{\sqrt{2}}(\mathbf{x_1} - \mathbf{x_2}), \tag{3}$$

$$\boldsymbol{\lambda} = \frac{1}{\sqrt{6}}(\mathbf{x_1} + \mathbf{x_2} - 2\mathbf{x_3}), \tag{4}$$

as follows. The exact string potential Eq. (1) consists of the so-called Y-string, or three-string term,

$$V_{\text{string}} = V_Y = \sigma\sqrt{\frac{3}{2}(\boldsymbol{\rho}^2 + \boldsymbol{\lambda}^2 + 2|\boldsymbol{\rho} \times \boldsymbol{\lambda}|)}, \tag{5}$$

$$\text{when} \begin{cases} 2\boldsymbol{\rho}^2 - \sqrt{3}\boldsymbol{\rho} \cdot \boldsymbol{\lambda} \geq -\rho\sqrt{\boldsymbol{\rho}^2 + 3\boldsymbol{\lambda}^2 - 2\sqrt{3}\boldsymbol{\rho} \cdot \boldsymbol{\lambda}} \\ 2\boldsymbol{\rho}^2 + \sqrt{3}\boldsymbol{\rho} \cdot \boldsymbol{\lambda} \geq -\rho\sqrt{\boldsymbol{\rho}^2 + 3\boldsymbol{\lambda}^2 + 2\sqrt{3}\boldsymbol{\rho} \cdot \boldsymbol{\lambda}} \\ 3\boldsymbol{\lambda}^2 - \boldsymbol{\rho}^2 \geq -\frac{1}{2}\sqrt{(\boldsymbol{\rho}^2 + 3\boldsymbol{\lambda}^2)^2 - 12(\boldsymbol{\rho} \cdot \boldsymbol{\lambda})^2}. \end{cases}$$

and three angle-dependent two-part string, or the so-called V-string, terms,

$$V_{string} = \sigma \left(\sqrt{\frac{1}{2}(\rho^2 + 3\lambda^2 + 2\sqrt{3}\boldsymbol{\rho}\cdot\boldsymbol{\lambda})} + \sqrt{\frac{1}{2}(\rho^2 + 3\lambda^2 - 2\sqrt{3}\boldsymbol{\rho}\cdot\boldsymbol{\lambda})} \right) \qquad (6)$$

$$\text{when} \begin{cases} 2\rho^2 - \sqrt{3}\boldsymbol{\rho}\cdot\boldsymbol{\lambda} \geq -\rho\sqrt{\rho^2 + 3\lambda^2 - 2\sqrt{3}\boldsymbol{\rho}\cdot\boldsymbol{\lambda}} \\ 2\rho^2 + \sqrt{3}\boldsymbol{\rho}\cdot\boldsymbol{\lambda} \geq -\rho\sqrt{\rho^2 + 3\lambda^2 + 2\sqrt{3}\boldsymbol{\rho}\cdot\boldsymbol{\lambda}} \\ 3\lambda^2 - \rho^2 \leq -\frac{1}{2}\sqrt{(\rho^2 + 3\lambda^2)^2 - 12(\boldsymbol{\rho}\cdot\boldsymbol{\lambda})^2} \end{cases}$$

$$V_{string} = \sigma \left(\sqrt{2}\rho + \sqrt{\frac{1}{2}(\rho^2 + 3\lambda^2 + 2\sqrt{3}\boldsymbol{\rho}\cdot\boldsymbol{\lambda})} \right) \qquad (7)$$

$$\text{when} \begin{cases} 2\rho^2 - \sqrt{3}\boldsymbol{\rho}\cdot\boldsymbol{\lambda} \geq -\rho\sqrt{\rho^2 + 3\lambda^2 - 2\sqrt{3}\boldsymbol{\rho}\cdot\boldsymbol{\lambda}} \\ 2\rho^2 + \sqrt{3}\boldsymbol{\rho}\cdot\boldsymbol{\lambda} \leq -\rho\sqrt{\rho^2 + 3\lambda^2 + 2\sqrt{3}\boldsymbol{\rho}\cdot\boldsymbol{\lambda}} \\ 3\lambda^2 - \rho^2 \geq -\frac{1}{2}\sqrt{(\rho^2 + 3\lambda^2)^2 - 12(\boldsymbol{\rho}\cdot\boldsymbol{\lambda})^2} \end{cases}$$

$$V_{string} = \sigma \left(\sqrt{2}\rho + \sqrt{\frac{1}{2}(\rho^2 + 3\lambda^2 - 2\sqrt{3}\boldsymbol{\rho}\cdot\boldsymbol{\lambda})} \right) \qquad (8)$$

$$\text{when} \begin{cases} 2\rho^2 - \sqrt{3}\boldsymbol{\rho}\cdot\boldsymbol{\lambda} \leq -\rho\sqrt{\rho^2 + 3\lambda^2 - 2\sqrt{3}\boldsymbol{\rho}\cdot\boldsymbol{\lambda}} \\ 2\rho^2 + \sqrt{3}\boldsymbol{\rho}\cdot\boldsymbol{\lambda} \geq -\rho\sqrt{\rho^2 + 3\lambda^2 + 2\sqrt{3}\boldsymbol{\rho}\cdot\boldsymbol{\lambda}} \\ 3\lambda^2 - \rho^2 \geq -\frac{1}{2}\sqrt{(\rho^2 + 3\lambda^2)^2 - 12(\boldsymbol{\rho}\cdot\boldsymbol{\lambda})^2} \end{cases} \cdot$$

Here, the reasons for the lack of use of the exact potential Eq. (1) become apparent: i) it is a genuine three-body operator with a complicated and unusual ("area term") angular dependence under the square-root of the most important term (the Y-junction string potential) that leads to the non-conservation of the individual Jacobi relative coordinates' angular momenta and hugely complicates the equations of motion; ii) the square-roots appearing in all four functional forms of the potential make this task even more difficult; iii) the presence of four different functional forms of the potential depending on the configuration space angles makes the integration of the equations of motion difficult as one cannot easily separate the angular and radial integrals.

In Sect. 2 we give a summary of how we address the above three problems. A summary of our results is shown in Sect. 3. The final Section 4 contains a discussion of our results.

2   Approximations

First we address the above three problems: first, we deal with the angular momentum recoupling algebra necessary to deal with the non-conserved "partial" angular momenta; second we deal with the square root(s) in the Y-string potential, and third we address all four forms of the string potential together.

Perhaps the most common, and the simplest approximation to the exact string potential Eq. (1) is the Y-string, or the three-string potential, Eq. (5), that is

used in all geometries, i.e., even when one of the angles exceeds 120°. In that way one avoids the cumbersome transition to the V-string potentials, see problem iii) above. Still, even this simplified approximation suffers from two difficulties mentioned above: i) an unusual ("area term") angular dependence under the square-root that leads to the non-conservation of the individual Jacobi coordinates' angular momenta; ii) the square-root. We shall address these problems in successive steps: i) the area term turns out to be exactly (analytically) integrable in the harmonic oscillator basis, that boils down to some (complicated) angular momenta recoupling algebra and the value of a particular one-dimensional integral. Problem ii), the overall square root, can be treated, at first, by a series expansion, i.e. in perturbation theory, using the angular algebra solution to problem i) and the numerical evaluation of the remaining one-dimensional integral. It turns out that the crucial ingredient for the solution of this problem is the application of the so-called hyper-spherical coordinates/angles [12], more specifically the cosines of the relative angle θ between the Jacobi coordinates ρ, λ and of the hyper-angle 2χ defined by the ratio of the moduli ρ, λ of the two Jacobi coordinates. Finally, the third issue iii) (the presence of four different functional forms of the potential) can be tackled as well, by numerically evaluating a two-dimensional integral in a restricted region of the $\chi - \theta$ sub-hyper-space.

3   Summary of Results

In the following we summarize the results of our study of the low-lying parts of the energy spectra of three quarks confined by a pure Y-string potential, without two-quark potentials, in four different approximations: 1) the area-dependent part of the three-string potential as the first order perturbation of the harmonic oscillator; 2) the area-dependent part of the three-string potential as the first order perturbation of the non-harmonic linear potential, i.e. the (approximate) three-string potential expanded up to the first power in hyper-spherical angles; 3) the (approximate) three-string potential to all orders in power expansion in hyper-spherical harmonics, without taking into account the transition(s) to two-string potentials; 4) the exact minimal-length string potential to all orders in power expansion in hyper-spherical harmonics, while taking into account the transition(s) to two-string potentials. Our results are shown in Table 1 and Fig. 3.

An attractive Y-string potential always splits the N=K=2 band states into degenerate $SU_{FS}(6)$ multiplets: $[20, 1^+], [70, 2^+], [56, 2^+], [70, 0^+]$, (in order of descending mass) following approximately the Bowler and Tynemouth (BT) [13] separation rule of 2:2:1. This rule is obeyed by approximations 1) and 2) exactly and by approximation 3) at the level of one per cent corrections. The exact result 4) leads to the 2.25:2.18:1 splitting, i.e. the largest violation of the BT rule is less than 13%.

The mass difference between the first (hyper-) radial excitation of the ground state, that is the "Roper multiplet" $[56', 0^+]$, and the odd-parity K=N=1 $[70, 1^-]$ multiplet is entirely determined by the difference between and the first (hyper-) angular and the first (hyper-) radial excitation eigen-energies in a linearly rising hyper-radial potential, which is always negative.
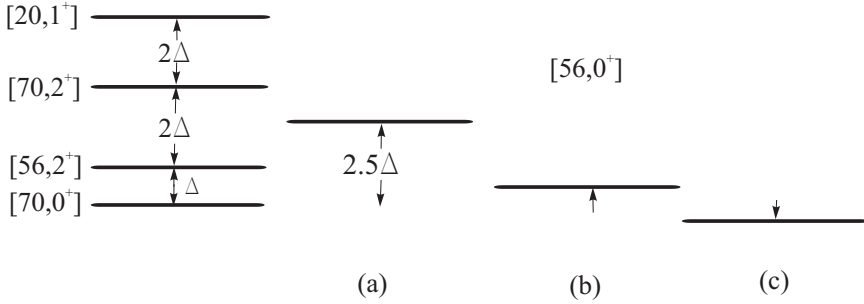
Fig.3. Depiction of the energy splitting of the K = 2 states of the hyper-spherical linear potential spectrum due to attractive three-body potentials: (a) the first-order perturbation approximation to the "harmonic Y-string" potential; (b) the first-order perturbation approximation to the first-power expansion in hyper-spherical coordinates of the "three-string" potential (see text for definition); (c) non-perturbative results of the "three-string" potential solved in hyper-spherical coordinates. The left-hand side of the diagram involving the $[20, 1^+], [70, 2^+], [56, 2^+], [70, 0^+]$ multiplets is common to both kinds of potentials, follows the Bowler-Tynemouth rule 2:2:1 to 1%; only the position of the $[56, 0^+]$ multiplet (containing the Roper resonance) is variable.

In other words, the Roper resonance cannot be lowered below the odd-parity K=N=1 states, irrespective of the string tension constant and the quark masses, which are the only free parameters in this theory. Consequently, the energy spectrum pattern can not be improved, as compared with the desired/experimental one, by a straightforward application of the Y-string three-body potential.

Table 1. The eigen-values of the unperturbed (solution to the hyper-central approximation, see the text) energy $E^{(0)}_{N_K,K}$, and the two perturbative ($E^{(1)}_{N_K,K,L}$, $E^{(2)}_{N_K,K,L}$), and two non-perturbative ($E^{(3)}_{N_K,K,L}$, $E^{(4)}_{N_K,K,L}$) approximations, where the last one $E^{(4)}_K$; is the exact (numerical) result, for the various low-lying K = 0,1,2 states (with all allowed orbital waves L).

K	N_K	$[SU(6), L^P]$	$E^{(0)}_{N_K,K}$	$E^{(1)}_{N_K,K,L}$	$E^{(2)}_{N_K,K,L}$	$E^{(3)}_{N_K,K,L}$	$E^{(4)}_{N_K,K,L}$
0	0	$[56, 0^+]$	3.8175	4.0000	4.6658	4.5182	4.5218
1	1	$[70, 1^-]$	4.6582	5.3333	5.6934	5.5132	5.5176
0	1	$[56, 0^+]$	5.2630	6.6667	6.4326	6.2290	6.2340
2	2	$[70, 0^+]$	5.4290	6.3333	6.3942	6.2493	6.2665
2	2	$[56, 2^+]$	5.4290	6.4667	6.4907	6.3199	6.3279
2	2	$[70, 2^+]$	5.4290	6.7333	6.6837	6.4604	6.4617
2	2	$[20, 1^+]$	5.4290	7.0000	6.8767	6.5993	6.5999

4   Discussion

We have examined the qualitative and quantitative features of the energy spectrum in the Y-string three-quark potential and its differences from the two-body,

or the Δ-shaped string one. For this purpose we have studied the low-lying states of the three-quark system (the "baryon") in the Y-string potential (the Δ-string potential had been studied in Ref. [14]). It turns out that the three lowest-lying bands of states that form the (only) set of well-established ("four-star") resonances, do *not* as yet allow a clear distinction to be made between these two types of potentials: there are too few states in these shells, and their wave functions are (tightly) constrained by the permutation symmetry. This is a bit of a surprise, as these two string potentials have (very) different functional forms, which we expected to predict different physics:

So, it turns out that there is only one possible clue to the form of the confining potential in the low-lying baryon resonance spectrum, *viz.* the Roper resonance's (abnormally low) mass, that perhaps could be used to draw conclusions about the existence and/or preponderance of one kind of potential over the other. We have shown, however, that the Y-shaped string always leads to a Roper resonance that is heavier than the lowest-lying odd-parity resonance. This does not mean that the spectra of the Y- and the two-body potentials are identical, rather, it means that one must go to the higher lying bands, and in particular to higher orbital angular momentum states, in order to see the difference between the two.

A detailed study of the possible interference of the two- and three-body potentials on the position of the first hyper-radial excitation (the "Roper resonance") remains a task for the future. Moreover, the behavior of the Y-string in higher orbital angular momentum states remains another place to look for the differences from the Δ-string.

References

1. V. Dmitrašinović, M. Šuvakov and T. Sato, submitted to Phys. Rev. **D** (2008).
2. X. Artru, Nucl. Phys. **B 85**, 442 (1975).
3. H. G. Dosch and V. Mueller, Nucl. Phys. **B 116**, 470 (1976).
4. J. Carlson, J.B. Kogut, and V. R. Pandharipande, Phys. Rev. **D 27**, 233 (1983); *ibid.* **D 28**, 2807 (1983).
5. S. Capstick and N. Isgur, Phys. Rev. **D 34**, 2809 (1986).
6. W. H. Blask, U. Bohn, M. G. Huber, B. Ch. Metsch, and H. R. Petry, Z. Phys. **A 337**, 327 (1990).
7. Y. Koma, E.-M. Ilgenfritz, T. Suzuki, and H. Toki, Phys. Rev. **D 64**, 014015 (2001).
8. G. S. Bali, Phys. Rep. **343**, 1 (2001).
9. T. T. Takahashi, H. Matsufuru, Y. Nemoto, and H. Suganuma, Phys. Rev. Lett. **86**, 18 (2001); Phys. Rev D **65**, 114509 (2002).
10. C. Alexandrou, P. De Forcrand, A. Tsapalis, Phys. Rev. **D 65**, 054503,(2002).
11. U. Löring, B. C. Metsch, H. R. Petry, Eur. Phys. J. **A 10**, 395 (2001).
12. Yu. A. Simonov, Sov. J. Nucl. Phys. **3**, 461 (1966) [Yad. Fiz. **3**, 630 (1966)].
13. K.C. Bowler and B.F. Tynemouth, Phys. Rev. **D 27**, 662 (1983); K.C. Bowler, P.J. Corvi, A.J.G. Hey, P.D. Jarvis and R.C. King, Phys.Rev. **D 24**, 197 (1981).
14. J.M. Richard and P. Taxil, Nucl.Phys. **B 329**, 310, (1990).

Masses of heavy tetraquarks in the relativistic quark model*

D. Ebert[a], R. N. Faustov[b], V. O. Galkin[b]

[a]Institut für Physik, Humboldt–Universität zu Berlin, Germany
[b]Dorodnicyn Computing Centre, Russian Academy of Sciences, Moscow, Russia

Abstract. The masses of the ground and excited heavy tetraquarks with hidden charm are calculated within the relativistic diquark-antidiquark picture.

Recently, significant experimental progress has been achieved in charmonium spectroscopy. Several new charmonium-like states, such as X(3872), Y(4260), Y(4360), Y(4660), Z(4248), Z(4430), etc., were observed [1] which cannot be simply accommodated in the quark-antiquark ($c\bar{c}$) picture. These states and especially the charged ones can be considered as indications of the possible existence of exotic multiquark states. In this talk we briefly review our papers [2,3] where we calculated masses of the ground and excited states of heavy tetraquarks in the framework of the relativistic quark model based on the quasipotential approach in quantum chromodynamics. For our calculations we use the diquark-antidiquark picture to reduce a complicated relativistic four-body problem to the subsequent two more simple two-body problems. The first step consists in the calculation of the masses, wave functions and form factors of the diquarks, composed from light and heavy quarks. At the second step, a heavy tetraquark is considered to be a bound diquark-antidiquark system. It is important to emphasize that we do not consider the diquark as a point particle but explicitly take into account its structure by calculating the form factor of the diquark-gluon interaction in terms of the diquark wave functions. Details of the relativistic quark model and calculations can be found in [2,3].

In the diquark-antidiquark picture of heavy tetraquarks both scalar S (antisymmetric in flavour $(Qq)_{S=0} = [Qq]$) and axial vector A (symmetric in flavour $(Qq)_{S=1} = \{Qq\}$) diquarks are considered. Therefore we get the following structure of the $(Qq)(\bar{Q}\bar{q}')$ ground (1S) states (C is defined only for $q = q'$):

- Two states with $J^{PC} = 0^{++}$:

$$X(0^{++}) = (Qq)_{S=0}(\bar{Q}\bar{q}')_{S=0}$$
$$X(0^{++\prime}) = (Qq)_{S=1}(\bar{Q}\bar{q}')_{S=1}$$

---

* Talk presented by D. Ebert

- Three states with $J = 1$:

$$X(1^{++}) = \frac{1}{\sqrt{2}}[(Qq)_{S=1}(\bar{Q}\bar{q}')_{S=0} + (Qq)_{S=0}(\bar{Q}\bar{q}')_{S=1}]$$

$$X(1^{+-}) = \frac{1}{\sqrt{2}}[(Qq)_{S=0}(\bar{Q}\bar{q}')_{S=1} - (Qq)_{S=1}(\bar{Q}\bar{q}')_{S=0}]$$

$$X(1^{+-\prime}) = (Qq)_{S=1}(\bar{Q}\bar{q}')_{S=1}$$

- One state with $J^{PC} = 2^{++}$:

$$X(2^{++}) = (Qq)_{S=1}(\bar{Q}\bar{q}')_{S=1}.$$

The orbitally excited (1P, 1D ...) states are constructed analogously. As we find, a very rich spectrum of tetraquarks emerges. However the number of states in the considered diquark-antidiquark picture is significantly less than in the genuine four-quark approach.

The diquark-antidiquark model of heavy tetraquarks predicts the existence of a flavour SU(3) nonet of states with hidden charm or beauty ($Q = c, b$): four tetraquarks $[(Qq)(\bar{Q}\bar{q}), q = u, d]$ with neither open or hidden strangeness, which have electric charges 0 or ± 1 and isospin 0 or 1; four tetraquarks $[(Qs)(\bar{Q}\bar{q})$ and $(Qq)(\bar{Q}\bar{s}), q = u, d]$ with open strangeness ($S = \pm 1$), which have electric charges 0 or ± 1 and isospin $\frac{1}{2}$; one tetraquark $(Qs)(\bar{Q}\bar{s})$ with hidden strangeness and zero electric charge. Since we neglect in our model the mass difference of u and d quarks and electromagnetic interactions, the corresponding tetraquarks will be degenerate in mass. A more detailed analysis [4] predicts that the tetraquark mass differences can be of a few MeV so that the isospin invariance is broken for the $(Qq)(\bar{Q}\bar{q})$ mass eigenstates and thus in their strong decays. The (non)observation of such states will be a crucial test of the tetraquark model.

In Table 1 we compare our results (EFG) for the masses of the ground and excited charm diquark-antidiquark bound states with the predictions of Refs. [4] and with the masses of the observed highly-excited charmonium-like states [1]. We assume that the excitations occur only between the bound diquark and antidiquark. Possible excitations of diquarks are not considered. Our calculation of the heavy baryon masses supports such a scheme [5]. In this table we give our predictions only for some of the masses of the orbitally and radially excited states for which possible experimental candidates are observed. The differences in some of the presented theoretical mass values can be attributed to the substantial distinctions in the used approaches. We describe the diquarks dynamically as quark-quark bound systems and calculate their masses and form factors, while in Refs.[4] they are treated only phenomenologically. Then we consider the tetraquark as purely the diquark-antidiquark bound system. In distinction, Maini et al. consider a hyperfine interaction between all quarks which, e.g., causes the splitting of 1^{++} and 1^{+-} states arising from the SA diquark-antidiquark compositions. From Table 1 we see that our dynamical calculation supports the assumption [4] that X(3872) can be the axial vector 1^{++} tetraquark state composed from the scalar and axial vector diquark and antidiquark in the relative 1S state. Recent Belle and BaBar results indicate the existence of a second X(3875) particle a

Table 1. Comparison of theoretical predictions for the masses of the ground and excited charm diquark-antidiquark states (in MeV) and possible experimental candidates.

State J^{PC}	Diquark content	Theory EFG	Theory [4]	Experiment state	Experiment mass[1]
1S					
0^{++}	$S\bar{S}$	3812	3723		
1^{++}	$(S\bar{A}+\bar{S}A)/\sqrt{2}$	3871	$3872^{\dagger}$	X(3872)	3871.4 ± 0.6
				X(3876)	$3875.2 \pm 0.7^{+0.9}_{-1.8}$
1^{+-}	$(S\bar{A}-\bar{S}A)/\sqrt{2}$	3871	3754		
0^{++}	$A\bar{A}$	3852	3832		
1^{+-}	$A\bar{A}$	3890	3882		
2^{++}	$A\bar{A}$	3968	3952	Y(3943)	$3943 \pm 11 \pm 13$
					$3914.3^{+4.1}_{-3.8}$
1P					
1^{--}	$S\bar{S}$	4244	4330 ± 70 $(cs\bar{c}\bar{s})$	Y(4260)	$4259 \pm 8^{+2}_{-6}$
					$4247 \pm 12^{+17}_{-32}$
1^{-}	$S\bar{S}$	4244		Z(4248)	$4248^{+44+180}_{-29-35}$
0^{-}	$(S\bar{A}\pm\bar{S}A)/\sqrt{2}$	4267			
1^{--}	$(S\bar{A}-\bar{S}A)/\sqrt{2}$	4284		Y(4260)	$4284^{+17}_{-16}\pm4$
1^{--}	$A\bar{A}$	4277			
1^{--}	$A\bar{A}$	4350		Y(4360)	$4361 \pm 9 \pm 9$
					4324 ± 24
2S					
1^{+}	$(S\bar{A}\pm\bar{S}A)/\sqrt{2}$	4431		Z(4430)	$4433\pm4\pm2$
0^{+}	$A\bar{A}$	4434			
1^{+}	$A\bar{A}$	4461	~ 4470		
2P					
1^{--}	$S\bar{S}$	4666		Y(4660)	$4664 \pm 11 \pm 5$
				X(4630)	4634^{+8+5}_{-7-8}

† input

few MeV above X(3872). This state could be naturally identified with the second neutral particle predicted by the tetraquark model [4]. On the other hand, in our model the lightest scalar 0^{++} tetraquark is predicted to be above the open charm threshold $D\bar{D}$ and thus to be broad, while in the model [4] it lies a few MeV below this threshold, and thus is predicted to be narrow. Our 2^{++} tetraquark also lies higher than the one in Ref.[4], thus making the interpretation of this state as Y(3943) less probable, especially if one averages the original Belle result with the recent BaBar value which is somewhat lower.

The discovery in the initial state radiation at B-factories of the Y(4260), Y(4360) and Y(4660) indicates an overpopulation of the expected charmonium 1^{--} states [1]. Maini et al. [4] argue that Y(4260) is the 1^{--} 1P state of the charm-strange diquark-antidiquark tetraquark. We find that Y(4260) cannot be interpreted in this way, since the mass of such $([cs]_{S=0}[\bar{c}\bar{s}]_{S=0})$ tetraquark is found to be ~ 200 MeV higher. A more natural tetraquark interpretation could be the 1^{--} 1P state

$([cq]_{S=0}[\bar{c}\bar{q}]_{S=0})$ $(S\bar{S})$ which mass is predicted in our model to be close to the mass of Y(4260) (see Table 1). Then the Y(4260) would decay dominantly into $D\bar{D}$ pairs. The other possible interpretations of Y(4260) are the 1^{--} 1P states of $(S\bar{A} - \bar{S}A)/\sqrt{2}$ and $A\bar{A}$ tetraquarks which predicted masses have close values. These additional tetraquark states could be responsible for the mass difference of Y(4260) observed in different decay channels. As we see from Table 1, the recently discovered resonances Y(4360) and Y(4660) in the $e^+e^- \to \pi^+\pi^-\psi'$ cross section can be interpreted as the excited 1^{--} 1P $(A\bar{A})$ and 2P $(S\bar{S})$ tetraquark states, respectively. The peak X(4630) very recently observed by Belle in $e^+e^- \to \Lambda_c^+\Lambda_c^-$ is consistent with a 1^{--} resonance Y(4660) and therefore has the same interpretation in our model.

Recently the Belle Collaboration reported the observation of a relatively narrow enhancement in the $\pi^+\psi'$ invariant mass distribution in the $B \to K\pi^+\psi'$ decay [1]. This new resonance, $Z^+(4430)$, is unique among other exotic meson candidates, since it is the first state which has a non-zero electric charge. Different theoretical interpretations were suggested [1]. Maiani et al. [4] gave qualitative arguments that the $Z^+(4430)$ could be the first radial excitation (2S) of a diquark-antidiquark $X_{u\bar{d}}^+(1^{+-}; 1S)$ state $(A\bar{A})$ with mass 3882 MeV. Our calculations indicate that the $Z^+(4430)$ can indeed be the 1^+ 2S $[cu][\bar{c}\bar{d}]$ tetraquark state. It could be the first radial excitation of the ground state $(S\bar{A} - \bar{S}A)/\sqrt{2}$, which has the same mass as X(3872). The other possible interpretation is the 0^+ 2S $[cu][\bar{c}\bar{d}]$ tetraquark state $(A\bar{A})$ which has a very close mass. Measurement of the $Z^+(4430)$ spin will discriminate between these possibilities.

Encouraged by this discovery, the Belle Collaboration performed a study of $\bar{B}^0 \to K^-\pi^+\chi_{c1}$ and observed a double peaked structure in the $\pi^+\chi_{c1}$ invariant mass distribution. These two charged hidden charm peaks, Z(4051) and Z(4248), are explicitly exotic. We find no tetraquark candidates for the former, Z(4051), structure. On the other hand, we see from Table 1 that Z(4248) can be interpreted in our model as the charged partner of the 1^- 1P state $S\bar{S}$ or as the 0^- 1P state of the $(S\bar{A} \pm \bar{S}A)/\sqrt{2}$ tetraquark.

In summary, we calculated the masses of excited heavy tetraquarks with hidden charm in the diquark-antidiquark picture. In contrast to previous phenomenological treatments, we used the dynamical approach based on the relativistic quark model. Both diquark and tetraquark masses were obtained by numerical solution of the quasipotential wave equation with the corresponding relativistic potentials. The diquark structure was taken into account in terms of diquark wave functions. It is important to emphasize that, in our analysis, we did not introduce any free adjustable parameters but used their values fixed from our previous considerations of heavy and light hadron properties. It was found that the X(3872), Z(4248), Y(4260), Y(4360), Z(4430) and Y(4660) exotic meson candidates can be tetraquark states with hidden charm.

References

1. For recent review see e.g. G. V. Pakhlova talk at 34th International Conference on High Energy Physics (ICHEP 08), July 28-August 5, Philadelphia, 2008, USA, arXiv:0810.4114 [hep-ex].
2. D. Ebert, R. N. Faustov and V. O. Galkin, Phys. Lett. B **634**, 214 (2006); D. Ebert, R. N. Faustov, V. O. Galkin and W. Lucha, Phys. Rev. D **76**, 114015 (2007).
3. D. Ebert, R. N. Faustov and V. O. Galkin, arXiv:0808.3912 [hep-ph].
4. L. Maiani *et al.*, Phys. Rev. D **71**, 014028 (2005); Phys. Rev. Lett. **99**, 182003 (2007); Phys. Rev. D **72**, 031502(R) (2005).
5. D. Ebert, R. N. Faustov and V. O. Galkin, Phys. Rev. D **72**, 034026 (2005); Phys. Lett. B **659**, 612 (2008).

$\Xi^{12}C(0^+)$ and $\Xi^{16}O$ Potentials Derived from the SU_6 Quark-Model Baryon-Baryon Interaction[⋆]

Y. Fujiwara[a], M. Kohno[b] and Y. Suzuki[c]

[a] Department of Physics, Kyoto University, Kyoto 606-8502, Japan
[b] Physics Division, Kyushu Dental College, Kitakyushu 803-8580, Japan
[c] Department of Physics, and Graduate School of Science and Technology, Niigata University, Niigata 950-2181, Japan

There exists a renewed interest in interactions between hyperons and nuclei, since rich experimental data are expected to emerge from the strangeness experiments at J-PARC. In particular, our understanding on interactions between the octet-baryons ($B_8 = N$, Λ, Σ and Ξ) and light nuclei will be significantly improved by observing possible bound states and resonances of light hypernuclei. These interactions are also important as basic constructing blocks of heavier hypernuclei through sophisticated microscopic calculations of many-cluster systems. Needless to say, these hypernucleus data afford invaluable source of information for underlying baryon-baryon interactions, since the direct scattering data for the hyperon-nucleon (YN) interaction are still scarce and none exists for the hyperon-hyperon (YY) interaction. It is therefore important to apply models for the baryon-baryon interaction to finite nuclei, and to clarify characteristics of the interaction and its implications to hypernuclear physics.

We have developed a quark-model (QM) baryon-baryon interaction for the octet-baryons [1], which reproduces all the two-nucleon data and the low-energy YN scattering data. It is formulated in the (3q)-(3q) resonating-group method (RGM), using the spin-flavor SU_6 QM wave functions. A colored version of the one-gluon exchange Fermi-Breit interaction is fully incorporated with the flavor symmetry breaking, and effective meson-exchange potentials are introduced between quarks. The early version, the model FSS [2] includes only the scalar (S) and pseudoscalar (PS) meson exchange potentials, while the renovated version fss2 [3,4] introduces also the vector (V) meson exchange potentials and the momentum-dependent Bryan-Scott terms for the S and V mesons. One of the important differences between FSS and fss2 is that the former describes the LS forces only by the Fermi-Breit interaction, while the latter also contains the ordinary LS component originating from the S-meson exchange.

As an important application of our QM baryon-baryon interactions, we have carried out Faddeev calculations for the triton and the hypertriton in Ref. [5], in the most reliable framework of using the energy-independent renormalized RGM kernels [6]. The triton binding energy, predicted by fss2, is very close to the ex-

---

[⋆] Talk delivered by Y. Fujiwara

perimental value with about 350 keV less bound, and the Λ separation energy of the hypertriton is 262 keV vs. the experimental value, 130 ± 50 keV. In the hypertriton calculation, the detailed information is obtained for the central force of the ΛN interaction, since this system is S-wave dominant.

For the p-shell Λ-hypernuclei, some kinds of models inevitably need to be assumed so far, to connect properties of the Λ-hypernuclei and the underlying YN interactions. In our previous publications, we have studied $B_8\alpha$ [7,8] and $B_8(3N)$ potentials [9] based on the G-matrix calculations of our QM hyperon-baryon interaction within the framework of the lowest-order Brueckner theory. Here, (3N) stands for the triton or ^{3}He, and rigid translational-invariant harmonic-oscillator (h.o.) shell-model wave functions are assumed with the size parameters $\nu = 0.257$ fm^{-2} for α and and 0.18 fm^{-2} for the (3N) cluster. In these calculations, we have developed a new method to derive direct and knock-on terms of the interaction Born kernel from the YN G-matrices with explicit treatments of the nonlocality and the center-of-mass (c.m.) motion between the hyperon and the α cluster. This framework makes it possible to take into account the short-range correlations and other correlations related to the channel-coupling effect of baryon channels, which is a new feature of the YN and YY interactions. For example, a strong ΛN-ΣN coupling is caused by the strong tensor component of the one-pion exchange, and the very small single-particle (s.p.) spin-orbit force of the Λ hyperon is explained by a strong cancellation of the ordinary LS and the antisymmetric LS (LS$^{(-)}$) forces generated from the rich structure of the LS components of the Fermi-Breit interaction. [10] The G-matrix calculations are carried
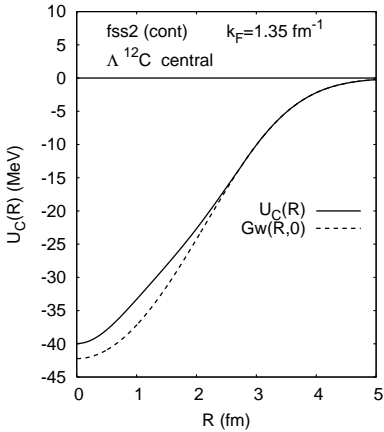
Fig.1. The zero-momentum Wigner transform (dashed curve) and the solution of the transcendental equation (solid curve) for the bound-state energy $E_B = -13.51$ MeV, obtained from the Wigner transform of $\Lambda^{12}C(0^+)$ Born kernel. The model is fss2 and $k_F = 1.35$ fm^{-1} is used.
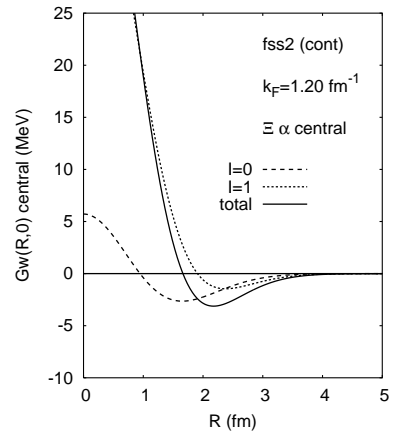
Fig.2. The central components of the zero-momentum Wigner transform for the $\Xi\alpha$ Born kernel. The contributions from the $I = 0$ and $I = 1$ components are separately shown. The model is fss2 and $k_F = 1.20$ fm^{-1} is used. The energy-independent QM RGM kernel is used.

out by assuming a constant Fermi momentum k_F, which is a parameter in the present framework. As in the Faddeev calculations of the triton and hypertriton, the energy-independent QM baryon-baryon interaction is used for the G-matrix calculation.

We extend this method to the B_8 $^{12}C(0^+)$ and B_8 ^{16}O systems, assuming the h.o. shell-model wave functions with $\nu = 0.20$ fm^{-2} for ^{12}C and 0.16 fm^{-2} for ^{16}O. Our main interest is to find new features appearing in the core nuclei involving the p-shell orbits. For the G-matrix calculation, we use $k_F = 1.35$ fm^{-1}, which corresponds to the normal saturation density.

As an example of Λ-core potentials, we show in Fig. 1 the $\Lambda^{12}C(0^+)$ potential for the $^{13}_{\Lambda}C$ ground state, calculated from the model fss2. Since the $\Lambda^{12}C(0^+)$ Born kernel, derived from the ΛN G-matrix folding is nonlocal, we have calculated the Wigner transform in the WKB-RGM approach [11]. The effective local potential is then obtained by solving the transcendental equation for the Wigner transform. Figure 1 also shows the zero-momentum Wigner transform with the dashed curve, which is already a good approximation to the effective local potential (solid curve). This potential predicts the bound-state energy $E_B = -13.51$ MeV, which is used for the input of the transcendental equation. We compare in Table 1 our QM predictions for the bound-state energies of light Λ hypernuclei with available experimental data. The bound-state energies are calculated by solving the Lippmann-Schwinger equations for the Λ-core Born kernels. The result for the hypertriton is taken from the Faddeev calculations in Ref. [5]. We find that the present G-matrix approach can give reasonable results for the Λ s.p. potentials in light nuclei, if an appropriate Fermi momentum for each system is chosen.

The Σ-core and Ξ-core interactions are generally repulsive, except for a special case like $^4_{\Sigma}He$. The origin of the repulsion in the Σ-core potential is the quark-Pauli effect which appears in the isospin $I = 3/2$ ^3S state for the most compact SU_3 (30) configuration. On the other hand, the isospin $I = 0$ channel of the ΞN interaction, the $^1S_0$ H-particle channel in particular, is attractive owing to the color-

Table 1. Comparison of the ground-state energies of some light Λ hypernuclei between the QM predictions and the experiment. The energies are measured from the Λ separation threshold. The unit is in MeV. The listed Fermi momenta k_F are used for the G-matrix calculations except for the hypertriton $^3_{\Lambda}H$.

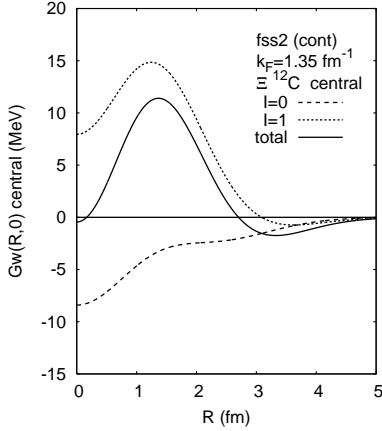| System	k_F (fm^{-1})	fss2	FSS	exp't [12]
$^3_{\Lambda}H$	Faddeev [5]	-0.262	-0.790	-0.13 ± 0.05
$^4_{\Lambda}H(0^+)$	1.07	-1.55	-2.29	-2.04 ± 0.04
$^4_{\Lambda}He(0^+)$				-2.39 ± 0.03
$^4_{\Lambda}H(1^+)$	1.07	-0.97	-0.32	-0.99 ± 0.04
$^4_{\Lambda}He(1^+)$				-1.24 ± 0.05
$^5_{\Lambda}He$	1.20	-3.43	-2.41	-3.12 ± 0.02
$^{13}_{\Lambda}C$	1.35	-13.90	-11.31	-11.69 ± 0.12
$^{17}_{\Lambda}O$	1.35	-16.04	-13.37	

Fig.3. The same as Fig 2, but for the $\Xi^{12}C(0^+)$ Born kernel. The model is fss2 and $k_F = 1.35$ fm^{-1} is used for the G-matrix calculation.
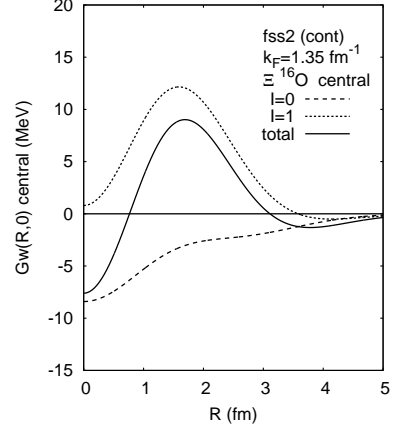
Fig.4. The same as Fig. 3, but for the $\Xi^{16}O$ zero-momentum Wigner transform.

magnetic term of the Fermi-Breit interaction. The $I = 1$ ΞN interaction is repulsive, but involves a strong channel-coupling effect with the $\Sigma\Lambda$ channel. Since the extension of the Wigner transform to the negative q^2 is not easy numerically, we only discuss the zero-momentum Wigner transform, $G_W^C(R, 0)$, which we call the "B_8-core potential" in the following. The $\Xi^{12}C(0^+)$ and $\Xi^{16}O$ potentials, obtained as the zero-momentum Wigner transform of the folding kernels for the G-matrix interaction with the Fermi momentum $k_F = 1.35$ fm^{-1}, are illustrated in Figs. 3 and 4 for fss2. We find a weak attraction in the surface area around $R \sim 3$ - 4 fm, which is a common feature to the previous $\Xi\alpha$ potential shown in Fig. 2. The present potentials, however, also possess an attractive pocket in the short-range region with $R \leq 1.2$ fm, which originates from the strong attraction in the isospin $I = 0$ component. This feature is clearly related to the p-orbit of the core nuclei. Such a structure of the nuclear potentials should appreciably influence on the Coulombic bound states for the Ξ^- atoms.

References

1. Y. Fujiwara, Y. Suzuki, and C. Nakamoto, Prog. Part. Nucl. Phys. **58** (2007), 439.
2. Y. Fujiwara, C. Nakamoto, and Y. Suzuki, Phys. Rev. Lett. **76**, 2242 (1996); Phys. Rev. C **54**, 2180 (1996).
3. Y. Fujiwara, T. Fujita, M. Kohno, C. Nakamoto, and Y. Suzuki, Phys. Rev. C **65**, 014002 (2002).
4. Y. Fujiwara, M. Kohno, C. Nakamoto, and Y. Suzuki, Phys. Rev. C **64**, 054001 (2001).
5. Y. Fujiwara, Y. Suzuki, M. Kohno, and K. Miyagawa Phys. Rev. C **77**, 027001 (2008).
6. Y. Suzuki, H. Matsumura, M. Orabi, Y. Fujiwara, P. Descouvemont, M. Theeten, and D. Baye, Phys. Lett. **B659** (2008), 160.
7. Y. Fujiwara, M. Kohno, and Y. Suzuki, Nucl. Phys. **A784** (2007), 161.

8. Y. Fujiwara, M. Kohno, and Y. Suzuki, Prog. Theor. Phys. **120** (2008), 289.

9. Y. Fujiwara, Y. Suzuki, C. Nakamoto, M. Kohno, and K. Miyagawa, *Proceedings on the IX International Conference on Hypernuclear and Strange Particle Physics* (HYP2006), edited by J. Pochodzalla and Th. Walcher, (Springer-Verlag, Berlin, Heidelberg, 2007), p. 307.

10. Y. Fujiwara, M. Kohno, and Y. Suzuki, nucl-th/0808.0628.

11. H. Horiuchi, Prog. Theor. Phys. **64** (1980), 184; K. Aoki and H. Horiuchi, Prog. Theor. Phys. **68** (1982), 1658; 2028.

12. H. Bandō, T. Motoba, and J. Žofka, Int. J. of Mod. Phys. A **5** (1990), 4021.

Gluons in Point Form QCD

W. Klink

Department of Physics and Astronomy University of Iowa, Iowa City, Iowa, USA

Abstract. Point form quantum field theory is used to analyze the QCD gluon vacuum and bound state problems. An algebra of operators formed from gluon creation and annihilation operators is used to generate a total four momentum operator from the gluon self coupling terms. The vacuum is then the Lorentz invariant state which is annihilated by the four-momentum operator. Such a state is obtained from the generalization of the coupled-cluster technique, familiar from nuclear physics. An example in which the color symmetry is SU(2) is given.

1 Point Form Quantum Field Theory

In point form field theory [1] all interactions are in the four-momentum operator and Lorentz transformations are kinematic. Interactions are introduced via vertices, products of local free fields, which are integrated over the forward hyperboloid to give the interacting four-momentum operator.

The four-momentum operator P^μ is written as the sum of free and interacting four-momentum operators, $P^\mu = P^\mu(fr) + P^\mu(I)$. To guarantee the relativistic covariance of the theory, it is required that

$$[P^\mu, P^\nu] = 0, \tag{1}$$

$$U_\Lambda P^\mu U_\Lambda^{-1} = (\Lambda^{-1})^\mu_\nu P^\nu, \tag{2}$$

where U_Λ is the unitary operator representing the Lorentz transformation Λ. These "point form" equations [1] lead to the eigenvalue problem

$$P^\mu |\Psi_p> = p^\mu |\Psi_p>, \tag{3}$$

where p^μ is the four-momentum eigenvalue and $|\Psi_p>$ the eigenvector of the four-momentum operator, which acts in generalized fermion-antifermion-boson Fock spaces. Then the physical vacuum and physical bound and scattering states should all arise as the appropriate solutions of the eigenvalue Eq.(3). What is unusual in Eq.(3) is that the momentum operator has interaction terms. But since the momentum and energy operators commute and can be simultaneously diagonalized, they have common eigenvectors. One of the important properties of the point form is that since the Lorentz generators have no interactions, the action of global Lorentz transformations on operators and states is simple.

2 Gluons

Gluons are massless vector particles that transform as representations of the little group E(2), the euclidean group in two dimensions [2]; a four dimensional nonunitary irrep of E(2) generates four polarization degrees of freedom, labeled by α. A standard four-vector $k^{st} = (1, 0, 0, 1)$ leaves E(2) invariant and the helicity boost, $B(k)$, which gives the four-momentum k, generates a gluon state with transformation properties

$$|k, \alpha, a >: = U_{B(k)}|k^{st}, \alpha, a >,$$
$$U_\Lambda|k, \alpha, a > = U_\Lambda U_{B(k)}|k^{st}, \alpha, a >$$
$$= \sum |\Lambda k, \alpha', a > \Lambda_{\alpha'\alpha}(e_W),$$
$$U_g|k, \alpha, a > = \sum |k, \alpha, a' > D_{a'a}(g),$$

where $\Lambda(e_W) = B^{-1}(\Lambda k)\Lambda B(k)$ is a euclidean Wigner "rotation", g is an element of the internal symmetry (color) group and a, a' are color indices.

Many gluon states are most simply obtained from gluon creation and annihilation operators:

$$|k, \alpha, a > = g^\dagger(k, \alpha, a)|0 >$$
$$g(k, \alpha, a)|0 > = 0, \forall k, \alpha, a$$
$$[g(k, \alpha, a), g^\dagger(k', \alpha', a')] = -g_{\alpha,\alpha'}k_0\delta^3(\mathbf{k} - \mathbf{k}')\delta_{aa'}$$
$$U_\Lambda g(k, \alpha, a)U_\Lambda^{-1} = \sum g(\Lambda k, \alpha', a)\Lambda_{\alpha,\alpha'}(e_W)$$
$$U_g g(k, \alpha, a)U_g^{-1} = \sum g(k, \alpha, a')D_{a'a}(g)$$
$$P_{free}^\mu = -\sum \int dk k^\mu g^\dagger(k, \alpha, a)g_{\alpha,\alpha}g(k, \alpha, a);$$

the auxiliary condition eliminating the 0 and 3 components is the annihilation operator condition, $\sum k_\alpha^{st} g_{\alpha\alpha}g(k, \alpha, a) = 0$. $dk := \frac{d^3k}{2k}$.

The free gluon field is then

$$G_a^\mu(x) = \int dk B^{\mu\alpha}(k)(e^{-ik\cdot x}g(k, \alpha, a) + e^{ik\cdot x}g^\dagger(k, \alpha, a));$$
$$\partial G_{\mu,a}^+(x)/\partial x_\mu = i \int dk k^\mu B_{\mu\alpha}(k)g_{\alpha,\alpha}e^{-ik\cdot x}g(k, \alpha, a)$$
$$= i \sum \int dk e^{-ik\cdot x}k_\alpha^{st} g_{\alpha\alpha}g(k, \alpha, a)$$
$$= 0;$$

this last relation shows the connection between the auxiliary condition and the Lorentz gauge condition. In fact, because Lorentz transformations are kinematic, the only gauge transformations allowed are those that leave the Lorentz gauge condition invariant.

Gauge invariance then fixes the field tensor to be

$$F_a^{\mu\nu}(x) = \frac{\partial G_a^\nu}{\partial x_\mu} - \frac{\partial G_a^\mu}{\partial x_\nu} - \alpha c_{a,b,c} G_b^\mu(x)G_c^\nu(x)$$

where $c_{a,b,c}$ are the color structure constants and α is the strong bare coupling constant.

By integrating the stress energy tensor generated by the field operators over the forward hyperboloid, the pure glue part of the four-momentum operator takes on the form

$$P^\mu_{glue} = P^\mu_{ke} + P^\mu_{tri} + P^\mu_{quar}$$

$$P^\mu_{quar} = \alpha^2 \sum \int dx^\mu dk_1 dk_2 dk_3 dk_4 c_{a,b,c} c_{a,b',c'}$$

$$B^{\mu\alpha_1}(k_1)B^{\nu\alpha_2}(k_2)B^{\alpha_3}_\mu(k_3)B^{\alpha_4}_\nu(k_4)$$

$$(e^{-ik_1 \cdot x}g(k_1,\alpha_1,b) + e^{ik_1 \cdot x}g^\dagger(k_1,\alpha_1,b))$$

$$(e^{-ik_2 \cdot x}g(k_2,\alpha_2,c) + e^{ik_2 \cdot x}g^\dagger(k_2,\alpha_2,c))$$

$$(e^{-ik_3 \cdot x}g(k_3,\alpha_3,b') + e^{ik_3 \cdot x}g^\dagger(k_3,\alpha_3,b'))$$

$$(e^{-ik_4 \cdot x}g(k_4,\alpha_4,c') + e^{ik_4 \cdot x}g^\dagger(k_4,\alpha_4,c'))$$

$$P^\mu_{tri} = i\alpha \sum c_{a,b,c} \int dx^\mu dk_1 dk_2 dk_3$$

$$(B^{\nu\alpha_1}(k_1)k^\mu_1 - B^{\mu\alpha_1}(k_1)k^\nu_1)B^{\alpha_2}_\mu(k_2)B^{\alpha_3}_\nu(k_3)$$

$$(e^{-ik_1 \cdot x}g(k_1,\alpha_1,a) - e^{ik_1 \cdot x}g^\dagger(k_1,\alpha_1,b))$$

$$(e^{-ik_2 \cdot x}g(k_2,\alpha_2,b) + e^{ik_2 \cdot x}g^\dagger(k_2,\alpha_2,b))$$

$$(e^{-ik_3 \cdot x}g(k_3\alpha_3,c) + e^{ik_3 \cdot x}g^\dagger(k_3,\alpha_3,c))$$

$$P^\mu_{ke} = -\sum \int dk k^\mu g^\dagger(k,\alpha,a)g_{\alpha\alpha}g(k,\alpha,a)$$

3   The Gluon Vacuum Equations

Neglecting the quark sector, the gluon vacuum structure can be analyzed by writing the vacuum as $|\Omega> = F|0>$ so that $P^\mu_{glue}|\Omega> = P^\mu_{glue}F|0> = 0$. Since there are no quarks, the operator F will act only in the gluon space; it must satisfy the properties of being invariant under Lorentz and color transformations. So write

$$F = f_0 I + \sum \int dk_1 dk_2 f_{k_1,\beta_1,a-1;k_2\beta_2,a_2}$$

$$g^\dagger(k_1,\beta_1,a_1)g^\dagger(k_2,\beta_2,a_2) + ...$$

$$f_{k_1,\beta_1,a_1;k_2,\beta_2,a_2} = f_2((k_1+k_2)^2)B^{\mu\beta_1}(k_1)B^{\beta_2}_\mu(k_2)C^1_{1,a_1,a_2}$$

where $f_2((k_1+k_2)^2)$ is a Lorentz invariant function and C^1_{1,a_1,a_2} is a Clebsch-Gordan coefficient coupling the adjoint representation to itself to give the identity representation. There are no odd powers of gluon creation operators because of invariance under the internal symmetry. When quarks are coupled to the gluon sector, this will no longer be the case.

As an example of the structure of the gluon vacuum equations, choose SU(2) as the internal symmetry. The tri interactions do not contribute when acting on F; the general form of the equations arising from the quartic interactions are

$$(\alpha^2 \int dx^\mu (e^{-ik \cdot x}g + e^{ik \cdot x}g^\dagger)^4 - \int dv v^\mu g^\dagger g)F|0> = 0.$$

The lowest order equation resulting from these equations is

$$\alpha^2 \int dx^\mu [\int dk_1 dk_2 f_0 - 4 \int dk_1 dk_2 dk_3 f_2(k_2 + k_3)e^{-i(k_2+k_3)\cdot x}$$

$$+8 \int dk_1 dk_2 dk_3 dk_4 f_4(k_1 + k_2, k_3 + k_4)e^{-i(k_1+k_2+k_3+k_4)\cdot x}] = 0;$$

where the f's are Lorentz invariant functions of their arguments. More generally there is a hierarchy of equations in even powers of the gluon creation operators. By factoring out the infinite Lorentz volume at each level of the hierarchy, a set of recursive equations results, which have no infinities.

4 Glueballs

The simplest glueballs are bound states of two gluons, bound by their self interactions [3]. A two gluon state can be written as $|v, |\mathbf{k}|, j, \sigma, \lambda_1, \lambda_2 >$, where

$$|v, |\mathbf{k}|, j, \sigma\lambda_1\lambda_2 > = \int dR \sum C^1_{1,a_1 a_2} D^j_{\sigma, \lambda_1 - \lambda_2}(R)\, U_{B(v)} U_R$$

$$g^\dagger(k_1\alpha_1 a_1)g^\dagger(k_2\alpha_2 a_2)F|0>,$$

with $\mathbf{k}_1 = -\mathbf{k}_2 = \mathbf{k}$, $C^1_{1,a_1 a_2}$ a color Clebsch Gordan coefficient, and R a rotation.

Again a set of (bound state) equations in powers of the gluon creation operators results, generated from

$$(P^\mu - \lambda^\mu_v)|v, k, j, \sigma\lambda_1\lambda_2 > = 0.$$

Setting $j = \sigma = 0$ gives a scalar glueball.

References

1. E. P. Biernat, et al, Ann. Phys. 323 (2008) 1361.
2. This formalism is worked out in W. H. Klink, Nucl. Phys. A716 (2003) 158.
3. Potential models for glueballs can be found in V. Mathieu, et al, Phys. Rev. D 77 (2008)114022 and references cited therein.

Testing the usage of a generalization of the Witten-Veneziano relation in a bound-state approach to η and η′ mesons[*]

D. Horvatić[a], D. Blaschke[b,c,d], Yu. Kalinovsky[e], D. Kekez[f], D. Klabučar[g,h]

[a] Physics Department, Faculty of Science, University of Zagreb, Bijenička c. 32, 10000 Zagreb, Croatia

[b] Institute for Theoretical Physics, University of Wroclaw, Max Born pl. 9, 50-204 Wroclaw, Poland

[c] Bogoliubov Laboratory of Theoretical Physics, Joint Institute for Nuclear Research, 141980 Dubna, Russia

[d] Institute of Physics, University of Rostock, D-18051 Rostock, Germany

[e] Laboratory for Information Technologies, Joint Institute for Nuclear Research, 141980 Dubna, Russia

[f] Rudjer Bošković Institute, P.O.B. 180, 10002 Zagreb, Croatia

[g] Physics Department, Faculty of Science, University of Zagreb, Bijenička c. 32, 10000 Zagreb, Croatia

[h] Senior Associate of Abdus Salam ICTP, Trieste, Italy

Abstract. The results of the Dyson-Schwinger approach utilizing the Witten-Veneziano relation to obtain a description of the η and η′ mesons, are compared with the results obtained when Shore's generalization of the Witten-Veneziano relation is used instead. On the examples of three different model interactions, we find that irrespective of the concrete model dynamics, our Dyson-Schwinger approach is phenomenologically more successful in conjunction with the standard Witten-Veneziano relation than with the generalization valid, at least in principle, in all orders in the $1/N_c$ expansion.

1 Introduction

The complex of the η and η′ pseudoscalar mesons is an intriguing problem in the light-quark sector of the nonperturbative Quantum Chromodynamics (QCD). The mixing of the pertinent isospin-zero states should be such that the physical η meson is one of the (almost-)Goldstone bosons of the dynamical chiral symmetry breaking (DChSB) of QCD, whereas its partner η′ must be very massive (∼ 1 GeV) and remain such even in the chiral limit. For the correct η′ mass behavior, the non-abelian (gluon) axial anomaly of QCD is essential, and a way to extract its contribution is through the Witten-Veneziano (WV) relation [1,2].

We are particularly interested in the Dyson-Schwinger (DS) approach [3–8] to QCD and its modeling. In some variants of the DS approach (e.g., in Ref. [9]), the

---

[*] Talk delivered by D. Klabučar

WV relation has been used to obtain the description of the η-η′ complex. In the present paper, for three different DS models, we compare the usage of the WV relation with the usage of its recent generalization recently proposed by Shore [10,11]. The present paper in the Bled 2008 proceedings, is a shortened version of Ref. [12].

The DS approach [3–8] is the chirally well-behaved bound-state approach and thus the most suitable one to treat the light pseudoscalar mesons (those composed of the u, d and s quarks), for which DChSB is essential. One solves the DS equations (DSEs) for dressed quark propagators, which are then employed in Bethe-Salpeter equations (BSEs). Their solving yields quark-antiquark ($q\bar{q}′$) bound state amplitudes and corresponding masses $M_{q\bar{q}′}$.

To obtain the chiral behavior as in QCD, DS and BS equations must be solved in a consistent approximation. The rainbow-ladder approximation (RLA), where DChSB is well-understood, is still the most usual approximation in phenomenological applications. This also entails that in both DSE and BSE we employ the same effective interaction. Concretely, in the present paper we recall and utilize the results obtained *i)* in Refs. [13,14] by using the renormalization-group improved (RGI) interaction of Jain and Munczek [15], *ii)* in Ref. [9] by using the RGI gluon condensate-induced interaction [16], and *iii)* in Refs. [17,18] by using the separable interaction [19]. Such effective interactions must be modeled at least in the low-energy, nonperturbative regime in order to be phenomenologically successful – which above all means to be sufficiently strong in the low-momentum domain to yield DChSB. In the chiral limit (and *close* to it), light pseudoscalar (P) meson $q\bar{q}$ bound states (P $= \pi^{0,\pm}, K^{0,\pm}, \eta$) then simultaneously manifest themselves also as (*quasi-*)Goldstone bosons of DChSB. This enables one to work with the mesons as explicit $q\bar{q}$ bound states, while reproducing the results of the Abelian axial anomaly for the light pseudoscalars, i.e., the amplitudes for P $\to \gamma\gamma$ and $\gamma^\star \to P^0P^+P^-$. This is unique among the bound state approaches – e.g., see Refs. [5,20,22,21] and references therein. Nevertheless, one keeps the advantage of bound-state approaches that from the $q\bar{q}$ substructure one can calculate many important quantities (such as the pion, kaon and $s\bar{s}$ pseudoscalar decay constants: f_π, f_K and $f_{s\bar{s}}$) which are just parameters in most of other chiral approaches to the light-quark sector. The treatment [13,14,23,9] of the η-η′ complex is remarkable in that it is very successful in spite of the limitations of RLA. (Very recently, during the work on the present paper, the first and still simplified DS treatments of η and η′ beyond RLA appeared [24,25]. However, RLA treatments will probably long retain their usefulness in applications where simple modeling is desirable, as in the calculationally demanding finite-temperature calculations [18].) The RLA treatments [13,14,23,9,18] of the η-η′ complex relied on the Witten-Veneziano (WV) relation [1,2]. Nevertheless, Shore achieved [10,11] what can be considered as a generalization of the WV relation, and the purpose of the present paper is exploring the usage of this generalization in the DS context.

The paper is organized as follows: in the next section, we recapitulate the procedures and results of our previous treatments [14,9,18] relying on the WV relation (11), and present in Table I also their extension to the scheme of the four decay constants (and two mixing angles) of η and η′. In Section 3, we expose the

usage of the pertinent Shore's equations [10,11] in the context of DS approach. The last section concludes after giving the results of solving the pertinent equations.

2   η-η′ mass matrix from Witten-Veneziano relation

All $q\bar{q}'$ model masses $M_{q\bar{q}'}$ (q, q′ = u, d, s) used in the present paper, and corresponding $q\bar{q}'$ bound-state amplitudes, were obtained in Refs. [13,14,9,26,17,18] in RLA, i.e., with an interaction kernel which (irrespective of how one models the dynamics) cannot possibly capture the effects of the non-Abelian, gluon axial anomaly. Thus, when we form the η-η′ mass matrix

$$\hat{M}_{NA}^2 = \begin{bmatrix} M_{88}^2 & M_{80}^2 \\ M_{08}^2 & M_{00}^2 \end{bmatrix}, \tag{1}$$

in this case in the octet-singlet basis η_8-η_0 of the (broken) flavor-SU(3) states of isospin zero,

$$\eta_8 = \frac{1}{\sqrt{6}}(u\bar{u} + d\bar{d} - 2s\bar{s}), \qquad \eta_0 = \frac{1}{\sqrt{3}}(u\bar{u} + d\bar{d} + s\bar{s}), \tag{2}$$

this matrix (1), consisting of our calculated $q\bar{q}$ masses,

$$M_{88}^2 \equiv \langle\eta_8|\hat{M}_{NA}^2|\eta_8\rangle = \frac{2}{3}\left(M_{s\bar{s}}^2 + \frac{1}{2}M_{u\bar{u}}^2\right), \tag{3}$$

$$M_{00}^2 \equiv \langle\eta_0|\hat{M}_{NA}^2|\eta_0\rangle = \frac{2}{3}\left(\frac{1}{2}M_{s\bar{s}}^2 + M_{u\bar{u}}^2\right), \tag{4}$$

$$M_{80}^2 \equiv \langle\eta_8|\hat{M}_{NA}^2|\eta_0\rangle = M_{08}^2 = \frac{\sqrt{2}}{3}(M_{u\bar{u}}^2 - M_{s\bar{s}}^2) < 0, \tag{5}$$

is purely non-anomalous (NA), vanishing in the chiral limit. In the isospin limit, to which we adhere throughout, the pion is strictly decoupled from the gluon anomaly and $M_{u\bar{u}} = M_{d\bar{d}}$ is exactly our model pion mass M_π. Also the unphysical $s\bar{s}$ quasi-Goldstone's mass $M_{s\bar{s}}$ results from RLA BSE and does not include the contribution from the gluon anomaly. This is consistent with the fact that due to the Dashen-Gell-Mann-Oakes-Renner (DGMOR) relation, it is in a good approximation [13,14,9,18] given by $M_{s\bar{s}}^2 = 2M_K^2 - M_\pi^2$, i.e., by the kaon and pion masses protected from the anomaly by strangeness and/or isospin.

In our previous DS studies [13,14,9,26,17,18], to which we refer for all model details, the phenomenology of the non-anomalous sector was successfully reproduced, e.g., f_π, f_K, as well as the empirical masses M_π and M_K (see the upper part of Table 1), yielding a strongly non-diagonal $\hat{M}_{NA}^2$ (1). Its diagonalization leads to the eigenstates known as the nonstrange-strange (NS-S) basis,

$$\eta_{NS} = \frac{1}{\sqrt{2}}(u\bar{u} + d\bar{d}), \qquad \eta_S = s\bar{s}, \tag{6}$$

and to $\hat{M}_{NA}^2 = \text{diag}[M_\pi^2, M_{s\bar{s}}^2]$. In contrast to these mass-squared eigenvalues, the experimental masses are such that $(M_\pi^2)_{exp}\lambda^2(M_\eta^2)_{exp}$, and η′ is too heavy,

$(M_{\eta'})_{exp} = 958$ MeV, to be considered even as the $s\bar{s}$ quasi-Goldstone boson. This is the well-known $U_A(1)$ problem, resolved by the fact that the *complete* η-η' mass matrix $\hat{M}^2$ must contain the anomalous (A) part $\hat{M}_A^2$. That is, $\hat{M}^2 = \hat{M}_{NA}^2 + \hat{M}_A^2$.

However, $\hat{M}_A^2$ is inaccessible to RLA which yields our Goldstone pseudo-scalars. In Refs. [13,14,9,17,18], $\hat{M}_A^2$ was extracted from lattice data through the WV relation [the second equality in Eq. (11)]. The main purpose of the present paper, instead, is to approach η and η' through Shore's [10,11] recent generalization of that relation.

Before that, nevertheless, we review the usage of the WV relation in Refs. [13,14,9,17,18]. The expansion in the large number of colors, N_c, indicates that the leading approximation in that expansion describes the bulk of main features of QCD. The gluon anomaly is suppressed as $1/N_c$ and can be viewed as a perturbation in the large N_c expansion. In the SU(3) limit, it is coupled *only* to the singlet combination η_0 (2); only the η_0 mass receives, from the gluon anomaly, a contribution which, unlike quasi-Goldstone masses $M_{q\bar{q}'}$'s comprising $\hat{M}_{NA}^2$, does *not* vanish in the chiral limit. As discussed in Refs. [13,9], in the present bound-state context it is thus meaningful to include the effect of the gluon anomaly just on the level of a mass shift for the η_0 as the lowest-order effect, and retain the $q\bar{q}$ bound-state amplitudes and the corresponding mass eigenvalues $M_{q\bar{q}}$ as calculated by solving DSEs and BSEs with kernels in RLA.

References [13,14,9,17,18] thus break the $U_A(1)$ symmetry, and avoid the $U_A(1)$ problem, by shifting the η_0 (squared) mass by an amount denoted by 3β (in the notation of Refs. [14,9]). The complete mass matrix $\hat{M}^2 = \hat{M}_{NA}^2 + \hat{M}_A^2$ then contains the anomalous part $\hat{M}_A^2 = \text{diag}[0, 3\beta]$, where the anomalous η_0 mass shift 3β is related to the topological susceptibility of the vacuum, but in the present approach must be treated as a parameter to be determined outside of our RLA model, i.e., fixed by phenomenology or taken from the lattice calculations [27]. (The possibility of employing an additional microscopic model for the gluon anomaly contribution, such as the one of Ref. [28], is presently not considered.)

The SU(3) flavor symmetry breaking and its interplay with the gluon anomaly [9] modifies $\hat{M}_A^2 = \text{diag}[0, 3\beta]$ to

$$\hat{M}_A^2 = \beta \begin{bmatrix} \frac{2}{3}(1-X)^2 & \frac{\sqrt{2}}{3}(1-X)(2+X) \\ \frac{\sqrt{2}}{3}(1-X)(2+X) & \frac{1}{3}(2+X)^2 \end{bmatrix} , \qquad (7)$$

where X is the flavor symmetry breaking parameter. It is most often estimated as $X = f_\pi/f_{s\bar{s}} \sim 0.7 - 0.8$ (see, e.g., Refs. [30,29,14,9], although there are some other [14], of course related, estimates of X). Presently we also adopt $X = f_\pi/f_{s\bar{s}}$, which means that X is a calculated quantity in our approach. The employed models achieved good agreement with phenomenology [13,14,9,18], e.g., fitted the experimental value of $M_\eta^2 + M_{\eta'}^2$, for β around $0.26 - 0.28$ GeV^2. The anomaly contribution $\hat{M}_A^2$ then brings the complete M^2 rather close to a diagonal form for all considered models [13,14,9,18]; that is, to diagonalize M^2, only a relatively small rotation ($|\theta| \sim 13° \pm 2°$) of the η_8-η_0 basis states,

$$\eta = \cos\theta\,\eta_8 - \sin\theta\,\eta_0 , \qquad\qquad \eta' = \sin\theta\,\eta_8 + \cos\theta\,\eta_0 , \qquad (8)$$

is needed to align them with the mass eigenstates, i.e., with the physical η and η'. In contrast to this, the η-η' mass matrix in the NS-S basis (6),

$$\hat{M}^2 = \begin{bmatrix} M^2_{\eta_{NS}} & M^2_{\eta_S\eta_{NS}} \\ M^2_{\eta_{NS}\eta_S} & M^2_{\eta_S} \end{bmatrix} = \begin{bmatrix} M^2_\pi + 2\beta & \sqrt{2}\beta X \\ \sqrt{2}\beta X & M^2_{s\bar{s}} + \beta X^2 \end{bmatrix} \xrightarrow{\phi} \begin{bmatrix} M^2_\eta & 0 \\ 0 & M^2_{\eta'} \end{bmatrix} \quad (9)$$

is then strongly off-diagonal. The indicated diagonalization, given by

$$\eta = \cos\phi\,\eta_{NS} - \sin\phi\,\eta_S , \qquad \eta' = \sin\phi\,\eta_{NS} + \cos\phi\,\eta_S , \quad (10)$$

is thus achieved for a large NS-S state-mixing angle $\phi \sim 42° \pm 2°$. Of course, this is again in agreement with phenomenological requirements [14,9], since ϕ is fixed to the angle θ by the relation $\phi = \theta + \arctan\sqrt{2} = \theta + 54.74°$.

The invariant trace of the mass matrix (9), together with $M^2_{s\bar{s}} = 2M^2_K - M^2_\pi$ (from the DGMOR relation), gives the first equality in

$$\beta\,(2 + X^2) = M^2_\eta + M^2_{\eta'} - 2M^2_K = \frac{6}{f^2_\pi}\,\chi_{YM} . \quad (11)$$

The second equality is the Witten-Veneziano (WV) relation [1,2] between the η, η' and kaon masses and χ_{YM}, the topological susceptibility of the pure gauge, Yang-Mills theory. Thus, β does not need to be a free parameter, but can be determined from lattice results on χ_{YM}, so that no fitting parameters are introduced. For the three models [15,16,19] utilized in our treatments [13,14,9,18] of η and η', the bare quark mass parameters and the interaction parameters were fixed already in the non-anomalous sector, by requiring the good pion and kaon phenomenology. (See the π and K masses and decay constants in Table 1.) Then, following Refs. [9,18] in adopting the central value of the weighted average of the recent lattice results on Yang-Mills topological susceptibility [31–33],

$$\chi_{YM} = (175.7 \pm 1.5\,\text{MeV})^4 , \quad (12)$$

we have obtained the good descriptions of the η-η' phenomenology [13,14,9,18], exemplified by the first three columns (one for each DS models used) of the middle part of Table 1, giving the predictions for the η and η' masses and for the NS-S mixing angle ϕ.

The lowest part of the table, below the second horizontal dividing line, contains the results on the quantities (θ_0, θ_8, etc.) defined in the scheme with four η and η' decay constants and two mixing angles, introduced and explained in the following Section 3. Table 1 also compares these results of ours (in the first three columns) with the corresponding results of Shore's approach [10,11], in which the *experimental* values of the meson masses M_π, M_K, M_η, and $M_{\eta'}$, as well as the decay constants f_π and f_K (in contrast to our $q\bar{q}$ bound-state model predictions for these quantities) are used as inputs enabling the calculation of various decay constants in the η-η' complex and the two mixing angles θ_0 and θ_8 (corresponding to $\phi = 38.24°$ in our approach).

3 Usage of Shore's equations in DS approach

The WV relation was derived in the lowest-order approximation in the large N_c expansion. However, considerations by Shore [10,11] contain what amounts to

from Ref.	[14] & WV	[9] & WV	[18] & WV	Shore [10,11]	Experiment
M_π	137.3	135.0	140.0		$(138.0)^{\text{isospin}}_{\text{average}}$
M_K	495.7	494.9	495.0		$(495.7)^{\text{isospin}}_{\text{average}}$
$M_{s\bar{s}}$	700.7	722.1	684.8		
f_π	93.1	92.9	92.0		92.4 ± 0.3
f_K	113.4	111.5	110.1		113.0 ± 1.0
$f_{s\bar{s}}$	135.0	132.9	119.1		
M_η	568.2	577.1	542.3		547.75 ± 0.12
$M_{\eta'}$	920.4	932.0	932.6		957.78 ± 0.14
ϕ	$41.42°$	$39.56°$	$40.75°$	$(38.24°)$	
θ_0	$-2.86°$	$-5.12°$	$-6.80°$	$-12.3°$	
θ_8	$-22.59°$	$-24.14°$	$-20.58°$	$-20.1°$	
f_0	108.8	107.9	101.8	106.6	
f_8	122.6	121.1	110.7	104.8	
f_η^0	5.4	9.6	12.1	22.8	
$f_{\eta'}^0$	108.7	107.5	101.1	104.2	
f_η^8	113.2	110.5	103.7	98.4	
$f_{\eta'}^8$	-47.1	-49.5	-38.9	-37.6	

Table 1. The results of employing the WV relation (11) in our DS approach for the three dynamical models used in Refs. [14,9,18], compared with the results of Shore's analysis [10,11] and with the experimental results. The first column was obtained by the WV-recalculation of the results of Ref. [14], which in turn used the Jain-Munczek *Ansatz* for the gluon propagator [15]. Column 2: the results based on Ref. [9], which used the OPE-inspired, gluon-condensate-enhanced gluon propagator [16]. Column 3: the results based on Ref. [18], which utilized the separable *Ansatz* for the dressed gluon propagator [19]. Column 4: The results of Shore [10,11], who used the lattice result $\chi_{\text{YM}} = (191\,\text{MeV})^4$ of Ref. [32], and not the weighted average (12), in contrast to us. Column 5: the experimental values. All masses and decay constants are in MeV, and angles are in degrees. For more details, see text.

the generalization of the WV relation, which is valid to all orders in $1/N_c$. Among the relations he derived through the inclusion of the gluon anomaly in DGMOR relations, the following are pertinent for the present paper:

$$(f_{\eta'}^0)^2 M_{\eta'}^2 + (f_\eta^0)^2 M_\eta^2 = \frac{1}{3}\left(f_\pi^2 M_\pi^2 + 2f_K^2 M_K^2\right) + 6A\,, \qquad (13)$$

$$f_{\eta'}^0 f_{\eta'}^8 M_{\eta'}^2 + f_\eta^0 f_\eta^8 M_\eta^2 = \frac{2\sqrt{2}}{3}\left(f_\pi^2 M_\pi^2 - f_K^2 M_K^2\right)\,, \qquad (14)$$

$$(f_{\eta'}^8)^2 M_{\eta'}^2 + (f_\eta^8)^2 M_\eta^2 = -\frac{1}{3}\left(f_\pi^2 M_\pi^2 - 4f_K^2 M_K^2\right)\,, \qquad (15)$$

where A is the full QCD topological charge parameter, which is presently unknown, but in the large N_c limit, it reduces to YM topological susceptibility: $A = \chi_{\text{YM}} + \mathcal{O}(1/N_c)$. Besides f_π, they contain f_K and the *four* decay constants [34–36], $f_{\eta'}^0, f_\eta^8, f_\eta^0$, and $f_{\eta'}^8$, associated with the two pseudoscalars η and η'.

Adding Eqs. (13) and (15), one gets the relation

$$(f_{\eta'}^0)^2 M_{\eta'}^2 + (f_\eta^0)^2 M_\eta^2 + (f_\eta^8)^2 M_\eta^2 + (f_{\eta'}^8)^2 M_{\eta'}^2 - 2f_K^2 M_K^2 = 6A \qquad (16)$$

which is the analogue of the standard WV formula (11), to which it reduces in the large N_c limit where $A \to \chi_{YM}$, the $f_{\eta'}^0, f_\eta^8, f_K \to f_\pi$ limit, and the limit of vanishing subdominant decay constants (since η and η' are dominantly η_8 and η_0, respectively), i.e., $f_\eta^0, f_{\eta'}^8 \to 0$. Nevertheless, we will need to use not just this single equation, but the three equations (13)-(15) from Shore's generalization.

These four η and η' decay constants are often parameterized in terms of two decay constants, f_8 and f_0, and two mixing angles, θ_8 and θ_0:

$$f_\eta^8 = \cos\theta_8 \, f_8 \,, \qquad f_\eta^0 = -\sin\theta_0 \, f_0 \,, \qquad f_{\eta'}^8 = \sin\theta_8 \, f_8 \,, \qquad f_{\eta'}^0 = \cos\theta_0 \, f_0 \,. \quad (17)$$

This is the so-called two-angle mixing scheme, which shows explicitly that it is inconsistent to assume that the mixing of the decay constants follows the pattern (8) of the mixing of the states η_8 and η_0 [34–36,30,37,29].

The advantage of our model is that, as we shall see, we are able to calculate the f_8 and f_0 parts of the physical decay constants (17) from the $q\bar{q}$ substructure. However, we cannot keep the full generality of Shore's approach, which allows for the mixing with the gluonic pseudoscalar operators, and therefore employs the definition [10,11] of the decay constants which, in general, due to the gluonic contribution, differs from the following standard definition through the matrix elements of the axial currents $A^{a\,\mu}(x)$:

$$\langle 0|A^{a\,\mu}(x)|P(p)\rangle = i f_P^a \, p^\mu e^{-ip\cdot x}, \qquad a = 8, 0; \qquad P = \eta, \eta' \,. \quad (18)$$

Nevertheless, Shore's definition [10,11] coincides with the above standard one in the non-singlet channel, where there cannot be any admixture of the pseudoscalar gluonic component. Similarly, since our BS solutions (from Refs. [13,14,9,18]) are the pure $q\bar{q}$ states, without any gluonic components, using Shore's definition would not help us calculate the gluon anomaly influence on the decay constants. We thus employ the standard definitions (18), also used by, e.g., Gasser, Leutwyler, and Kaiser [34–36], as well as by Feldmann, Kroll, and Stech (FKS) [30,37,29].

Equivalently to $f_{\eta'}^0, f_\eta^8, f_\eta^0$, and $f_{\eta'}^8$, defined by Eq. (18), one has four related but different constants $f_{\eta'}^{NS}, f_\eta^{NS}, f_{\eta'}^S$, and $f_{\eta'}^S$, if instead of octet and singlet axial currents ($a = 8, 0$) in Eq. (18) one uses the nonstrange-strange axial currents ($a = $ NS, S)

$$A_{NS}^\mu(x) = \frac{1}{\sqrt{3}} A^{8\,\mu}(x) + \sqrt{\frac{2}{3}} A^{0\,\mu}(x) = \frac{1}{2}\left[\bar{u}(x)\gamma^\mu\gamma_5 u(x) + \bar{d}(x)\gamma^\mu\gamma_5 d(x)\right], \quad (19)$$

$$A_S^\mu(x) = -\sqrt{\frac{2}{3}} A^{8\,\mu}(x) + \frac{1}{\sqrt{3}} A^{0\,\mu}(x) = \frac{1}{\sqrt{2}}\bar{s}(x)\gamma^\mu\gamma_5 s(x) \,. \quad (20)$$

The relation between the two equivalent sets is thus

$$\begin{bmatrix} f_\eta^{NS} & f_\eta^S \\ f_{\eta'}^{NS} & f_{\eta'}^S \end{bmatrix} = \begin{bmatrix} f_\eta^8 & f_\eta^0 \\ f_{\eta'}^8 & f_{\eta'}^0 \end{bmatrix} \begin{bmatrix} \frac{1}{\sqrt{3}} & -\sqrt{\frac{2}{3}} \\ \sqrt{\frac{2}{3}} & \frac{1}{\sqrt{3}} \end{bmatrix} \,. \quad (21)$$

Of course, this other quartet of η and η' decay constants can also be parameterized in terms of other two constants and two other mixing angles:

$$f_\eta^{NS} = \cos\phi_{NS}\, f_{NS}\,,\quad f_\eta^S = -\sin\phi_S\, f_S\,,\quad f_{\eta'}^{NS} = \sin\phi_{NS}\, f_{NS}\,,\quad f_{\eta'}^S = \cos\phi_S\, f_S\,,$$
$$(22)$$

where f_{NS} and f_S are given by the matrix elements

$$\langle 0|A_{NS}^\mu(x)|\eta_{NS}(p)\rangle = i f_{NS}\, p^\mu e^{-ip\cdot x}\,,\qquad \langle 0|A_S^\mu(x)|\eta_S(p)\rangle = i f_S\, p^\mu e^{-ip\cdot x}\,,\quad (23)$$

while $\langle 0|A_{NS}^\mu(x)|\eta_S(p)\rangle = 0$ and $\langle 0|A_S^\mu(x)|\eta_{NS}(p)\rangle = 0$.

In the NS-S basis, it is possible to recover a scheme with a single mixing angle ϕ through the application of the Okubo-Zweig-Iizuka (OZI) rule [30,37,29]. For example, $f_{NS} f_S \sin(\phi_{NS} - \phi_S)$ differs from zero just by an OZI-suppressed term [29]. Neglecting this term thus implies $\phi_{NS} = \phi_S$. (Refs. [30,37,29] denote $f_{NS}, f_S, \phi_{NS}, \phi_S$ by, respectively, f_q, f_s, ϕ_q, ϕ_s.) In general, neglecting the OZI-suppressed terms, i.e., application of the OZI rule, leads to the so-called FKS scheme [30,37,29], which exploits a big practical difference between the (in principle equivalent) parameterizations (17) and (22): while θ_8 and θ_0 differ a lot from each other and from the octet-singlet *state* mixing angle $\theta \approx (\theta_8 + \theta_0)/2$, the NS-S decay-constant mixing angles are very close to each other and both can be approximated by the state mixing angle: $\phi_{NS} \approx \phi_S \approx \phi$. Therefore one can deal with only this one angle, ϕ, and express the physical η-η' decay constants as

$$\begin{bmatrix} f_\eta^8 & f_\eta^0 \\ f_{\eta'}^8 & f_{\eta'}^0 \end{bmatrix} = \begin{bmatrix} f_{NS}\cos\phi & -f_S\sin\phi \\ f_{NS}\sin\phi & f_S\cos\phi \end{bmatrix} \begin{bmatrix} \frac{1}{\sqrt{3}} & \sqrt{\frac{2}{3}} \\ -\sqrt{\frac{2}{3}} & \frac{1}{\sqrt{3}} \end{bmatrix}. \qquad (24)$$

This relation is valid also in our approach, where η and η' are the simple η_{NS}-η_S mixtures (10). In our present DS approach, mesons are pure $q\bar{q}$ BS solutions, without any gluonium admixtures, which are prominent possible sources of OZI violations. Therefore, our decay constants are calculated quantities, $f_{NS} = f_{u\bar{u}} = f_{d\bar{d}} = f_\pi$ and $f_S = f_{s\bar{s}}$, in agreement with the OZI rule. Our DS approach is thus naturally compatible with the FKS scheme, and we can use the η and η' decay constants (24) with our calculated $f_{NS} = f_\pi$ and $f_S = f_{s\bar{s}}$ in Shore's equations (13)-(15).

4   Results and conclusions

All quantities appearing on the right-hand side of Eqs. (13)-(15), namely M_π, M_K, f_π, and f_K, are calculated in our DS approach [14,9,18] (for the three dynamical models [15,16,19]), *except* the full QCD topological charge parameter A. Since it is at present unfortunately not yet known, we follow Shore and approximate it by the Yang-Mills topological susceptibility χ_{YM}.

On the left-hand side of Eqs. (13)-(15), the model results for $f_{NS} = f_\pi$ and $f_S = f_{s\bar{s}}$ and Eq. (24) reduce the unknown part of the four η and η' decay constants f_η^0, $f_{\eta'}^0$, f_η^8, and $f_{\eta'}^8$, down to the mixing angle ϕ. The three Shore's equations (13)-(15) can then be solved for ϕ, M_η and $M_{\eta'}$, providing us with the upper three lines

Inputs:	from Ref. [14]		from Ref. [9]		from Ref. [18]	
$\chi_{YM}^{1/4}$	175.7	191	175.7	191	175.7	191
M_η	485.7	499.8	482.8	496.7	507.0	526.2
$M_{\eta'}$	815.8	931.4	818.4	934.9	868.7	983.2
ϕ	46.11°	52.01°	46.07°	51.85°	40.86°	47.23°
θ_0	1.84°	7.74°	1.39°	7.17°	−6.69°	−0.33°
θ_8	−17.90°	−12.00°	−17.6°	−11.85°	−20.47°	−14.11°
f_0	108.8	108.8	107.9	107.9	101.8	101.8
f_8	122.6	122.6	121.1	121.1	110.7	110.7
f_η^0	-3.5	-14.7	-2.6	-13.5	11.9	0.6
$f_{\eta'}^0$	108.8	107.9	107.9	107.1	101.1	101.8
f_η^8	116.7	119.9	115.4	118.5	103.7	107.4
$f_{\eta'}^8$	-37.7	-25.5	-37.6	-24.9	-38.7	-27.0

Table 2. The results of the three DS models obtained through Shore's equations (13)-(15) for the two values of χ_{YM} approximating A: $(175.7\,\text{MeV})^4$ and $(191\text{MeV})^4$. Columns 1 and 2: The results when the non-anomalous inputs for Eqs. (13)-(15), namely $M_\pi, M_K, f_\pi = f_{NS}, f_{s\bar{s}} = f_S$ and f_K, are taken from Ref. [14], which uses Jain–Munczek *Ansatz* interaction [15]. Columns 3 and 4: The results for the non-anomalous inputs from Ref. [9] using OPE-inspired interaction nonperturbatively dressed by gluon condensates [16]. Columns 5 and 6: The results for the inputs from Ref. [18] using the separable *Ansatz* interaction [19]. All masses and decay constants, as well as $\chi_{YM}^{1/4}$, are in MeV, and angles are in degrees.

of Table 2. For each of the three different dynamical models which we used in our previous DS studies [13,14,9,26,17,18], these results are displayed for $\chi_{YM} = (175.7\,\text{MeV})^4$ as in Refs. [9,18] and for $\chi_{YM} = (191\,\text{MeV})^4$ [32] (adopted by Shore [10,11]). The lower part of the table, displaying various additional results, is then readily obtained through Eq. (24) and/or the following useful relations [29,14]:

$$f_8 = \sqrt{\frac{1}{3}f_{NS}^2 + \frac{2}{3}f_S^2}\,, \quad \theta_8 = \phi - \arctan\left(\frac{\sqrt{2}f_S}{f_{NS}}\right)\,, \qquad (25)$$

$$f_0 = \sqrt{\frac{2}{3}f_{NS}^2 + \frac{1}{3}f_S^2}\,, \quad \theta_0 = \phi - \arctan\left(\frac{\sqrt{2}f_{NS}}{f_S}\right)\,. \qquad (26)$$

Note that f_0 and f_8 do not result from solving of Eqs. (13)-(15), but are the calculated predictions of a concrete dynamical DS model, independently of Shore's equations.

For all three quite different (RGI [15,16] and non-RGI [19]) dynamical models which we used in our previous DS studies [13,14,9,26,17,18], the situation with the results turns out to be rather similar. The most conspicuous feature is that η and η' masses are both much too low when the weighted average $\chi_{YM} = (175.7 \pm 1.5\,\text{MeV})^4$ of Refs. [31–33] is used, in contrast to the results from the standard WV relation, displayed in Table 1. If we single out just the highest of these values $(191\,\text{MeV})^4$ [32]), the masses improve somewhat. However, other results are spoiled – e.g., the mixing angle ϕ becomes too high to enable agreement with the experimental results on $\eta, \eta' \to \gamma\gamma$ decays, which require $\phi \sim 40°$ [9].

When we turn to the lower parts of Tables 1 and 2, where the results for the η and η' decay constants, and the corresponding two mixing angles θ_0 and θ_8, are given, we notice a feature common to all our results, as well as Shore's (also given in Table 1). The diagonal ones, $f_{\eta'}^0$ and f_η^8, are all of the order of f_π, being larger by some 10% to 30%. The off-diagonal ones, $f_{\eta'}^8$ and f_η^0, are, on the other hand, in general strongly suppressed. This is expected, as η' is mostly singlet, and η is mostly octet. The feature that may be surprising is that Shore's results (which, to be sure, were obtained [10,11] in quite a different way from ours) are more similar to our results obtained through the standard WV relation, than to our results obtained through Shore's Eqs. (13)-(15).

All in all, inspection and comparison of the results in Table 2 with the results (in Table 1) from the analogous calculations but using the standard WV relation to construct the complete η-η' mass matrix, leads to the conclusion that the DS approach with the standard WV relation (11) is phenomenologically more successful, yielding the masses closer to the experimental ones. This may seem surprising, as Shore's generalization is in principle valid to all orders in $1/N_c$, while the standard WV relation is a lowest order $1/N_c$ result. Nevertheless, one must be aware that we do not yet have at our disposal the full QCD topological charge parameter A, and that we (along with Shore) had to use its lowest $1/N_c$ approximation, χ_{YM}. Also, we should recall from Sections 1 and 2 that the very usage of the RLA assumed that the anomaly is implemented on the level of the anomalous mass only, as a lowest order $1/N_c$ correction [13,14,9,17,18]. Thus, with respect to the orders in $1/N_c$, the usage of the standard WV relation is consistent in the present formulation of our DS approach, whereas the usage of Shore's generalization is not, which is probably the cause of its lesser phenomenological success. However, the usage of Shore's generalization in the DS context as exposed here, will likely find its application at finite temperatures. Namely, there it may help alleviate the difficulties met due to the usage of the standard WV relation in the DS approach at $T > 0$, as discussed in Ref. [18].

References

1. E. Witten, Nucl. Phys. **B156**, 269 (1979).
2. G. Veneziano, Nucl. Phys. **B159**, 213 (1979).
3. For example, see Refs. [4–8] for recent reviews and references on various applications of the DS approach.

4. R. Alkofer and L. von Smekal, Phys. Rept. **353**, 281 (2001).
5. C. D. Roberts, arXiv:nucl-th/0007054.
6. C. D. Roberts and S. M. Schmidt, Prog. Part. Nucl. Phys. **45**, S1 (2000).
7. A. Holl, C. D. Roberts, and S. V. Wright, arXiv:nucl-th/0601071.
8. C. S. Fischer, J. Phys. G **32**, R253 (2006).
9. D. Kekez and D. Klabučar, Phys. Rev. D **73**, 036002 (2006).
10. G. M. Shore, Nucl. Phys. **B744**, 34 (2006).
11. G. M. Shore, hep-ph/0701171.
12. D. Horvatić, D. Blaschke, Yu. Kalinovsky, D. Kekez and D. Klabučar, arXiv:0710.5650 [hep-ph], accepted for publication in European Physical Journal A.
13. D. Klabučar and D. Kekez, Phys. Rev. D **58**, 096003 (1998).
14. D. Kekez, D. Klabučar, and M. D. Scadron, J. Phys. G **26**, 1335 (2000).
15. P. Jain and H. J. Munczek, Phys. Rev. D **48**, 5403 (1993).
16. D. Kekez and D. Klabučar, Phys. Rev. D **71**, 014004 (2005).
17. D. Horvatić, D. Blaschke, D. Klabučar, and A. E. Radzhabov, arXiv:hep-ph/0703115.
18. D. Horvatić, D. Klabučar and A. E. Radzhabov, Phys. Rev. D **76**, 096009 (2007) [arXiv:0708.1260 [hep-ph]].
19. D. Blaschke, G. Burau, Y. L. Kalinovsky, P. Maris, and P. C. Tandy, Int. J. Mod. Phys. A **16**, 2267 (2001).
20. D. Kekez, B. Bistrović, and D. Klabučar, Int. J. Mod. Phys. A **14**, 161 (1999).
21. B. Bistrović and D. Klabučar, Phys. Lett. B **478**, 127 (2000); Phys. Rev. D **61**, 033006 (2000).
22. R. Alkofer and C. D. Roberts, Phys. Lett. B **369**, 101 (1996).
23. D. Kekez and D. Klabučar, Phys. Rev. D **65**, 057901 (2002).
24. O. Lakhina and P. Bicudo, arXiv:0708.0984.
25. M. S. Bhagwat, L. Chang, Y. X. Liu, C. D. Roberts, and P. C. Tandy, arXiv:0708.1118.
26. D. Blaschke, D. Horvatić, D. Klabučar, and A. E. Radzhabov, hep-ph/0703188, in *Proceedings of the Mini-Workshop "Progress in Quark Models", Bled, Slovenia, 2006*, editors B. Golli, M. Rosina, and S. Širca (DMFA - založništvo, Ljubljana 2006), p. 20.
27. B. Alles, M. D'Elia, and A. Di Giacomo, Nucl. Phys. **B494**, 281 (1997).
28. D. Blaschke, H. P. Pavel, V. N. Pervushin, G. Ropke, and M. K. Volkov, Phys. Lett. B **397**, 129 (1997).
29. Th. Feldmann, Int. J. Mod. Phys. A **15**, 159 (2000).
30. Th. Feldmann, P. Kroll, and B. Stech, Phys. Rev. D **58**, 114006 (1998).
31. B. Lucini, M. Teper, and U. Wenger, Nucl. Phys. **B715**, 461 (2005).
32. L. Del Debbio, L. Giusti, and C. Pica, Phys. Rev. Lett. **94**, 032003 (2005).
33. B. Alles, M. D'Elia, and A. Di Giacomo, Phys. Rev. D **71**, 034503 (2005).
34. J. Gasser and H. Leutwyler, Nucl. Phys. **B250**, 465 (1985).
35. H. Leutwyler, Nucl. Phys. Proc. Suppl. **64**, 223 (1998).
36. R. Kaiser and H. Leutwyler, hep-ph/9806336, in *Proceedings of the Workshop "Non-perturbative methods in quantum field theory", Adelaide, Australia, 1998*, editors A.W. Schreiber, A.G. Williams, and A.W. Thomas (World Scientific, Singapore 1998).
37. Th. Feldmann, P. Kroll, and B. Stech, Phys. Lett. B **449**, 339 (1999).

Parity doubling in the high baryon spectrum: near-degenerate three-quark quartets[*]

F. J. Llanes-Estrada[a], P. Bicudo[b], M. Cardoso[b], T. Van Cauteren[c]

[a] Dept. Física Teorica I, Univ. Complutense, Madrid 28040, Spain
[b] Instituto Superior Tecnico,1049-001 Lisboa, Portugal
[c] Dept. of Subatomic and Radiation Physics, Ghent University, Belgium

Abstract. We report on the first calculation of excited baryons with a chirally symmetric Hamiltonian, modeled after Coulomb gauge QCD (or upgraded from the Cornell meson potential model to a field theory in all of Fock-space) showing the insensitivity to chiral symmetry breaking. As has recently been understood, this leads to doubling between two hadrons of equal spin and opposite parity. As a novelty we show that three-quark Δ states group into quartets with two states of each parity, all four states having equal angular momentum J. Diagonalizing the chiral charge expressed in terms of quarks we show that the quartet is slightly split into two parity doublets by the tensor force, all splittings decreasing to zero high in the spectrum.

Our specific calculation is for the family of maximum-spin excitations of the Delta baryon. We provide a model estimate of the experimental accuracy needed to establish Chiral Symmetry Restoration in the high spectrum. We suggest that a measurement of masses of high-partial wave Δ resonances with an accuracy of 50 MeV should be sufficient to unambiguously establish the approximate degeneracy, and test the concept of running quark mass in the infrared.

The idea of chiral symmetry restoration has been around for a while, for example parity doubling was examined for the proton in the context of the linear sigma model in [1]. By current ideas we believe that this restoration should occur for higher excitations. Glozman and collaborators [2–8] (see also [9]) have theoretically examined $(q\bar{q})$ mesons, and also shown marginal empirical evidence for chiral symmetry restoration in both meson and hadron spectra, that rekindles interest on intermediate energy resonances. Chiral symmetry restoration, or more precisely, Spontaneous Chiral Symmetry Breaking Insensitivity high in the spectrum, is established as a strong prediction of the symmetry breaking pattern of QCD, and such prediction in an energy region where little else can be stated, needs to be confirmed or refuted by experiment.

The baryon spectrum is a more difficult theoretical problem given the minimum three-body wavefunction (as opposed to only quark-antiquark for mesons) and in this paper we provide the necessary theoretical background to understand parity doubling, in agreement with a prior study by Nefediev, Ribeiro and

---

[*] Talk presented by F. J. Llanes-Estrada

Szczepaniak [10], and give the first model estimate of what the experimental target-precision should be. This should help quantify what "high enough" in the spectrum means, to assist experimental planning.

We customarily employ a truncation of Coulomb-gauge QCD by ignoring the Faddeev-Popov operator and substituting the Coulomb kernel by its vacuum expectation value, that takes the usual linear plus Coulomb form. This can be seen as a field theory upgrade of the Cornell potential model. The Hamiltonian reads

$$H = -g_s \int d\mathbf{x} \Psi^\dagger(\mathbf{x}) \alpha \cdot \mathbf{A}(\mathbf{x}) \Psi(\mathbf{x}) + \text{Tr} \int d\mathbf{x} (\mathbf{E} \cdot \mathbf{E} + \mathbf{B} \cdot \mathbf{B})$$

$$+ \int d\mathbf{x} \Psi_q^\dagger(\mathbf{x})(-i\alpha \cdot \nabla + \beta m_q) \Psi_q(\mathbf{x}) + \frac{1}{2} \int d\mathbf{x} d\mathbf{y} \rho^a(\mathbf{x}) V_L(|\mathbf{x} - \mathbf{y}|) \rho^a(\mathbf{y}) \quad (1)$$

with a strong kernel containing a linear potential V_L, with string tension $\sigma = 0.135 \, \text{GeV}^2$, coupled to the color charge density $\rho^a(\mathbf{x}) = \Psi^\dagger(\mathbf{x}) T^a \Psi(\mathbf{x}) + f^{abc} \mathbf{A}^b(\mathbf{x}) \cdot \Pi^c(\mathbf{x})$. In our past work we have solved the BCS gap equation to spontaneously break chiral symmetry. This model has the same chiral structure of QCD, satisfying the Gell-Mann-Oakes-Renner relation, the low-energy theorems for pion scattering [14] and allowing computations of static pion-nucleon observables [15]. We have employed it in studies of gluodynamics [16] shown at this workshop that agree with lattice gauge theory and are of qualitative phenomenological interest. In any case, these play a minor role in the topic of this article, as the decreasing of the splittings is dominated by chiral symmetry breaking alone. For a reduced baryon sector application we are going to perform two more simplifications. We employ only the V_L linear potential, and neglect all magnetic interactions. This makes the Δ-nucleon mass splitting too small, but does not affect the Δ spectrum much.

We truncate the Fock space variationally, as customary, to the $|qqq\rangle$ minimum wavefunction. Since radial excitations of this system compete with multiquark excitations, we concentrate instead on maximum angular-momentum excitations $J = 3/2 + l$. Chiral forces are too weak to compensate large centrifugal forces and can hardly maintain $l = 3$ or $l = 4$, so one hopes to reduce the molecular component by studying the ground state in each J-channel, so that the $|qqq\rangle$ correlation remains important high in the spectrum.

As a rule of thumb, one needs to keep in the Fock-space expansion $|qqq\rangle + |qqqq\bar{q}\rangle + |qqqg\rangle + \ldots$ as many states as will be competitive by phase space considerations, considering the quark and gluon dynamical mass gaps established by lattice and Dyson-Schwinger studies. When pentaquark correlations are more abundant than three-quark correlations (see figure 1) the typical quark momentum will be lower than extrapolated from the ground-state baryons, so that chiral symmetry restoration will not be quite so fast.

This puts pentaquark correlations above 2 GeV, with the exception of possible meson-baryon resonances (as the Goldstone bosons avoid the mass-gap). In any case it seems well established that three-quark correlations play an important role in baryon-phenomenology, so it is worth examining the effect of a chiral transformation on a three-quark variational wavefunction $|N\rangle = F_{ijk} B_i^\dagger B_j^\dagger B_k^\dagger |0\rangle$.
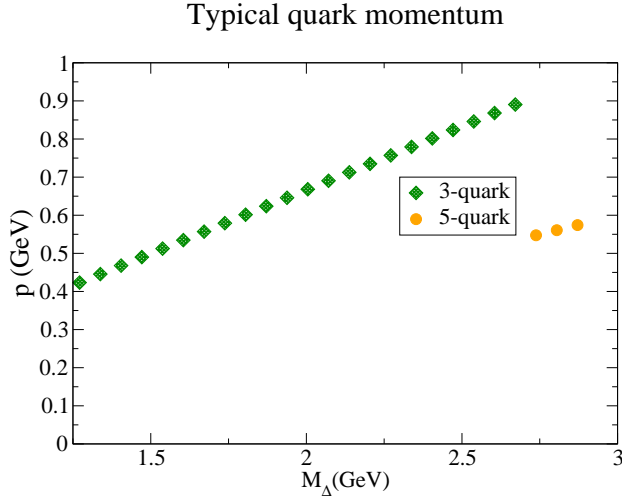
Typical quark momentum

Fig.1. The typical momentum of a quark in a three-quark state is (by kinetic energy considerations alone, with a running mass-gap) $|k\rangle \propto M_{\Delta_J}$. Plotted is the typical momentum in a three quarks and five quark wavefunction. At the jump the phase space for five-quark states is larger, so it is more likely that a baryon of that mass is in a five-quark configuration, and the typical momentum is therefore smaller. Hence chiral symmetry restoration has to be somewhat slower than three-quark models would indicate.

We proceed variationally and employ several types of wavefunctions, rational and Gaussian, but the lowest energy (binding the model's J-ground state from above by the Rayleigh-Ritz principle) is obtained by employing the chiral limit pion-wavefunction rescaled with two variational parameters in terms of Jacobi coordinates, $\sin\phi(k_\rho/\alpha_\rho)\sin\phi(k_\lambda/\alpha_\lambda)Y_l^{m_1}(\hat{k}_\rho)$. We have found the angular excitation in λ to be slightly higher in energy and neglect the correlation. Part of it though reenters the calculation upon (anti)symmetrizing the wavefunction, since quark exchange mixes the ρ and λ variables.

A typical variational search is represented in figure 2. Table 1 presents the intradoublet splittings. The interdoublet splittings, as well as improved precision on our three-body variational Montecarlo method, will be given in an upcoming publication. As can be seen from the table, the model doublet splittings drop with the orbital angular momentum. This is easy to understand from the structure of the model Hamiltonian. The kernel for baryons is proportional to

$$F^*_{s_1 s_2 s_3}(\mathbf{k}_1,\mathbf{k}_2)\, U^\dagger_{k_1 s_1} U_{k_1+q\lambda_1}\, U^\dagger_{k_2 s_2} U_{k_2-q\lambda_2} \tag{2}$$
$$\times F_{\lambda_1\lambda_2 s_3}(\mathbf{k}_1+\mathbf{q},\mathbf{k}_2-\mathbf{q})$$

that, upon becoming insensitive to the gap angle, $\sin\phi(k >> \Lambda_{QCD}) \to 0$, turns into

$$F^*_{s_1 s_2 s_3}\left(\delta_{s_1\lambda_1}+(\sigma\cdot\hat{k}_1\sigma\cdot\widehat{k_1+q})_{s_1\lambda_1}\right)\cdot \tag{3}$$
$$\left(\delta_{s_2\lambda_2}+(\sigma\cdot\hat{k}_2\sigma\cdot\widehat{k_2-q})_{s_2\lambda_2}\right)F_{\lambda_1\lambda_2 s_3}\,.$$
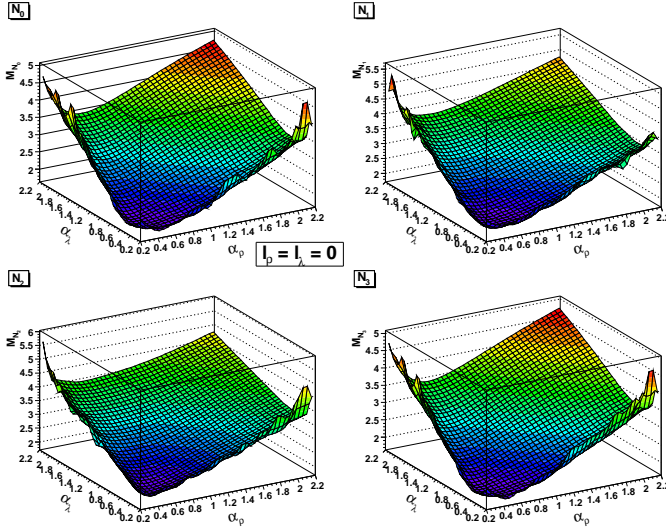
Fig.2. Variational minimum-energy search $E(\alpha_\rho, \alpha_\lambda)$ with a two-parameter family of functions. Best results are obtained when the (chiral-limit) pion wavefunction is rescaled and used to build the Jacobi-radial part of the Δ wavefunctions, $\sin\phi(k_\rho/\alpha_\rho)\sin\phi(k_\lambda/\alpha_\lambda)$. For maximum spin Δ states, $J = 3/2 + l_\rho$ the angular wavefunction before symmetrization is $Y_l^{m_1}(\hat{k}_\rho)$ (we set $l_\lambda = 0$ consistent with the variational approximation, but numerically symmetrize the spin-space wavefunction, which reintroduces it through exchanged-quarks).

Table 1. Experimental and computed doublet splittings. The entire quartet degenerates high in the spectrum, with the $+-$ parity doubling proceeding faster due to insensitivity to χSB and the interdoublet splitting decreasing slower, as they are due to the tensor force and dynamical. We give a preliminary calculation of the intradoublet splitting (parity degeneracy). From the decreasing theory splittings we deduce that an experimental measurement of the parity splitting $M_+ - M_-$ to an accuracy of 100, or better 50 MeV, should suffice to see the effect. Note that our excited splittings become compatible with zero within errors in the Montecarlo 9-d integral.

J	Exp. $M_+ - M_-$	Theory intradoublet
3/2	470(40)	450(100)
5/2	70(90)	400(100)
7/2	270(120)	50(100)
9/2	50(250)	200(100)
11/2	-	100(100)
13/2	-	100(100)

If instead of $F^*_{s_1 s_2 s_3}$ one substitutes its chiral partner $F^*_{s'_1 s_2 s_3}(\sigma \cdot \hat{k}_1)_{s'_1 s_1}$ (and the same for the ket), the two states are seen to be degenerate. Also apparent in Eq.(3) is the role of the tensor force in enforcing chiral cancellations.

Finally, the first computation of the parity doubling for baryons is presented in figure 3.
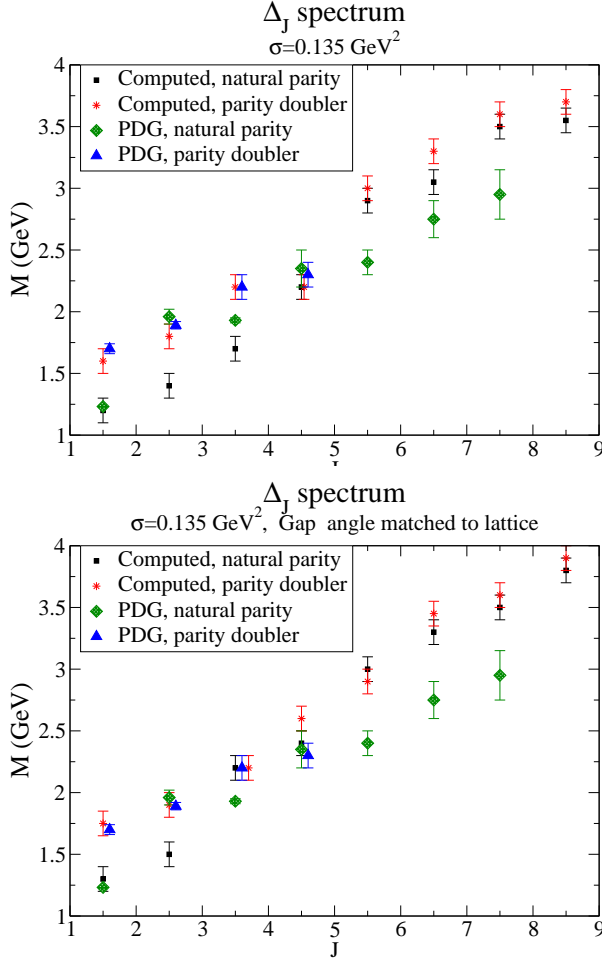

Fig.3. Parity doubling in the spin-excited Δ spectrum. Top: with infrared quark mass as calculated in the model (probably too low). Bottom: quark mass rescaled to fit Landau-gauge lattice data. The model clearly displays parity doubling. The experimental situation is still unclear, the degeneracy can be claimed for the $9/2$ states alone, and the chiral partners higher in the spectrum are not experimentally known.

Let us now show that there are indeed two closely separated baryon doublets, slightly split by tensor forces. We find convenient to employ the gap angle instead of the quark mass

$$\sin\phi(k) \equiv \frac{M(k)}{\sqrt{M(k)^2 + k^2}}$$

and the Dirac spinors can be easily parametrized as

$$U_{\kappa\lambda} = \frac{1}{\sqrt{2}} \begin{bmatrix} \sqrt{1 + \sin\phi_\kappa}\chi_\lambda \\ \sqrt{1 - \sin\phi_\kappa}\,\sigma \cdot \hat{\kappa}\chi_\lambda \end{bmatrix} \qquad (4)$$

$$V_{-\kappa\lambda} = \frac{1}{\sqrt{2}} \begin{bmatrix} -\sqrt{1 - \sin\phi_\kappa}\,\sigma \cdot \hat{\kappa}i\sigma_2\chi_\lambda \\ \sqrt{1 + \sin\phi_\kappa}\,i\sigma_2\chi_\lambda \end{bmatrix} . \qquad (5)$$

Substituting these spinors, and in terms of Bogoliubov-rotated quark and anti-quark normal modes B, D, the chiral charge takes the form

$$Q_a^5 = \int \frac{d^3k}{(2\pi)^3} \sum_{\lambda\lambda'ff'c} \left(\frac{\tau^a}{2}\right)_{ff'} \qquad (6)$$

$$(\cos\phi(k)$$

$$(\sigma\cdot\hat{\mathbf{k}})_{\lambda\lambda'} \left(B^\dagger_{k\lambda fc}B_{k\lambda'f'c} + D^\dagger_{-k\lambda fc}D_{-k\lambda'f'c}\right) +$$

$$\sin\phi(k)$$

$$(i\sigma_2)_{\lambda\lambda'} \left(B^\dagger_{k\lambda fc}D^\dagger_{-k\lambda'f'c} + B_{k\lambda fc}D_{-k\lambda'f'c}\right)) .$$

In the presence of Spontaneous Chiral Symmetry Breaking, $\sin\phi(k) \neq 0$, and the two terms in the second line are responsible for the non-linear realization of chiral symmetry in the spectrum. One can see this by applying the chiral charge on a hadron state to collect the same hadron state plus a pion. As in Jaffe, Pirjol and Scardiccio [11],

$$[Q_5^a, N_i^\pm] = \nu_0(\pi^2)\epsilon_{abc}\pi^c\Theta_{ij}^b N_j^\pm . \qquad (7)$$

(Here, i and j are the chiral multiplet indices).
Eq. (7) is easy to derive because the $i\sigma_2$ matrix couples the quark-antiquark pair to pseudoscalar quantum numbers, so the terms in the second line of eq.(6) provide an interpolating field for the pion. In fact, if the vacuum is variationally chosen as the BCS ground state $|\Omega\rangle$ with $B|\Omega\rangle = 0$, $D|\Omega\rangle = 0$, $\sin\phi(k)$ then provides precisely the RPA pion wavefunction in the chiral limit, and the terms with $\sin\phi(k)$ become the RPA pion-creation operator.

If instead Chiral Symmetry was not spontaneously broken in QCD, $M(k) \simeq 0$ and $\sin\phi(k) \simeq 0$. As a consequence, it is obvious that the chiral charge would not change the particle content since the second line of eq.(6) would vanish, and the first line is made of quark and antiquark number operators. Then chiral symmetry would be linearly realized in Wigner-Weyl mode where hadrons come in degenerate opposite-parity pairs

$$[Q_5^a, N_i^+] = \Theta_{ij}^a N_j^-$$
$$[Q_5^a, N_i^-] = \Theta_{ij}^a N_j^+ .$$

The parity change follows from the $\sigma\cdot\hat{k}$ p-wave present in the first line of eq.(6).

In fact, the contemporary realization is that both phenomena are simultaneously realized in QCD. The vacuum is not annihilated by the chiral charge, forcing spontaneous symmetry breaking, but the mass gap angle has compact support and if, in a hadron, the typical quark momentum is high, as illustrated in

figure 4, its wavefunction is insensitive to Chiral Symmetry Breaking. Therefore one asymptotically recovers degenerate Glozman parity doublets. We will in the following drop the isospin index.
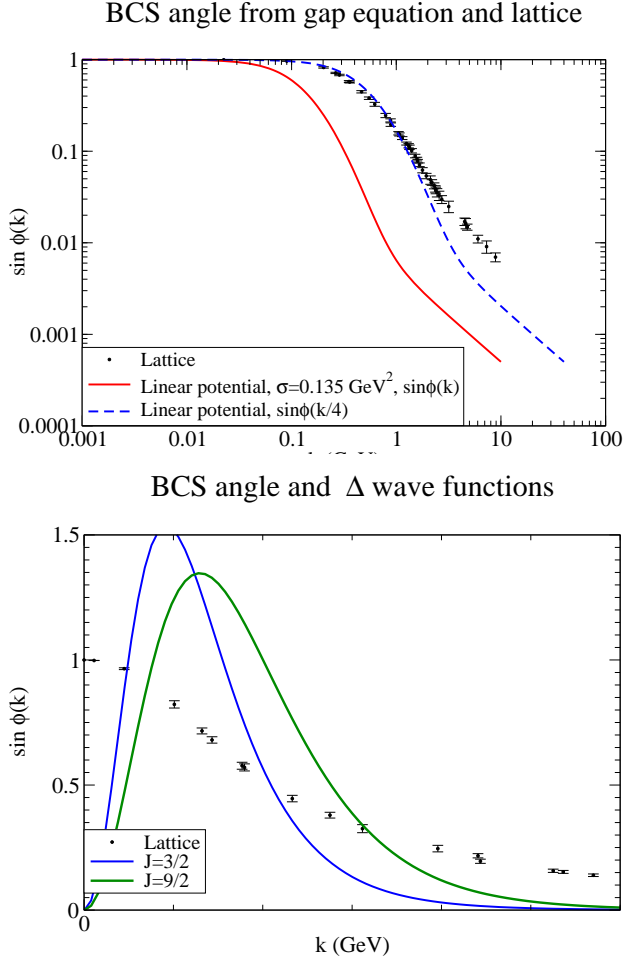
BCS angle from gap equation and lattice

BCS angle and Δ wave functions

Fig.4. The sine of the gap angle $M(k)/\sqrt{(M(k)^2 + k^2)}$ has limited support if the chiral-symmetry breaking quark mass remains of order Λ_{QCD} or less. Top: we show the running mass from a model computation for a linear potential with string tension $\sigma = 0.135\ GeV^2$, and its rescaling to match Landau-gauge data [12,13] (no Coulomb-gauge lattice data for the quark mass is known to us). Bottom: Quark-momentum distributions for $\Delta_{3/2}$ and $\Delta_{9/2}$ with simple variational wavefunctions. The quark-momentum distribution for higher hadron resonances has smaller overlap with this gap angle, and therefore the quarks in those hadrons behave effectively as if they were massless. Hence they become insensitive to the gap angle, and chiral symmetry is restored in Wigner-Weyl mode with degenerate multiplets.

If a given resonance is high enough in the spectrum so the quarks have a momentum distribution peaked higher than the support of the gap angle, as in figure 4, only the first line of Eq.(6) is active. $Q_5|N\rangle$ contains also three quarks, but one of them is spin-rotated from $B_{k\lambda}$ to $\sigma\cdot\hat{k}_{\lambda\lambda'}B_{k\lambda'}$. Successive application of the chiral charge spin-rotates further quarks, changing each time the parity of the total wavefunction. However the sequence of states ends since $\sigma\cdot\hat{k}\sigma\cdot\hat{k} = \mathbb{I}$. In fact, starting with an arbitrary such wavefunction, one generates a quartet

$$|N_0^P\rangle = \sum F_{ijk}^P B_i^\dagger B_j^\dagger B_k^\dagger |\Omega\rangle$$

$$|N_1^{-P}\rangle = \frac{1}{3}\sum F_{ijk}^P$$

$$\left(\left(\sigma\cdot\hat{k}_i B^\dagger\right)_i B_j^\dagger B_k^\dagger + \text{permutations}\right)|\Omega\rangle$$

$$|N_2^P\rangle = \frac{1}{3}\sum F_{ijk}^P$$

$$\left(\left(\sigma\cdot\hat{k}_i B^\dagger\right)_i \left(\sigma\cdot\hat{k}_j B^\dagger\right)_j B_k^\dagger + \text{permutations}\right)|\Omega\rangle$$

$$|N_3^{-P}\rangle = \sum F_{ijk}^P$$

$$\left(\sigma\cdot\hat{k}_i B^\dagger\right)_i \left(\sigma\cdot\hat{k}_j B^\dagger\right)_j \left(\sigma\cdot\hat{k}_k B^\dagger\right)_k |\Omega\rangle$$

that is the natural basis to discuss chiral symmetry restoration in baryons, through wavefunctions that are linear combinations $|N\rangle = \sum c_i|N_i\rangle$.

Because the Hamiltonian and the chiral charge commute, they can be diagonalized simultaneously.

The quartet then separates into two doublets connected by the chiral charge

$$Q_5(N_0 - N_2) = N_1 - N_3 \qquad (8)$$
$$Q_5(N_1 - N_3) = N_0 - N_2$$
$$Q_5(N_0 + 3N_2) = 3(3N_1 + N_3)$$
$$Q_5(3N_1 + N_3) = 3(N_0 + 3N_2)$$

Since the quartet can be divided into two two-dimensional irreducible representations of the chiral group, (with different eigenvalues of Q_5^2, 1 and 9 respectively), the masses of the two doublets may also be different, and the interdoublet splitting becomes a dynamical question. However, the splitting within the doublet *must vanish* asymptotically. This is a prediction following from first principles-understanding of QCD alone. Should it not be borne experimentally, it would falsify the theory.

Of course, parity doubling is a property of a more general class of theories than QCD. Even for fixed (not running) quark mass, when the typical momenta are high enough $\langle k\rangle >> m$ in the kinetic energy, the effects of the quark mass are negligible. Parity doubling then comes down to whether the interaction terms are also chiral symmetry violating or not.

To round off this work, let us look ahead to what the highly excited spin spectrum may reveal. The J-dependence of the fall-off of the splittings $M_+ - M_-$

is an observable that reveals the underlying chiral theory. If precise data becomes available at ELSA or Jefferson Lab (note the EBAC, Excited Baryon Analysis Center effort [19]), in particular for the Δ_J with $J = 7/2, 9/2, 11/2$ parity doublets, one should be able to distinguish between the typical $1/\sqrt{l}$ fall-off for non-chiral models and the faster drop for chiral theories. (Higher yet in the spectrum, also the chiral theory may take on the $1/\sqrt{l}$ behavior due to the small remaining current quark mass that falls only logarithmically)[1].

Since the two doublets are closely degenerate, both positive and negative parity ground states will have a nearby resonance with identical quantum numbers. Given the width of those states, it is likely they will only be distinguished by very careful exclusive decay analysis. Meanwhile, if interpreted as only one resonance, their decay pattern will defy intuition.

It is also worth remarking that the spin-orbit interaction is very small in the low-lying spectrum, due to cancellations between scalar and vector potentials and the Thomas precession [20]. However, higher in the spectrum, the vector $\gamma_0\gamma_0$ potential comes forward, and it is known to present larger spin-orbit splittings than found to date. Therefore not all splittings in a given baryon shell will disappear alike: while parity splittings must decrease fast by chiral symmetry, other spin-orbit splittings will stay constant or even grow. This is demanded by a necessary cancellation between $L \cdot S$, centrifugal forces $l(l + 1)$ and tensor forces. This has been explicitly shown for mesons in [21].

Table 2. Total width, exclusive pion-nucleon width and semiinclusive pion width (decay to one pion plus any other particles excluding pions) for the ground state Δ_J resonances. All units MeV. Data adapted from PDG[23] .

J^P	Γ	$\Gamma_{\pi N}$	$\Gamma_{\pi X}$
$\frac{3}{2}^+$	118(2)	118(2)	118(2)
$\frac{3}{2}^-$	300(100)	50(30)	190(90)
$\frac{5}{2}^+$	330(60)	42(18)	$< 80(20)$
$\frac{5}{2}^-$	350(150)	40(30)	-
$\frac{7}{2}^+$	285(50)	115(35)	170(30)
$\frac{7}{2}^-$	400(150)	30(20)	-
$\frac{9}{2}^+$	400(150)	30(20)	-
$\frac{9}{2}^-$	400(180)	35(25)	-
$\frac{11}{2}^+$	450(150)	50(40)	-
$\frac{11}{2}^-$	-	-	-
$\frac{13}{2}^+$	-	-	-
$\frac{13}{2}^-$	400(200)	20(12)	-
$\frac{13}{2}^+$	550(300)	30(25)	-

[1] Other authors have argued that flattening of the potential in a non-relativistic quark model for large distances due to screening (string-breaking) also leads to parity degeneracy [18]. We are preparing an additional paper that will provide the necessary detail for chiral models to distinguish them.

   It has also been pointed out [8,22,10] that the pion decouples from the very excited resonances due to the falling overlap between the $\Delta*$ wavefunctions and $\sin\phi(k)$ (the pion wavefunction in the chiral limit). This might already be observable in the known widths for pion decays, that decrease even with larger phase space, see table 2. There are lattice calculations addressing low-excited baryons [24], but it is still a long way to go until highly excited states can be examined.

References

 1. C. E. Detar and T. Kunihiro, Phys. Rev. D **39**, 2805 (1989).
 2. L. Y. Glozman, Phys. Lett. B **475** (2000) 329.
 3. L. Y. Glozman, Prog. Part. Nucl. Phys. **50** (2003) 247.
 4. R. F. Wagenbrunn and L. Y. Glozman, Phys. Lett. B **643**, 98 (2006).
 5. T. D. Cohen and L. Y. Glozman, Mod. Phys. Lett. A **21**, 1939 (2006).
 6. T. D. Cohen and L. Y. Glozman, Phys. Rev. D **65**, 016006 (2002) [arXiv:hep-ph/0102206].
 7. T. D. Cohen and L. Y. Glozman, Int. J. Mod. Phys. A **17**, 1327 (2002) [arXiv:hep-ph/0201242].
 8. L. Y. Glozman, A. V. Nefediev and J. E. F. Ribeiro, Phys. Rev. D **72**, 094002 (2005).
 9. D. Jido, T. Hatsuda and T. Kunihiro, Phys. Rev. Lett. **84**, 3252 (2000) [arXiv:hep-ph/9910375].
10. A. V. Nefediev, J. E. F. Ribeiro and A. P. Szczepaniak, JETP Lett. **87**, 271 (2008).
11. R. L. Jaffe, D. Pirjol and A. Scardicchio, Phys. Rev. Lett. **96**, 121601 (2006); Phys. Rev. D **74**, 057901 (2006).
12. P. O. Bowman, U. M. Heller, D. B. Leinweber, M. B. Parappilly and A. G. Williams, Nucl. Phys. Proc. Suppl. **161**, 27 (2006).
13. M. B. Parappilly, P. O. Bowman, U. M. Heller, D. B. .. Leinweber, A. G. Williams and J. B. Zhang, Phys. Rev. D **73**, 054504 (2006).
14. P. Bicudo, S. Cotanch, F. J. Llanes-Estrada, P. Maris, E. Ribeiro and A. Szczepaniak, Phys. Rev. D **65** (2002) 076008.
15. P. J. A. Bicudo, G. Krein and J. E. F. Ribeiro, Phys. Rev. C **64** (2001) 025202; P. Bicudo and J. Ribeiro, Phys. Rev. C **55** (1997) 834.
16. P. Bicudo, S. R. Cotanch, F. J. Llanes-Estrada and D. G. Robertson, Eur. Phys. J. C **52** (2007) 363; F. J. Llanes-Estrada, P. Bicudo and S. R. Cotanch, Phys. Rev. Lett. **96** (2006) 081601.
17. M. Shifman and A. Vainshtein, Phys. Rev. D **77**, 034002 (2008).
18. J. Segovia, D. R. Entem and F. Fernandez, Phys. Lett. B **662** (2008) 33.
19. B. Julia-Diaz, T. S. Lee, A. Matsuyama, T. Sato and L. C. Smith, Phys. Rev. C **77** (2008) 045205.
20. N. Isgur, Phys. Rev. D **62** (2000) 014025 [arXiv:hep-ph/9910272].
21. P. Bicudo, Phys. Rev. D **76** (2007) 094005 [arXiv:hep-ph/0703114].
22. L. Y. Glozman, Phys. Rev. Lett. **99**, 191602 (2007) [arXiv:0706.3288 [hep-ph]].
23. W. M. Yao *et al.* [Particle Data Group], J. Phys. G **33** (2006) 1.
24. T. T. Takahashi and T. Kunihiro, Phys. Rev. D **78**, 011503 (2008) [arXiv:0801.4707 [hep-lat]].

Λ(1405) and X(3872) as multiquark systems

S. Takeuchi

Japan College of Social Work, Kiyose, Tokyo 204-8555, Japan

Abstract. We have investigated the effects of (q$\overline{q}$) pairs on the baryons and mesons by employing two examples: Λ(1405) and X(3872). The Λ(1405) resonance is treated as a q^3-q$\overline{q}$ scattering which couples to the q^3 orbital $(0s)^2 0p$ state by the one-gluon exchange interaction. Due to the coupling of this q^3 state, we find that a peak appears at around 1405 MeV. We also investigate the system by employing a baryon-meson model with a separable interaction. By simplifying the model, we can clarify the mechanism and condition to form a peak. As for the X(3872), we investigate q$\overline{q}$c$\overline{c}$ isospin 1 and 0 systems with the orbital correlation. For the isospin 0 system, we also consider its coupling to the c$\overline{c}$ state. The results show that there can be a bound state of q$\overline{q}$c$\overline{c}$ with J^{PC} = 1^{++}, which is a coupled state of the J/ψ-ρ(or ω) and D-D* molecules with a multiquark configuration in the short range region. Both of the two examples indicate that an extra (q$\overline{q}$) pair may play important roles especially in the excited hadrons.

1 Λ(1405) by a quark model[1]

Properties of the Λ(1405) is hard to understand; the conventional quark picture, which assumes the q^3 $(0s)^2(0p)$ configuration, cannot give the observed Λ(1405) light mass, nor the large splitting between Λ(1405) and Λ(1520) [2]. Moreover, since Λ(1405) has a large width, the mixing between this q^3 state and the continuum should not be neglected.

To describe Λ(1405) as a peak in the baryon-meson scattering, we have investigated q^3-q$\overline{q}$ scattering system with a q^3 pole [1]. The scattering is solved by employing the Quark Cluster Model (QCM). The pole, which we assume the flavor-singlet q^3 $(0s)^2(0p)$ state, is treated as a bound state embedded in the continuum (BSEC). In the present model, the effective quark interaction consists of the one-gluon exchange (OGE) and the instanton-induced interaction (Ins) as well as the linear confinement potential. With a parameter set which reproduces both of the observed S-wave flavor-octet baryon and meson mass spectra, we perform the Σπ-N$\overline{K}$ coupled channel QCM.

We found that the peak energy can be 1405 MeV, namely by about 30 MeV below the N$\overline{K}$ threshold in the spin $\frac{1}{2}$ isospin 0 channel even if the mass of the q^3 pole without the coupling is taken to be the conventional quark model value, which is above the threshold by about 55 MeV. The peak disappears when the

---

[1] This work has been done in collaboration with Kiyotaka Shimizu (Sophia University) [1].
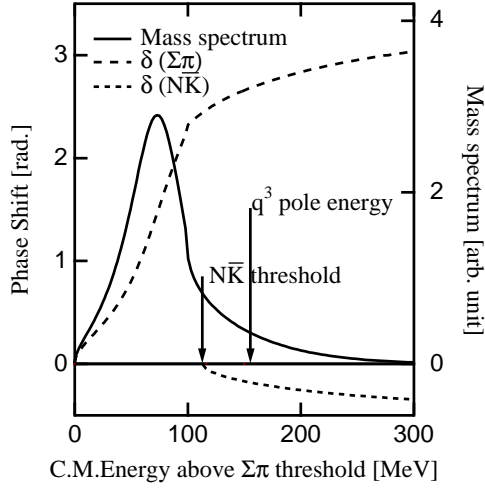
Fig.1. Mass spectrum and the phase shift (δ) of the $\Sigma\pi$ and $N\overline{K}$ coupled channel QCM.

coupling to the q^3 pole is switched off. The obtained peak width agrees with the experiments reasonably well. The $N\overline{K}$ scattering length is roughly half of the observed value [3]. For details, please check our paper [1].

2 $\Lambda(1405)$ by a baryon-meson model[2]

Recently, it was reported that a baryon-meson model with the chiral unitary approach can reproduce the $\Lambda(1405)$ peak without the help of an quark pole [4,5]. Then a new question arises: there should be the flavor-singlet q^3 state, which is supposed to affect the baryon-meson scattering in this energy region.

To investigate the mechanism and condition to form the peak, we employ a simple baryon-meson model with the semi-relativistic kinematics.

$$T = V + VG^{(0)}T \tag{1}$$

$$G_P^{(0)} = i \int \frac{d^4q}{(2\pi)^4} \frac{M}{\Omega} \frac{1}{E_{tot} - q^0 - \Omega + i\epsilon} \frac{1}{q^{02} - \omega^2 + i\epsilon}$$

$$= \int \frac{d^3q}{(2\pi)^3} \frac{mM}{\omega\Omega} \frac{1}{2m} \frac{1}{E_{tot} - q^0 - \Omega + i\epsilon} , \tag{2}$$

where $M[m]$ is the baryon [meson] mass, $\Omega = \sqrt{M^2 + \mathbf{q}^2}$, and $\omega = \sqrt{m^2 + \mathbf{q}^2}$.

The model also includes BSEC, which can be considered as the flavor-singlet q^3 pole, or more accurately, as a pole not originated from the baryon-meson degrees of freedom. We divide the model space into P (the baryon-meson space) and Q (the BSEC space). Because the Q-space contains only one state, we can safely

---

[2] This work has been done in collaboration with Kiyotaka Shimizu (Sophia University).

set $V_{QQ} = 0$. Using $P + Q = 1$, we obtain the T-matrix as:

$$T = T^{(P)} + (1 + V_{PP}G_P)V_{PQ}G_Q V_{QP}(1 + G_P V_{PP}) , \qquad (3)$$

where $T^{(P)}$ is the T-matrix solved within the P-space.

The potential we employ is separable:

$$V_{PP} = \sum_{i<j} f_{ij} \frac{V_0}{8} \exp[-\frac{1}{4}a^2(p^2 + p'^2)] \qquad (4)$$

$$V_{PQ} = V_0' \sum_i f_i'(c_1 + c_p b^2 p^2) \exp[-\frac{1}{4}b^2 p^2] . \qquad (5)$$

Here V_0 is taken so that the strength of the potential is the same as that of the chiral model approach. The factor f_{ij} corresponds to the Casimir operator in the flavor space, $\langle F_{Bi} \cdot F_{Mj} \rangle$, when we investigate the chiral-unitary type model. This we call the FF-type in the following. To investigate the quark model, we also use f_{ij} whose channel dependence is color-magnetic-like: $\langle -(\lambda \cdot \lambda)(\sigma \cdot \sigma) \rangle$, which we call λλσσ-type. As shown in Table 1, the FF-type interaction is strongly attractive both in the $N\overline{K}$ and $\Sigma\pi$ channels, while λλσσ-type is attractive in the $\Sigma\pi$ channel, but not in the $N\overline{K}$ channel. We also show the f_i' value for the transfer potential. This is calculated by assuming that the pole is flavor-singlet for the FF-type, while we use the quark model value for the λλσσ-type.

Table 1. Matrix elements f_{ij} and f_i' for the FF-type and and λλσσ-type models.

FF-type	$\Sigma\pi$	$N\overline{K}$	$\Lambda\eta$	ΞK
$\Sigma\pi$	-8	$\sqrt{6}$	0	$-\sqrt{6}$
$N\overline{K}$		-6	$3\sqrt{2}$	0
$\Lambda\eta$			0	$-3\sqrt{2}$
ΞK				-6
f_i'	$\sqrt{\frac{3}{8}}$	$-\frac{1}{2}$	$\sqrt{\frac{1}{8}}$	$\frac{1}{2}$

λλσσ-type	$\Sigma\pi$	$N\overline{K}$	$\Lambda\eta$	ΞK
$\Sigma\pi$	$-\frac{16}{3}$	$\frac{116\sqrt{7}}{21}$	$-\frac{16\sqrt{105}}{105}$	0
$N\overline{K}$		0	$\frac{28\sqrt{15}}{15}$	0
$\Lambda\eta$			$\frac{112}{15}$	$-\frac{40\sqrt{70}}{21}$
ΞK				$-\frac{160}{21}$
$V_0' f_i'$	140	-85	53	$-$

The condition to form the resonance by about 30MeV below the $N\overline{K}$ threshold and 80 MeV above the $\Sigma\pi$ threshold, which is numerically we confirmed in this work, is as follows. (A) Suppose there is no Q-space, there has to be a strong attraction in the $N\overline{K}$ channel, but not in the $\Sigma\pi$ channel. Otherwise, there may be a $\Sigma\pi$ bound state or threshold enhancement, but it is impossible to form a resonant peak by 80 MeV above the $\Sigma\pi$ threshold. (B) Suppose the $N\overline{K}$ channel is not attractive enough, it is necessary to introduce the Q-space. In the case (B), there is another kind of condition to have a 'broad' peak. All the continuum states except for those below the pole energy push the pole state downwards by the interaction V_{QP}. On the other hand, the width is governed by the size of V_{QP} at around the

pole energy, where p is about 0.75 fm^{-1}. So, suppose the interaction V_{QP} is proportional to p^2 (the c_p term), the real part of the pole energy reduces more rapidly than the imaginary part increases. This will result a narrow peak. In contrast to this, the c_1 term tends to produce a peak with a broader width.
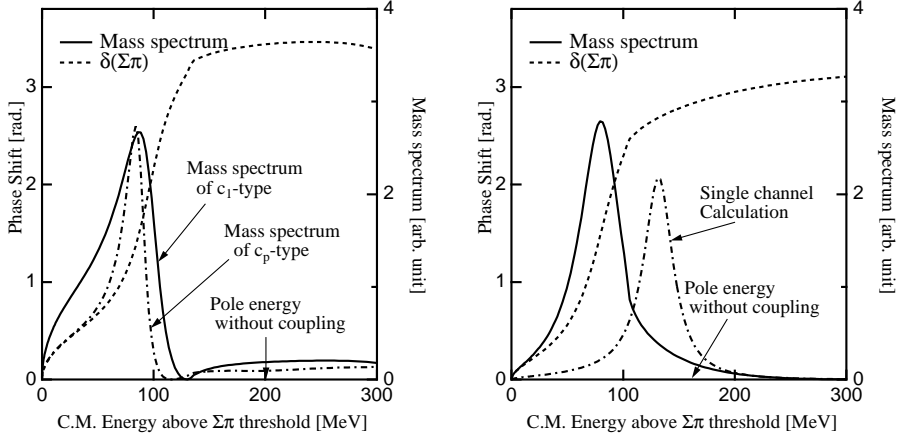

Fig.2. Mass spectrum and the phase shift (δ) given by the baryon-meson model with the FF-type (left figure) or the CM-type (right figure) potential.

It is found that the FF-type model can reproduce the peak without introducing an extra pole if the cutoff energy of the baryon-meson interaction is rather high. This situation is similar to the chiral unitary approach. One of the key points here is that the green function, eq. (2), contains the m/ω factor, which suppresses the strong attraction in the $\pi\Sigma$ channel. This picture corresponds to the condition (A) mentioned above.

When one uses the form factor which corresponds to the baryon and meson sizes in the quark model, however, the effective cutoff becomes lower, and the interaction becomes weaker. In such a case, the model requires an extra pole, which can be considered as the flavor-singlet q^3 pole, to reproduce the observed peak (Figure 2). The situation corresponds to the condition (B). By assuming $c_1 \neq 0$ and and $c_p = 0$ (c_1-type in the Figure 2), the peak actually becomes broad. The $N\overline{K}$ scattering length becomes $-1.68 + i0.42$, which also agrees well with the experimental value, $-(1.70 \pm 0.07) + i(0.68 \pm 0.04)$ [3].

When we employ the $\lambda\lambda\sigma\sigma$-type interaction, we find that the model reproduces a peak similar to the original one by introducing the q^3 pole. The situation also corresponds to the condition (B). Here, we use the c_1-type for the simplicity, though both of the c_1 and c_p have nonzero values in the quark model picture, which can be obtained by keeping the center of mass momentum of the quark system equal to zero.

Table 2. Matrix elements of the interactions between $q\bar{q}$ pairs. The color-magnetic interaction, $-\langle(\lambda \cdot \lambda)(\sigma \cdot \sigma)\rangle$, is denoted as CMI, the pair-annihilating term of OGE (OGE-a), the spin-color part of the instanton induced interaction (Ins), and estimate value by a typical parameter set, E.

color	spin	flavor	CMI	OGE-a	Ins	E[MeV]	States
1	0	1	−16	0	12	84	η
1	0	8	−16	0	−6	−327	π, K
1	1	1	16/3	0	0	63	ω
1	1	8	16/3	0	0	63	ρ
8	0	1	2	0	3/4	41	
8	0	8	2	0	−3/8	15	
8	1	1	−2/3	9/2	9/4	97	
8	1	8	−2/3	0	−9/8	−34	$c\bar{c}q\bar{q}$ with $J^{PC}=0^{++},1^{+-},1^{++},2^{++}$

We argue that both of the pole originated from the quark degrees of freedom and the baryon-meson continuum play important roles to form the Λ(1405) resonance[6].

3   X(3872)[3]

After the discovery and the confirmations of the peak X(3872) and enhancement X(3941) in the $\pi^+\pi^- J/\psi$ channel [8,9], many works on these peaks have been reported. The peak X(3872) does not seem a simple $c\bar{c}$ state, as was summarized in, *e.g.*, Ref. [10]. The fitting of the $\pi\pi$ mass spectrum of the experiment suggests that the peak X(3872) is $\rho + J/\psi$ with $J^{PC} = 1^{++}$ [11]. Many theoretical works have also been performed. It was suggested that this peak is a higher partial wave of the charmonium state, a DD^* molecule, a $q\bar{q}c\bar{c}$ multiquark state, or the bound state of the charmonium with a glue-ball, $c\bar{c}g$. The situation is summarized, *e.g.*, in ref. [12].

One of the most promising explanations is that the peak is a $q\bar{q}c\bar{c}$ state. The width of the X(3872) is narrow, less than 2.3 MeV [9]; namely, its decay to the DD channel should be forbidden. This restricts the spin-parity of the state. It seems that 1^{++} state is the strongest candidate [12].

In this work, the $q\bar{q}c\bar{c}$ systems are investigated by a quark model with the orbital correlations. The model hamiltonian has the long-range π- and σ-meson exchange between quarks in addition to OGE and Ins.

The wave function of the $q\bar{q}c\bar{c}$ systems consists of the color, flavor, spin, and orbital parts. The flavor part is taken to be $q\bar{q}c\bar{c}$. The spin of the $q\bar{q}$, as well as that of $c\bar{c}$, is taken to be 1, so that the C-parity is kept positive within this part. The total spin is also taken to be 1. The orbital correlation is fully taken into account by performing the the stochastic variational approach. The color part has two

---

[3] This work has been partially done in collaboration with Amand Faessler, Thomas Gutsche, Valery E. Lyubovitskij (X(3872), Inst. für Theo. Physik, Universität Tübingen) and published in Ref. [7].
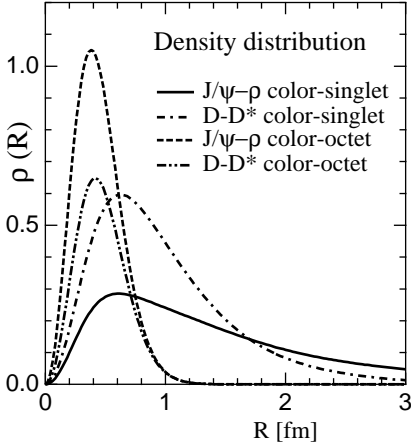
Table 3: Binding energies of the $q\bar{q}c\bar{c}$ state.

IJ^{PC}	11^{++}	01^{++}
Parameter set A	26 MeV	5 MeV
Parameter set B	5 MeV	Not bound
Parameter set A + c$\bar{c}$-pole	26 MeV	~25 MeV

Fig.3. Density distribution of the $q\bar{q}c\bar{c}$ bound state in the T=1 J^{PC}=1^{++} channel.

components: the one where the $c\bar{c}$ pair is color-singlet, $(J/\psi\rho)_{11}$, and the color-octet one, $(J/\psi\rho)_{88}$.

Since the hyperfine interaction between the quarks is inversely proportional to m_{quark}, properties of this system depend mainly on the interaction between the light quark-antiquark pair. In Table 2, we show the matrix elements of relevant interactions: the color-magnetic interaction (CMI), the pair-annihilating term of OGE (OGE-a), Ins, and an estimate by a typical parameter set used for a quark model. The most attractive pair is the color-singlet, spin 0, flavor-octet, which exists, *e.g.* in the pion. There is another weak, but still attractive pair: the color-octet, spin 1, flavor-octet one. Such a pair is found in the $q\bar{q}c\bar{c}$ isospin T=1 systems. T=0 pairs may also be attractive if OGE-a and Ins are weak, whose size is not well known in these channels.

By using a parameter set which gives correct baryon and meson spectrum, we find a J^{PC} = 1^{++} bound state for each of the T=1 and 0 channels (Table 3). The absolute value of the binding energy, however, depends on the strength of the σ-meson exchange: we can also find a parameter set which gives equally good hadron mass spectrum, but gives a bound state only for the T=1 state.

In Figure 3, the density distribution of the $(J/\psi\rho)_{11}$ and $(J/\psi\rho)_{88}$ components in the T=1 bound state is shown as a function of relative distance between J/ψ and ρ. The $(J/\psi\rho)_{11}$ component, having a long tail, looks like a J/ψ-ρ molecule. $(J/\psi\rho)_{88}$, in which the confinement keeps the two color-octet mesons close, has large overlap to $(DD^*)_{11}$. So, we also show the the density distribution of the $(DD^*)_{11}$ and $(DD^*)_{88}$ components as a function of relative distance between D and D* in the figure. The $(DD^*)_{11}$ component has also a long tail, which looks again like a molecule.

The obtained bound state, however, is not a simple two-meson molecule. The multiquark component, where quarks in different color-singlet mesons are also correlated, is found to be important; suppose the orbital wave function is re-

stricted to $\phi_{J/\psi}\phi_\rho\psi(R_{J/\psi\rho})$ and $\phi_D\phi_{D*}\psi(R_{DD*})$ without inter-meson quark correlation, the binding energy reduces by 17 MeV.

As for the T=0 channel, there should be a mixing between the $q\bar{q}c\bar{c}$ state and the $c\bar{c}$ excited state. We assume that it occurs by OGE, as we did in Λ(1405), and that the mass of $c\bar{c}$ state is 3950 MeV, which corresponds to the value calculated by Godfrey *et al.* [13]. When this coupling is switched on, we find that the binding energy increases by about 20 MeV (the precise value depends on the parameters). Namely, masses of the isospin 1 state and 0 state can be close to each other, which may cause a rather large mixing between these states.

Since the isospin symmetry of this system is broken as seen from $m_{D\pm} - m_{D^0}$ = 4.78 MeV, X(3872) may be a superposition of the above two bound states. Actually, a toy model of two free scattering channels and two poles with T=0 and 1, shows us that the threshold difference mixes the isospin of the shallow bound state considerably.

We consider that feature of the system can be explained by a two-meson molecule with a short-ranged attractive multiquark configuration and the excited $c\bar{c}$ core state.

References

1. S. Takeuchi and K. Shimizu, Phys. Rev. C **76**, 035204 (2007).
2. See, *e.g.*, M. Furuichi, K. Shimizu, and S. Takeuchi, Phys. Rev. C **68**, 034001 (2003).
3. A. D. Martin, Nucl. Phys. B **179**, 33 (1981).
4. E. Oset and A. Ramos, Nucl. Phys. A **635**, 99(1998).
5. T. Hyodo, *et al*, Phys. Rev. C **78**, 025203 (2008).
6. S. Takeuchi and K. Shimizu, in preparation.
7. S. Takeuchi, V. E. Lyubovitskij, T. Gutsche and A. Faessler, Nucl. Phys. A **790** (2007) 502; S. Takeuchi, in preparation.
8. S. K. Choi *et al.* [Belle Collaboration], Phys. Rev. Lett. **91**, 262001 (2003).
9. C. Amsler *et al.* [Particle Data Group], Phys. Lett. **B667**, 1 (2008).
10. G. Bauer, Int. J. Mod. Phys. A **21**, 959 (2006).
11. D. V. Bugg, Phys. Rev. D **71**, 016006 (2005).
12. E. S. Swanson, Phys. Rept. **429**, 243 (2006) and references therein.
13. S. Godfrey and N. Isgur, Phys. Rev. D **32**, 189 (1985).

Charm and Charmonium Spectroscopy at Belle

M. Bračko, representing the Belle Collaboration

University of Maribor, Smetanova ulica 17, SI-2000 Maribor, Slovenia
Jožef Stefan Institute, Jamova cesta 39, SI-1000 Ljubljana, Slovenia

Abstract. The Belle experiment at the KEKB asymmetric-energy e^+e^- collider provides an excellent environment not only for B physics, but also for studies in charm and charmonium spectroscopy. Most important Belle achievements in this field include observations of several yet undiscovered particles and measurements of their properties. In this paper we report and briefly discuss most recent of these experimental results.

1   Introduction

The Belle detector [1] at the asymmetric-energy e^+e^- collider KEKB [2] has accumulated about 850 fb^{-1} of data by July 2008. The KEKB collider is called a *B-factory*; it operates with a peak luminosity that exceeds 1.7×10^{34} cm^{-2}s^{-1} at the $\Upsilon(4S)$ resonance, slightly above the $B\overline{B}$-production threshold, and the accumulated data set contains a large number of $B\overline{B}$ pairs. Although both B-factories—a similar collider called PEP-II delivers data to the *BABAR* detector—were initially designed for measurements of CP violation in the B-meson system, it was soon clear that excellent detector performance and large amount of experimental data also enable searches for new charm and charmonium states as well as studies of their properties.

2   Excited charmed strange mesons (D_{sJ})

The interest in D_{sJ} mesons received a boost after recent discoveries of two states: $D_{s0}^*(2317)^+$ in $D_s^+\pi^0$ decay mode[1] and $D_{s1}(2460)^+$ in $D_s^{*+}\pi^0$ mode, both observed with continuum $e^+e^- \to c\bar{c}$ events by the *BABAR* [3] and CLEO [4] collaborations, respectively. Belle confirmed the existence of the two states in continuum events [5], but also in $B \to \overline{D}D_{sJ}$ decays [6]. An angular analysis performed in the latter case, favours the $J^P = 0^+$ and 1^+ values for $D_{s0}^*(2317)^+$ and $D_{s1}(2460)^+$, respectively.

   Due to the D_s meson in their final state, the states $D_{s0}^*(2317)^+$ and $D_{s1}(2460)^+$ are most naturally interpreted as P-wave excited $c\bar{s}$ states with $j = |\mathbf{L} + \mathbf{S_{\bar{s}}}| = 1/2$, where $|\mathbf{L}| = 1$ is the orbital angular momentum and $\mathbf{S_{\bar{s}}}$ is the spin of the

---

[1] Charge-conjugated modes are implied, unless explicitly stated otherwise.

light $\bar{s}$-antiquark. Nonetheless, while the masses and widths of previously observed $D_{s1}(2536)^+$ and $D_{s2}(2573)^+$ are in relatively good agreement with potential model predictions, both the masses and widths of $D_{s0}^*(2317)^+$ and $D_{s1}(2460)^+$ states are smaller than expected (see Ref. [7] for a discussion of $c\bar{s}$ models). Additionally, the mass difference between the two newly observed states is much larger that the difference between the masses of $D_{s1}(2536)^+$ and $D_{s2}(2573)^+$. All these properties have led to interpretations of the $D_{s0}^*(2317)^+$ and $D_{s1}(2460)^+$ as four-quark states or at least as states with significant four-quark content. Experimentally, these interpretations could be tested in decays $\overline{B}^0 \to D_{sJ}^+ K^-$, where the initial $\overline{B}^0$-meson quark content ($b\bar{d}$) is completely different from the one in the $D_{sJ}^+ K^-$ final state ($c\bar{s}s\bar{u}$). However, Belle results [8] were not conclusive about the four-quark content of $D_{s0}^*(2317)^+$ and $D_{s1}(2460)^+$, but at least supported the claim that these two states do not belong to the same spin-doublet.

2.1 Observation of a new state $D_{sJ}(2700)^+$
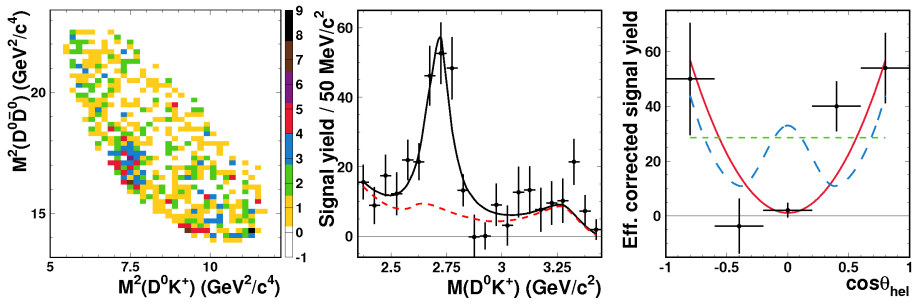
Fig.1. Left: Dalitz plot for $B^+ \to \overline{D}^0 D^0 K^+$ decays. **Centre**: B meson signal yield versus $M(D^0 K^+)$ for $M(D^0 \overline{D}^0) > 3.85\ \text{GeV}/c^2$. The solid curve denotes the total fit result, while the dotted curve shows the sum of non-$D_{sJ}(2700)^+$ components—including the $\psi(4160)$ reflection on the right. **Right**: Efficiency corrected $D_{sJ}(2700)^+$ helicity-angle distribution together with predictions for various spin hypotheses: $J = 0$ (dotted line), 1 (solid line) and 2 (dashed line).

In order to obtain further experimental data and help resolve the issues for D_{sJ} states, Belle recently performed an analysis of the $B^+ \to \overline{D}^0 D^0 K^+$ decays using a data sample containing about $449 \cdot 10^6$ $B\overline{B}$ pairs [9]. A study of the Dalitz plot for the ΔE-M_{bc} signal region[2] (see the left-most plot in Fig. 1) revealed that the decay $B^+ \to \overline{D}^0 D^0 K^+$ proceeds dominantly via quasi-two-body channels: $B^+ \to \psi(3770)K^+$ and $B^+ \to \overline{D}^0 D_{sJ}(2700)^+$. While the observed rate for $\psi(3770)$ production in B meson decays is consistent with our previous observation [10],

---

[2] The two kinematic variables identify B-meson candidates: $\Delta E \equiv E_B - E_{beam}$ and $M_{bc} \equiv 1/c^2 \sqrt{E_{beam}^2 - (p_B c)^2}$, where E_B and p_B are the energy and momentum of the B candidate, and E_{beam} is the beam energy, all expressed in the centre-of-mass (CM) frame.

the $D_{sJ}(2700)^+$ is a previously unobserved resonance in the D^0K^+ system (see the central plot in Fig. 1) with a mass of $M = (2708 \pm 9^{+11}_{-10})$ MeV/c^2 and a width of $\Gamma = (108 \pm 23^{+36}_{-31})$ MeV/c^2. The observed decay mode and angular analysis (see the right-most plot in Fig. 1) clearly favour the interpretation of $D_{sJ}(2700)^+$ as a $c\bar{s}$ meson with $J^P = 1^-$. The new meson could be a $c\bar{s}$ radially excited 2^3S_1 state [11] with a mass of $(2710 - 2720)$ MeV/c^2 or the 1^- chiral partner [12] of the $D_{s1}(2536)^+$ meson with a mass of (2721 ± 10) MeV/c^2. Additional measurements are needed for the new meson to distinguish between the two existing interpretations.

2.2 $D_{s1}(2460)^+$ - $D_{s1}(2536)^+$ Mixing

Another interesting result on D_{sJ} mesons comes from the recent study [13] of $D_{s1}(2536)^+$ mesons, produced inclusively in $e^+e^- \rightarrow D_{s1}(2536)^+X_{anything}$ reactions. The analysis is based on the e^+e^- continuum data set corresponding to 462 fb^{-1} and uses two decay modes for a $D_{s1}(2536)^+$ reconstruction, namely $D_{s1}(2536)^+ \rightarrow D^+\pi^-K^+$ and $D_{s1}(2536)^+ \rightarrow D^{*+}K^0_S$. The observed invariant mass $M_{D^+\pi^-K^+}$ and the invariant mass difference $M_{D^0\pi^+K^0_S} - M_{D^0\pi^+}$ for all selected $D^+\pi^-K^+$ and $D^0\pi^+K^0_S$ combinations are shown in Fig. 2. The ratio of branching fractions of the two studied decay modes is found to be: $\mathcal{B}(D_{s1}(2536)^+ \rightarrow D^+\pi^-K^+)/\mathcal{B}(D^0\pi^+K^0) = (3.27 \pm 0.18 \pm 0.37)\%$. The decay channel $D_{s1}(2536)^+ \rightarrow D^+\pi^-K^+$ is only the second observed three-body decay mode of the $D_{s1}(2536)^+$ meson (after $D_{s1}(2536)^+ \rightarrow D^+_s\pi^+\pi^-$) [14].

The large and clean $D_{s1}(2536)^+ \rightarrow D^{*+}K^0_S$ sample enables a partial-wave analysis for this decay mode. Heavy Quark Effective Theory (HQET) predicts that for an infinitely heavy c-quark the $D^{*+}K^0_S$ decay of the $|J^P = 1^+; j = 3/2\rangle$ state, $D_{s1}(2536)^+$, should proceed via a pure D-wave [15]. The same decay of its partner $D_{s1}(2460)^+$, the $|1^+; 1/2\rangle$ state, would proceed via a pure S-wave—if this was energetically allowed. Since the heavy quark symmetry is not exact, the two states can mix, and an S-wave component can appear in the decay $D_{s1}(2536)^+ \rightarrow D^*K$. Even if mixing is small, the S-wave contribution to the total width can be sizeable, since the D-wave contribution is strongly suppressed by the small energy release in this decay. Using a small polarization of $D_{s1}(2536)^+$ mesons produced in e^+e^- annihilations and performing a simultaneous fit to the three angles in the decay $D_{s1}(2536)^+ \rightarrow D^{*+}K^0_S; D^{*+} \rightarrow D^0\pi^+$, the measurement shows that the S-wave actually dominates. Its contribution to the total width in the decay $D_{s1}(2536)^+ \rightarrow D^{*+}K^0_S$ is $\Gamma_S/\Gamma_{total} = 0.72 \pm 0.05 \pm 0.01$. This result indicates there is a mixing between the two states: $D_{s1}(2536)^+$ and $D_{s1}(2460)^+$.

3   Charmonium and Charmonium-like States

There are several possible mechanisms of the charmonium(-like) particle production at B-factories: production in the B-meson decays, formation of C-even states in $\gamma\gamma$ processes and in e^+e^- annihilation into $J/\psi(c\bar{c})$, and creation of $J^{PC} = 1^{--}$ resonances in e^+e^- annihilation after the photon radiative return. Several of these
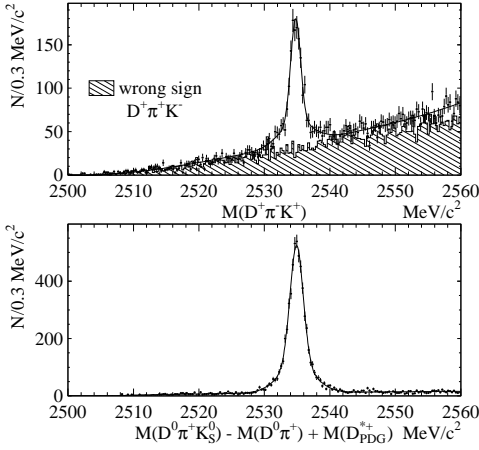
Fig.2. Invariant mass spectra of selected $D^+\pi^-K^+$ (**Top**) and $D^{*+}K^0_S$ (**Bottom**) combinations. The hatched histogram in the top plot shows the spectrum of wrong sign $D^+\pi^+K^-$ combinations. The $M(D^{*+}_{PDG})$ in the bottom denotes the D^{*+} nominal mass from Ref. [14].
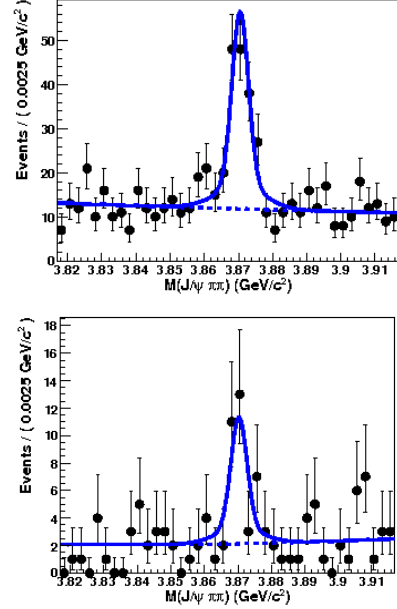
Fig.3. Invariant mass distributions of $J/\psi\pi^+\pi^-$ combinations for $B^+ \rightarrow K^+X(3872)$ (**Top**) and $B^0 \rightarrow K^0_S X(3872)$ (**Bottom**) decay candidates. The fit results are shown with solid curves.

charmonium(-like) particles have been recently discovered. The naming convention for these new X, Y, Z states indicates the lack of knowledge about their structure and properties at the time of discovery.

3.1 The X(3872) news

In 2003 Belle reported on the $B^+ \rightarrow K^+J/\psi\pi^+\pi^-$ analysis [16], where a narrow charmonium-like state X(3872) decaying to $J/\psi\pi^+\pi^-$ was discovered, and soon confirmed by CDF, D0 and *BABAR*[17]. In PDG2006 [14], the world average of the mass is (3871.2 ± 0.5) MeV/c^2 and the upper limit on its width, as measured by Belle, is 2.3 MeV. X(3872) does not appear to be a simple charmonium state and its quantum numbers are not yet determined. The observed X(3872) $\rightarrow \gamma J/\psi$ decay [18] (implying C = +1) as well as results of angular analyses [19,20] and studies of $J/\psi\pi^+\pi^-$ kinematical properties favour $J^{PC} = 1^{++}$ and 2^{-+} assignments. The latter possibility could have been ruled out by the study of $B \rightarrow KD^0\overline{D}^0\pi^0$ decays, where a near-threshold enhancement for the $D^0\overline{D}^0\pi^0$ invariant mass was observed at $(3875.4 \pm 0.7 \pm 1.1)$ MeV/c^2 [21]. However, since the invariant mass of the $D\overline{D}\pi$ peak was about 2σ higher than the world average value for X(3872), this result encouraged speculations about the two similar states, as predicted by a four-quark model of X(3872)[22]. Another interpretation of X(3872), a $D^0\overline{D}^{*0}$
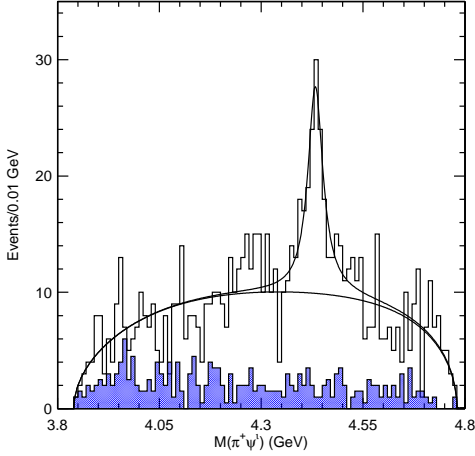
Fig.4. The $\pi^+\psi(2S)$ invariant mass distribution for events in the ΔE-M_{bc} signal region. The shaded histogram shows the scaled contribution from the ΔE sideband, while the solid curves correspond to the fit result.
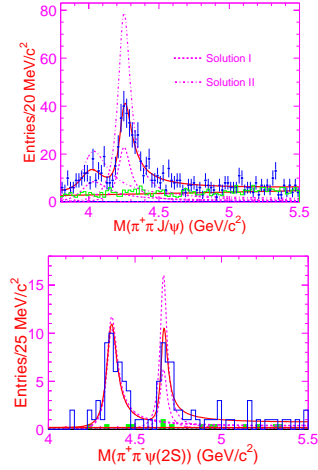
Fig.5. The mass distributions for $\pi^+\pi^- J/\psi$ (**Top**) and $\pi^+\pi^-\psi(2S)$ (**Bottom**) combinations from e^+e^- annihilation with the ISR photon. The curves show the fit and contributions of individual resonances for constructive (Solution I) and destructive (Solution II) interference.

molecule, is strongly motivated by the fact that the X(3872) mass is very close to the $D^0\overline{D}^{*0}$ threshold [23].

Belle recently reported on the updated X(3872) analysis, using the data sample of $657 \cdot 10^6$ $B\overline{B}$ pairs [24]. X(3872) $\rightarrow$ $J/\psi\pi^+\pi^-$ decays are reconstructed in both charged and neutral B decays (see Fig. 3), and the observed ratio of the branching fractions, $\mathcal{B}(B^0 \rightarrow K_S^0 X(3872))/\mathcal{B}(B^+ \rightarrow K^+ X(3872)) = 0.82 \pm 0.22 \pm 0.05$, is of the order of unity. Comparison of the neutral and charged B-meson signal can serve as a test for the four-quark hypothesis of X(3872), which predicts the existence of two four-quark states—$c\bar{c}u\bar{u}$ should be produced mainly in charged and $c\bar{c}d\bar{d}$ in neutral B-meson decays—with a mass difference of $\Delta M = (8 \pm 3)$ MeV/c^2 [22]. In contrast to this expectation, no mass difference between the X(3872) candidates in charged and neutral B-meson decay is observed: $\Delta M = (0.18 \pm 0.89 \pm 0.26)$ MeV/c^2. The measurements therefore favour the charm-meson molecular interpretation of X(3872), although the virtual state of two charm mesons is also not excluded [25].

3.2 Charged charmonium-like state: $Z^+(4430)$, ...

Recently a new charged state was observed by the B $\rightarrow$ $K\pi^\pm\psi(2S)$ Dalitz analysis, performed on a data sample with $657 \cdot 10^6$ $B\overline{B}$ pairs [26]. Both charged and neutral B decays are used, and the $\psi(2S)$ candidates are reconstructed in four decay modes: e^+e^-, $\mu^+\mu^-$, and $J/\psi\pi^+\pi^-$ with $J/\psi \rightarrow e^+e^-$, $\mu^+\mu^-$. After excluding the $K\pi$ Dalitz regions that correspond to $K^*(890)$ and $K_2^*(1430)$

Table 1. Properties of $J^{PC} = 1^{--}$ states (Y resonances) observed by Belle using the ISR technique.

Y state	Decay mode	M (MeV/c^2)	Γ (MeV)
Y(4008)	J/ψπ$^+$π$^-$	$4008 \pm 40^{+114}_{-28}$	$226 \pm 44 \pm 87$
Y(4260)	J/ψπ$^+$π$^-$	$4247 \pm 12^{+17}_{-32}$	$108 \pm 19 \pm 10$
Y(4360)	ψ(2S)π$^+$π$^-$	$4361 \pm 9 \pm 9$	$74 \pm 15 \pm 10$
Y(4660)	ψ(2S)π$^+$π$^-$	$4664 \pm 11 \pm 5$	$48 \pm 15 \pm 3$

mesons, a strong enhancement is seen in the $\pi^+\psi(2S)$ invariant mass distribution (Fig. 4). A fit with a Breit-Wigner shape yields a peak mass and width of $(4433 \pm 4 \pm 2)$ MeV/c^2 and (45^{+18+30}_{-13-13}) MeV, with a 6.5σ statistical significance. The observed resonance called Z$^+$(4430)—if confirmed by other experiments— would be the first charmonium-like meson candidate with non-zero charge, and could be interpreted as a charged molecular or a four-quark state. Systematic studies of B $\to$ K$\pi(c\overline{c})$ decays could reveal other similar neutral and charged partners [22]. During the preparation of this paper, a study was already reported, indicating the existence of a broad doubly peaked structure in the $\pi^+\chi_{c1}$ mass for exclusive $\overline{B}^0 \to K^-\pi^+\chi_{c1}$ decays [27].

3.3 Study of $J^{PC} = 1^{--}$ states using ISR

Initial-state radiation (ISR) has proven to be a powerful tool to search for 1^{--} states at B-factories, since it allows to scan a broad energy range of $\sqrt{s}$ below the initial e^+e^- CM energy, while the high luminosity compensates for the suppression due to the hard-photon emission. With the ISR technique, *BABAR* discovered Y(4260) state above D$^{(*)}\overline{D}^{(*)}$ threshold in the $e^+e^- \to \gamma_{ISR}Y(4260) \to \gamma_{ISR}J/\psi\pi^+\pi^-$ process [28].

Using the same method as *BABAR* on a data sample of 548 fb^{-1}, Belle recently confirmed the Y(4260) state, but also found another resonant structure, called Y(4008) (see the top plot of Fig. 5)[29]. A similar analysis was performed on a 673 fb^{-1} data sample to study the ISR e^+e^- annihilation process resulting in the $\psi(2S)\pi^+\pi^-$ final state [30]. The obtained $\psi(2S)\pi^+\pi^-$ mass distribution, shown in the bottom plot of Fig. 5, reveals two resonant structures, called Y(4360) and Y(4660). While Y(4660) still needs a confirmation, the former resonance, Y(4360), has a mass similar to the wide structure at (4324 ± 24) MeV/c^2, observed previously by *BABAR*[31]. Fit results for Belle measurements are summarized in Table 1. The four Y states observed in J/ψπ$^+$π$^-$ and ψ(2S)π$^+$π$^-$ decay modes are distinctive, although there is a hint that Y(4260) could also be seen in the ψ(2S)π$^+$π$^-$ decay mode [32]. The nature of Y states and their strong couplings to J/ψπ$^+$π$^-$ and ψ(2S)π$^+$π$^-$ are somewhat puzzling: such heavy charmonium(-like) states should decay mainly to D$^{(*)}\overline{D}^{(*)}$, but it seems that observed Y states do not match the peaks in $e^+e^- \to$ D$^{(*)\pm}$D$^{(*)\mp}$ cross sections, measured by Belle with ISR at $\sqrt{s} < 5$ GeV [33].
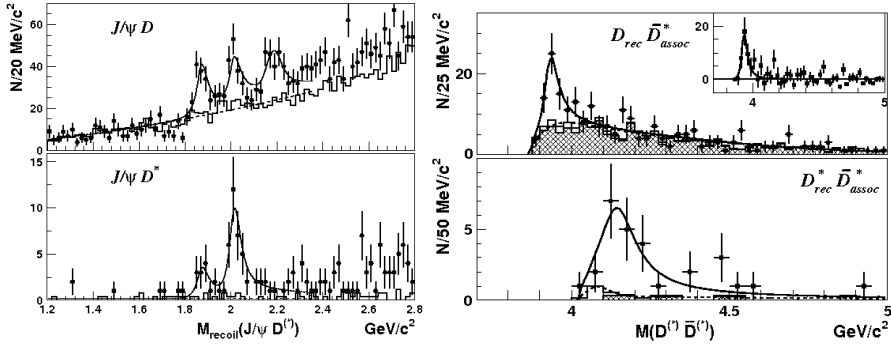
Fig.6. Left: $J/\psi D^{(*)}$ recoil mass distribution, showing peaks at D, D^* and $D^*\pi$ mass. Histograms show the scaled $D^{(*)}$ sidebands; curves indicate the total fit result (solid) and the background component (dashed). **Right**: The $D^{(*)}\overline{D}^{(*)}$ mass distributions for $e^+e^- \rightarrow J/\psi D^{(*)}\overline{D}^{(*)}$ events.

3.4 Double $c\overline{c}$ production in e^+e^- annihilation

Belle observed a surprisingly large double charmonium production in a study of the J/ψ and $\psi(2S)(\rightarrow J/\psi\pi^+\pi^-)$ recoil mass[3] spectrum for inclusive $e^+e^- \rightarrow J/\psi X$ processes [34]. The extracted $e^+e^- \rightarrow J/\psi(c\overline{c})$ cross-section was more than five times larger than values from the tree-level QCD calculation and still represents a challenge for theorists. The J/ψ recoil method was further improved

Table 2. Properties of two states observed in double $c\overline{c}$ production. Significance includes systematic uncertainties.

X state	Decay mode	M (MeV/c²)	Γ (MeV)	Significance (σ)
X(3940)	$D\overline{D}^{(*)}$	$3942^{+7}_{-6} \pm 6$	$37^{+26}_{-15} \pm 8$	5.7
X(4160)	$D^{(*)}\overline{D}^{(*)}$	$4156^{+25}_{-20} \pm 15$	$139^{+111}_{-61} \pm 21$	5.1

and used for studies of C = +1 charmonium states above $D\overline{D}$ threshold. A $D^{(*)}$ meson besides the J/ψ is reconstructed, and a constraint $M_{recoil}(J/\psi D^{(*)}) \sim M(\overline{D}^{(*)}_{PDG})$ is then applied to select $e^+e^- \rightarrow J/\psi D^{(*)}\overline{D}^{(*)}$ events (see the recoil mass distributions in Fig. 6). As a result of this method, two states, X(3940) and X(4160), were identified in the $D\overline{D}^*$ and $D^*\overline{D}^*$ distributions, respectively [35,36]. The fit results for the two peaks, shown in Fig. 6, are summarized in Table 2. Possible interpretation for these states include conventional $\eta_c(3S)$ and $\chi_{c0}(3P)$ charmonia.

---

[3] E.g. the J/ψ recoil mass, $M_{recoil}(J/\psi) = 1/c^2\sqrt{(E_{CM} - E^*)^2 - (cp^*)^2}$, is calculated in the CM frame with the total event energy (E_{CM}) and J/ψ energy and momentum (E^* and p^*).

4   Summary and Conclusions

The Belle experiment at the KEKB collider provides an excellent environment for charm and charmonium spectroscopy. As a result, many new particles have already been discovered during the Belle operation, and some of them — like $D_{sJ}(2700)^+$, $X(3872)$, $X(3940)$, $X(4160)$ and $Z^+(4430)$— are mentioned in this report. As new experimental data are still accumulated and many studies are ongoing, more interesting results on charm and charmonium spectroscopy are to be expected from Belle in the near future.

The Belle experimental results have already raised a lot of interest among theoretical physicists. Various interpretations for the nature and properties of newly observed states have been proposed. Some of the answers might be found in the near future, perhaps following also the ideas presented at this workshop.

References

1. A. Abashian *et al.* (Belle Coll.), Nucl. Instr. and Meth. A **479**, 117 (2002).
2. S. Kurokawa and E. Kikutani, Nucl. Instr. and Meth. A **499**, 1 (2003),
    and other papers included in this Volume.
3. B. Aubert *et al.* (B*A*B*AR* Coll.), Phys. Rev. Lett. **90**, 242001 (2003).
4. D. Besson *et al.* (CLEO Coll.), Phys. Rev. D **68**, 032002 (2003).
5. Y. Mikami *et al.* (Belle Coll.), Phys. Rev. Lett. **92**, 012002 (2004).
6. P. Krokovny *et al.* (Belle Coll.), Phys. Rev. Lett. **91**, 262002 (2003).
7. R. N. Cahn and J. D. Jackson, Phys. Rev. D **68**, 037502 (2003).
8. A. Drutskoy *et al.* (Belle Coll.), Phys. Rev. Lett. **94**, 061802 (2005);
    K. Abe *et al.* (Belle Coll.), Belle-CONF-0511, `arXiv:hep-ex/0507064`.
9. J. Brodzicka *et al.* (Belle Coll.), Phys. Rev. Lett. **100**, 092001 (2008).
10. R. Chistov *et al.* (Belle Coll.), Phys. Rev. Lett. **93**, 051803 (2004).
11. S. Godfrey and N. Isgur, Phys. Rev. D **32**, 189 (1985);
    F. E. Close *et al.*, Phys. Lett. B **647**, 159 (2007).
12. M. A. Nowak *et al.*, Acta Phys. Pol. B **35**, 2377 (2004).
13. V. Balagura *et al.* (Belle Coll.), Phys. Rev. D **77**, 032001 (2008).
14. W.-M. Yao *et al.* (Particle Data Group), J. Phys. G **33**, 1 (2006).
15. N. Isgur and M. Wise, Phys. Rev. Lett. **66**, 1130 (1991);
    M. Lu *et al.*, Phys. Rev. D **45**, 1553 (1992).
16. S.-K. Choi, *et al.* (Belle Coll.), Phys. Rev. Lett. **91**, 262001 (2003).
17. D. Acosta *et al.* (CDF II Coll.), Phys. Rev. Lett. **93**, 072001 (2004);
    V. M. Abazov *et al.* (D0 Coll.), Phys. Rev. Lett. **93**, 162002 (2004);
    B. Aubert *et al.* (B*A*B*AR*Coll.), Phys. Rev. D **71**, 071103 (2005).
18. K. Abe *et al.* (Belle Coll.), Belle-CONF-0540, `arXiv:hep-ex/0505037`.
19. K. Abe *et al.* (Belle Coll.), Belle-CONF-0541, `arXiv:hep-ex/0505038`.
20. A. Abulencia *et al.* (CDF Coll.), Phys. Rev. Lett. **98**, 132002 (2007).
21. G. Gokhroo *et al.* (Belle Coll.), Phys. Rev. Lett. **97**, 162002 (2006).
22. L. Maiani *et al.*, Phys. Rev. D **71**, 014028 (2005), and `arXiv:0708.3997 [hep-ph]`.
23. E. S. Swanson, Phys. Lett. B **588**, 189 (2004);
    N. A. Törnqvist, Phys. Lett. B **590**, 209 (2004).
24. K. Abe *et al.* (Belle Coll.), Belle-CONF-0711, `arXiv:0809.1224 [hep-ex]`.
25. E. Braaten and M. Lu, `arXiv:0710.5482 [hep-ph]`.
26. S.-K. Choi, *et al.* (Belle Coll.), Phys. Rev. Lett. **100**, 142001 (2008).

27. R. Mizuk *et al.* (Belle Coll.), `arXiv:0806.4098 [hep-ex]` (to appear in Phys. Rev. D).
28. B. Aubert *et al.* (*BABAR* Coll.), Phys. Rev. Lett. **95**, 142001 (2005).
29. C. Z. Yuan *et al.* (Belle Coll.), Phys. Rev. Lett. **99**, 182004 (2007).
30. X. L. Wang *et al.* (Belle Coll.), Phys. Rev. Lett. **99**, 142002 (2007).
31. B. Aubert *et al.* (*BABAR* Coll.), Phys. Rev. Lett. **98**, 212001 (2007).
32. Z. Q. Liu *et al.*, `arXiv:0805.3560 [hep-ex]`.
33. G. Pakhlova *et al.* (Belle Coll.), Phys. Rev. Lett. **98**, 092001 (2007).
34. K. Abe *et al.* (Belle Coll.), Phys. Rev. Lett. **89**, 142001 (2002);
    K. Abe *et al.* (Belle Coll.), Phys. Rev. D **70**, 071102 (2004).
35. K. Abe *et al.* (Belle Coll.), Phys. Rev. Lett. **98**, 082001 (2007).
36. P. Pakhlov *et al.* (Belle Coll.), Phys. Rev. Lett. **100**, 202001 (2008).

Pion electro-production in a dynamical model including quasi-bound three-quark states[⋆]

B. Golli[a,c] and S. Širca[b,c]

[a]Faculty of Education, University of Ljubljana, 1000 Ljubljana, Slovenia
[b]Faculty of Mathematics and Physics, University of Ljubljana, 1000 Ljubljana, Slovenia
[c]Jožef Stefan Institute, 1000 Ljubljana, Slovenia

Abstract. We present a method to calculate the pion electro-production amplitude in a framework of a coupled channel formalism incorporating quasi-bound quark-model states.

1 Introduction

In our previous work ([1] and [2]) we have developed a general method to incorporate excited baryons represented as quasi-bound quark-model states into a coupled channel calculation using the K matrix. The method has been applied to calculate pion scattering amplitudes in the energy region of low-lying P11 and P33 resonances. In addition to the elastic channel we have included the $\pi\Delta$ and σN ($\sigma\Delta$) channels where the σ-meson models the correlated two-pion decay. We have been able to explain a rather intriguing behaviour of the scattering amplitudes in these two partial waves in the range of invariant energies from the threshold up to $W \sim 1700$ MeV. In this work we show how the formalism can be extended to the calculation of electro-production amplitudes.

2 Incorporating quark-model states into multi-channel formalism

We consider a class of chiral quark models in which mesons (the pion and the sigma meson in our case) couple linearly to the quark core:

$$H_{\text{meson}} = \int dk \sum_{lmt} \left\{ \omega_k\, a^\dagger_{lmt}(k) a_{lmt}(k) + \left[V_{lmt}(k) a_{lmt}(k) + V^\dagger_{lmt}(k)\, a^\dagger_{lmt}(k) \right] \right\},$$

where $a^\dagger_{lmt}(k)$ is the creation operator for a meson with angular momentum l and the third components of spin m and isospin t. In the case of the pion, we include only $l = 1$ pions, and $V_{mt}(k) = -v(k) \sum_{i=1}^{3} \sigma^i_m \tau^i_t$ is the general form of the pion source, with the quark operator, $v(k)$, depending on the model. It includes also

---

[⋆] Talk delivered by B. Golli

the possibility that the quarks change their radial function which is specified by the reduced matrix elements $V_{BB'}(k) = \langle B\|V(k)\|B'\rangle$, where B are the bare baryon states (e.g. the bare nucleon, Δ, Roper, ...)

We have shown that in such models it is possible to find an exact expression for the K matrix without explicitly specifying the form of the asymptotic states. In the basis with good total angular momentum J and isospin T, the elements of the K matrix take the form:

$$K_{H'H}^{JT} = -\pi \mathcal{N}_H \langle \Psi_{JT}^H \| V(k) \| \widetilde{\Psi}_{B'} \rangle, \qquad \mathcal{N}_H = \sqrt{\frac{\omega E_{B'}}{kW}}, \tag{1}$$

where ω and k are the energy and momentum of the meson. Here Ψ_{JT}^H is the principal value state corresponding to channel H specified by the meson (π, σ, ...) and the baryon B (N, Δ, ...):

$$|\Psi_{JT}^H\rangle = \mathcal{N}_H \left\{ \sum_{\mathcal{R}} c_{\mathcal{R}}^H |\Phi_{\mathcal{R}}\rangle + [a^\dagger(k)|\widetilde{\Psi}_B\rangle]^{JT} + \sum_{H'} \int \frac{dk\, \chi_{JT}^{H'H}(k)}{\omega_k + E(k) - W} [a^\dagger(k)|\widetilde{\Psi}_{B'}\rangle]^{JT} \right\}. \tag{2}$$

The first term is the sum over *bare* tree-quark states $\Phi_{\mathcal{R}}$ involving different excitations of the quark core, the next term corresponds to the free meson and the baryon (N or Δ) and defines the channel, the third term introduces meson clouds around different isobars. The sum in the latter term includes also inelastic channels in which case the integration over the mass of unstable intermediate hadrons (σ-meson, Δ-isobar, ...) is implied. The state $\widetilde{\Psi}_{B'}$ in Eqs (1) and (2) represents either the nucleon or the intermediate Δ with invariant mass M; in the latter case it is equal to (2) with H = (π, N) and normalized as $\langle \widetilde{\Psi}_\Delta(M')|\widetilde{\Psi}_\Delta(M)\rangle = \delta(M-M')$, $E(k)$ is the energy of the recoiled baryon (nucleon or Δ). The on-shell meson amplitudes $\chi_{JT}^{H'H}$ are proportional to the corresponding matrix elements of the on-shell K matrix

$$K_{H'H} = \pi \mathcal{N}_{H'} \mathcal{N}_H \chi_{JT}^{H'H}(k_{H'}). \tag{3}$$

From the variational principle for the K matrix it is possible to derive the integral equation for the amplitudes which is equivalent to the Lippmann-Schwinger equation for the K matrix. The resulting expression for $\chi_{JT}^{H'H}$ can be written in the form

$$\chi_{JT}^{H'H}(k) = -\sum_{\mathcal{R}} c_{\mathcal{R}}^H \mathcal{V}_{H'\mathcal{R}}(k) + \mathcal{D}_{JT}^{H'H}(k) \tag{4}$$

where $\mathcal{V}_{H\mathcal{R}}$ are the dressed matrix elements of the interaction V_{lmt} between the resonant state and the baryon state in channel H, and $\mathcal{D}_{JT}^{H'H}$ is the background contribution.

3   T and K matrices for πN electro-production

We start with the definition of the T matrix for the pion electro-production on the nucleon:

$$T_{\pi N \gamma N} = -\pi \langle \Psi^{(+)}(m_s, m_t; \mathbf{k}_0, t)|H_\gamma|\Psi_N(m_s', m_t'; \mathbf{k}_\gamma, \mu)\rangle, \tag{5}$$

where m_s and m_t are the third components of baryon spin and isospin, $\mathbf{k}_0$ and t are the outgoing pion momentum and the third component of isospin, and $\mathbf{k}_\gamma$ and μ the momentum (along the coordinate z-axis) and the polarization of the incident photon. The interaction Hamiltonian is taken in the form

$$H_\gamma = \int d\mathbf{k}_\gamma \sum_\mu \left[V_\gamma(\mu, \mathbf{k}_\gamma) a_\mu(\mathbf{k}_\gamma) + \text{h.c.} \right] ,$$

$$V_\gamma(\mu, \mathbf{k}_\gamma) = \frac{1}{\sqrt{2\pi}^3} \tilde{V}_\gamma(\mu, \mathbf{k}_\gamma) , \qquad \tilde{V}_\gamma(\mu, \mathbf{k}_\gamma) = \frac{e_0}{\sqrt{2\omega_\gamma}} \int d\mathbf{r}\, \boldsymbol{\varepsilon}_\mu \cdot \mathbf{j}(\mathbf{r}) e^{i\mathbf{k}_\gamma \cdot \mathbf{r}} . \quad (6)$$

The state representing the photon-nucleon system reads

$$|\Psi_N(m_s', m_t'; \mathbf{k}_\gamma, \mu)\rangle = \mathcal{N}_\gamma a_\gamma^\dagger(\mathbf{k}_\gamma)|\Psi_N(m_s' m_t')\rangle , \qquad \mathcal{N}_\gamma = \sqrt{k_\gamma \omega_\gamma}\sqrt{\frac{E_N^\gamma}{W}} . \quad (7)$$

Here $\omega_\gamma = (W^2 - M_N^2 - Q^2)/2W$, $k_\gamma^2 = \omega_\gamma^2 + Q^2$, $E_N^\gamma = W - \omega_\gamma$, with Q^2 measuring the photon virtuality. We perform the spin-isospin decomposition of the outgoing state

$$|\Psi^{(+)}(m_s, m_t; \mathbf{k}_0, t)\rangle = \sum_{lmJT} i^l Y_{lm}^*(\hat{\mathbf{k}}_0)|\Psi_{JT}^{(+)}(M_J, M_T; k_0, l, m, t)\rangle C_{\frac{1}{2} m_s l m}^{JM_J} C_{\frac{1}{2} m_t 1 t}^{TM_T} . \quad (8)$$

Commuting $a_\gamma^\dagger$ in (5) to the left and using the expansion (8), we can write the T matrix in the JT basis as

$$T_{\pi N \gamma N}^{JT} = -\pi \mathcal{N}_\gamma \langle \Psi_{JT}^{(+)}(M_J M_T; k_0, l)|V_\gamma(\mu, \mathbf{k}_\gamma)|\Psi_N(m_s' m_t')\rangle . \quad (9)$$

The electro-production amplitude is proportional to (9) through $T = \sqrt{k_0 k_\gamma / 8\pi}\, \mathcal{M}$, hence

$$\mathcal{M}_{\pi N}^{JT} = -\frac{\mathcal{N}_\gamma}{\sqrt{k_0 k_\gamma}} \langle \Psi_{JT}^{(+)}(M_J M_T; k_0, l)|\tilde{V}_\gamma(\mu, \mathbf{k}_\gamma)|\Psi_N(m_s' m_t')\rangle . \quad (10)$$

The amplitudes proportional to the elements of the K matrix are obtained by replacing the state $\Psi_{JT}^{(+)}$ by the corresponding principal value state:

$$\mathcal{M}_H^{KJT} = -\frac{\mathcal{N}_\gamma}{\sqrt{k_0 k_\gamma}} \langle \Psi_{JT}^H(M_J M_T; k_0, l)|\tilde{V}_\gamma(\mu, \mathbf{k}_\gamma)|\Psi_N(m_s' m_t')\rangle . \quad (11)$$

The procedure to calculate the electro-production amplitudes in our formalism is the following: we first evaluate (11) using (2) as obtained in pion scattering, and then compute (10) using $\mathcal{M} = \mathcal{M}^K + iT\mathcal{M}^K$. (This equation trivially follows from the Heitler's equation $T = K + iTK$ since the proportionality factor between T and $\mathcal{M}$ is the same as between K and $\mathcal{M}^K$.) In principle, this equation involves also the matrix elements corresponding to Compton scattering. They can be neglected since they are orders of magnitude smaller than those containing strong interaction. In the P11 case we have

$$\mathcal{M}_{\pi N}(W) = \mathcal{M}_{\pi N}^K(W) + i\left[T_{\pi N \pi N}(W)\mathcal{M}_{\pi N}^K(W) + \overline{T}_{\pi N \pi \Delta}(W)\overline{\mathcal{M}}_{\pi \Delta}^K(W) \right.$$

$$\left. + \overline{T}_{\pi N \sigma N}(W)\overline{\mathcal{M}}_{\sigma N}^K(W) \right] . \quad (12)$$

We have further simplified the equation by using averaged values for amplitudes involving the $\pi\Delta$ and the σN channels and thus avoiding integration over the corresponding invariant masses. In the P33 case we have also added the $\pi N(1440)$ channel, while the σN channel has been replaced by the $\sigma\Delta$ channel.

4   The behaviour of the amplitudes close to a resonance

From (3) and (4) it follows that close to a resonance, denoted by $\mathcal{R}$, the K matrix element between the elastic channel and the πB channel can be cast in the form

$$K_{\pi B\pi N} = -\pi\sqrt{\frac{\omega_0\omega_B E_N E_B}{k_0 k_B W^2}}\, c_{\mathcal{R}}^B \mathcal{V}_{NR}(k_0) + K_{\pi B\pi N}^{\text{background}}.$$

After some rearrangements, the principal value states (2) take the form

$$|\Psi^H\rangle = -K_{\pi B\pi N}\sqrt{\frac{k_0 W}{\pi^2\omega_0 E_N}}\frac{\sqrt{\mathcal{Z}_{\mathcal{R}}}}{\mathcal{V}_{NR}}|\widehat{\Psi}^{\text{res}}\rangle + |\Psi^{H\,\text{non-res}}\rangle$$

with

$$|\widehat{\Psi}_{\mathcal{R}}^{\text{res}}\rangle = \frac{1}{\sqrt{\mathcal{Z}_{\mathcal{R}}}}\left\{|\Phi_{\mathcal{R}}\rangle - \int dk\,\frac{\mathcal{V}_{NR}(k)[a^\dagger(k)|\Psi_N\rangle]^{JT}}{\omega_k + E_N(k) - M} - \sum_B\int dk\,\frac{\mathcal{V}_{BR}(k)[a^\dagger(k)|\widehat{\Psi}_B\rangle]^{JT}}{\omega_k + E_B(k) - M}\right\}.$$

(the inclusion of the σN channel in the P11 case is straightforward). We can now split the K-matrix type amplitudes (11) into the resonant part containing the pole and the "non-resonant" part:

$$\mathcal{M}_H^K = \sqrt{\frac{\omega_\gamma E_N^\gamma}{k_0 W}}\sqrt{\frac{k_0 W}{\pi^2\omega_0 E_N}}\frac{\sqrt{\mathcal{Z}_{\mathcal{R}}}}{\mathcal{V}_{NR}} K_{NH}\langle\widehat{\Psi}_{\mathcal{R}}^{(\text{res})}(W)|\tilde{V}_\gamma|\Psi_N\rangle + \mathcal{M}_H^{K\,(\text{non})}. \qquad (13)$$

We see that the resonant matrix elements depend on a particular channel (H) only through the K matrix element referring to that channel. Next we plug (13) into (12) and take into account the relation between the T and the K matrix (T = K + iTK). The resonant part of the electro-production amplitudes then reads

$$\mathcal{M}_N^{(\text{res})} = \sqrt{\frac{\omega_\gamma E_N^\gamma}{k_0 W}}\sqrt{\frac{k_0 W}{\pi^2\omega_0 E_N}}\frac{\sqrt{\mathcal{Z}_{\mathcal{R}}}}{\mathcal{V}_{NR}}\langle\widehat{\Psi}_{\mathcal{R}}^{(\text{res})}(W)|\tilde{V}_\gamma|\Psi_N\rangle\, T_{\pi N\pi N}, \qquad (14)$$

while the non-resonant part satisfies

$$\mathcal{M}_N^{(\text{non})} = \mathcal{M}_N^{K\,(\text{non})} + i\left[T_{\pi N\pi N}\mathcal{M}_N^{K\,(\text{non})} + \overline{T}_{\pi N\pi\Delta}\overline{\mathcal{M}}_\Delta^{K\,(\text{non})} + \overline{T}_{\pi N\sigma N}\overline{\mathcal{M}}_\sigma^{K\,(\text{non})}\right].$$

Let us note that $\langle\widehat{\Psi}_{\mathcal{R}}^{(\text{res})}(W)|\tilde{V}_\gamma|\Psi_N\rangle$ is the electro-excitation amplitude for the resonance $\mathcal{R}$. For a sufficiently weak meson field the state $\widehat{\Psi}$ is dominated by the bare-three quark core surrounded by a cloud of pions, which is a familiar form of a baryon state in chiral-quark models. The relation (14) can be rewritten in a

more familiar form by noting that the elastic part of the K matrix can be written as

$$K_{\pi N \pi N} = \pi \frac{\omega_0 E_N}{k_0 W} \frac{\mathcal{V}_{N\mathcal{R}}^2}{\mathcal{Z}_{\mathcal{R}}(M_{\mathcal{R}})} = \frac{\frac{1}{2}\Gamma_{el}}{M_{\mathcal{R}} - W} \,, \tag{15}$$

where Γ_{el} is the elastic width of the resonance. Expressing $\mathcal{V}_{N\mathcal{R}}$ from (15) we get

$$\mathcal{M}_N^{(res)} = i\sqrt{\frac{\omega_\gamma E_N^\gamma \Gamma_{el}}{2\pi k_0 W \Gamma_{tot}^2}} \, \langle \widehat{\Psi}_{\mathcal{R}}^{(res)}(W) | \tilde{V}_\gamma | \Psi_N \rangle \,, \tag{16}$$

where we have taken into account that at the resonance $T_{\pi N \pi N} = i\Gamma_{el}/\Gamma_{tot}$.

5 Multipole decomposition for the P11 and P33 wave

Expanding (6) into multipoles, we have in the P33 case:

$$M_{1+}^{(3/2)} = \sqrt{\frac{\omega_\gamma E_N^\gamma}{6k_0 W}} \langle \Psi_{JT}^{(+)} \| \tilde{V}_\gamma^{M1} \| \Psi_N \rangle \,, \qquad E_{1+}^{(3/2)} = -\sqrt{\frac{\omega_\gamma E_N^\gamma}{30k_0 W}} \langle \Psi_{JT}^{(+)} \| \tilde{V}_\gamma^{E2} \| \Psi_N \rangle \,, \tag{17}$$

and in the P11 ($J = T = \frac{1}{2}$) case

$$M_{1-}^{(1/2)} = \sqrt{\frac{\omega_\gamma E_N^\gamma}{6k_0 W}} \langle \Psi_{JT}^{(+)} \| \tilde{V}_{\gamma\,(IV)}^{M1} \| \Psi_N \rangle \,, \quad M_{1-}^{(0)} = \sqrt{\frac{\omega_\gamma E_N^\gamma}{18k_0 W}} \langle \Psi_{JT}^{(+)} \| \tilde{V}_{\gamma\,(IS)}^{M1} \| \Psi_N \rangle \,,$$

related to π^0 production amplitude on the proton as $M_{1-}^p = M_{1-}^{(0)} + \frac{1}{3} M_{1-}^{(1/2)}$, and on the neutron as $M_{1-}^n = M_{1-}^{(0)} - \frac{1}{3} M_{1-}^{(1/2)}$. Here IV and IS denote the isovector and the isoscalar part of the interaction, respectively. The same formulas apply to the $\mathcal{M}^K$ amplitudes. (Similar relations can be derived for the scalar amplitudes.)

The transverse electro-excitation amplitudes are defined in terms of the helicity amplitudes A_{M_J}. In the P33 case we separate them into the magnetic dipole and the electric quadrupole part:

$$M1 = -\frac{1}{2} \left[\sqrt{3} A_{\frac{3}{2}} + A_{\frac{1}{2}} \right] = -\frac{\sqrt{8}}{3} \langle \widehat{\Psi}_{\mathcal{R}}^{(res)} \| \tilde{V}_\gamma(M1) \| \Psi_N \rangle \,, \tag{18}$$

$$E2 = \frac{1}{2\sqrt{3}} \left[A_{\frac{3}{2}} - \sqrt{3} A_{\frac{1}{2}} \right] = \sqrt{\frac{8}{45}} \langle \widehat{\Psi}_{\mathcal{R}}^{(res)} \| \tilde{V}_\gamma(E2) \| \Psi_N \rangle \,. \tag{19}$$

Taking into account (17) and (16) we reproduce the familiar relation

$$M_{1+}^{(3/2)} = if\,M1 \,, \qquad E_{1+}^{(3/2)} = if\,E2 \,, \qquad f = \sqrt{\frac{3\omega_\gamma E_N^\gamma \Gamma_{el}}{8\pi k_0 W \Gamma_{tot}^2}} \,.$$

In the P11 case only one transverse helicity amplitude appears and we find

$$A_{\frac{1}{2}}^{p,n} = \sqrt{\frac{2}{3}} \left[\langle \widehat{\Psi}_{\mathcal{R}}^{(res)} \| \tilde{V}^{M1}(IS) \| \Psi_N \rangle \pm \frac{1}{\sqrt{3}} \langle \widehat{\Psi}_{\mathcal{R}}^{(res)} \| \tilde{V}^{M1}(IV) \| \Psi_N \rangle \right]$$

(the reduced matrix elements appear only in the angular momentum, the third component of the isospin are $M_T = m_t' = \frac{1}{2}$).

6   Preliminary results in the N(1440) sector

The P33 wave amplitudes in the region of the $\Delta(1232)$ have been extensively in-vestigated in our previous works (see e.g. [3] and [4]). Since the electro-production amplitudes are dominated by the resonant contribution, they follow the shape of the elastic T matrix accordingly to (14).

This is not the case in the P11 wave. In Fig. 1 we show some preliminary re-sults (without including the $\pi\Delta$ and the σN channels) for the electro-production amplitude in the region of the N(1440) resonance showing the important role of the background processes. These are dominated by the nucleon pole contribution, the contribution from the second term in (2) (t-channel), and by a u-channel-type process with the Δ in the intermediate state. Below the resonance, the contribu-tion of the resonant term is almost negligible. The resonant contribution itself is dominated by the pion cloud and the admixture of the nucleon component which considerably reduces the contribution. This point is still under investigation; we expect that inclusion of higher resonances may cure this deficiency.
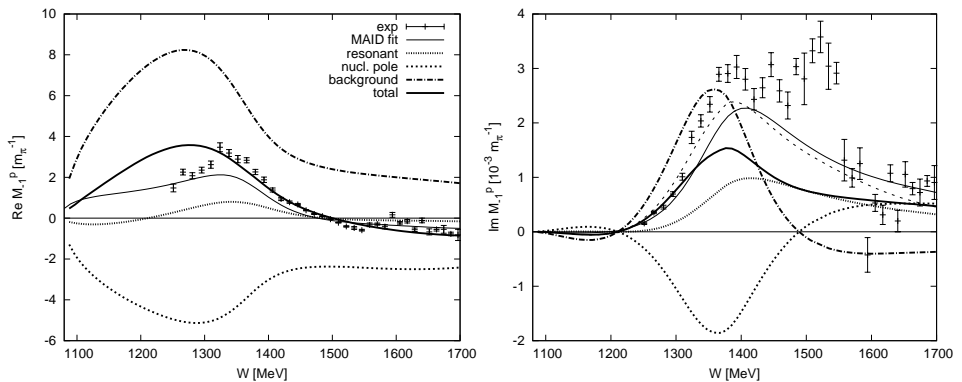

Fig.1. The real (left panel) and the imaginary (right panel) parts of the electro-production amplitudes M_{1-}^p for the P11 partial waves. The MAID result is taken from [5]; the ex-perimental points from [6]. The thin dashed curve in the right panel shows the effect of omitting the nucleon component in the resonant state.

References

1. B. Golli and S. Širca, to be published in Eur. Phys. J. A, arXiv:0708.3759 [hep-ph]
2. B. Golli and S. Širca in: B. Golli, M. Rosina, S. Širca (eds.), *Proceedings of the Mini-Workshop "Hadron Structure and Lattice QCD"*, July 9–16, 2007, Bled, Slovenia, p. 61.
3. M. Fiolhais, B. Golli, S. Širca, Phys. Lett. B **373**, 229 (1996)
4. P. Alberto, L. Amoreira, M. Fiolhais, B. Golli, and S. Širca, Eur. Phys. J. A **26** (2005) 99.
5. D. Drechsel, S. S. Kamalov, L. Tiator, Eur. Phys. J. A **34** (2007) 69.
6. R. Arndt et al., Phys. Rev. C **52** (1995) 2120; R. Arndt et al., Phys. Rev. C **69** (2004) 035213.

Searching for tetraquarks on the lattice

Saša Prelovšek

Department of Physics, University of Ljubljana and Jozef Stefan Institute, Ljubljana, Slovenia

Abstract. The observed mass pattern of scalar resonances below 1 GeV gives preference to the tetraquark assignment over the conventional $\bar{q}q$ assignment for these states. We present a search for tetraquarks with isospins $0, 1/2, 1$ in lattice QCD using diquark anti-diquark interpolators [1]. We determine three energy levels for each isospin using the variational method. The ground state is consistent with the scattering state, while the two excited states have energy above 2 GeV. Therefore we find no indication for light tetraquarks at our range of pion masses $344 - 576$ MeV.

1 Introduction

The observed mass pattern of scalar mesons below 1 GeV, illustrated in Fig. 1, does not agree with the expectations for the conventional $\bar{q}q$ nonet. The observed ordering $m_\kappa < m_{a0(980)}$ can not be reconciled with the conventional $\bar{u}s$ and $\bar{u}d$ states since $m_{\bar{u}s} > m_{\bar{u}d}$ is expected due to $m_s > m_d$. This is the key observation which points to the tetraquark interpretation, where light scalar tetraquark resonances may be formed by combining a "good" scalar diquark

$$[qQ]_a \equiv \epsilon_{abc}[q_b^T C\gamma_5 Q_c - Q_b^T C\gamma_5 q_c] \quad (\text{color and flavor anti} - \text{triplet}) \quad (1)$$

with a "good" scalar anti-diquark $[\bar{q}\bar{Q}]_a$ [2]. The states $[qq]_{\bar{3}_f,3_c} [\bar{q}\bar{q}]_{3_f,\bar{3}_c}$ form a flavor nonet of color-singlet scalar states, which are expected to be light. In this case, the $I = 1$ state $[us][\bar{d}\bar{s}]$ with additional valence pair $\bar{s}s$ is naturally heavier than the $I = 1/2$ state $[ud][\bar{d}\bar{s}]$ and the resemblance with the observed spectrum speaks for itself.

Light scalar tetraquarks have been extensively studied in phenomenological models [2], but there have been only few lattice simulations [3–6]. The main obstacle for identifying possible tetraquarks on the lattice is the presence of the scattering contributions in the correlators. All previous simulations considered only $I = 0$ and a single correlator, which makes it difficult to disentangle tetraquarks from the scattering. The strongest claim for σ as tetraquark was obtained for $m_\pi \simeq 180 - 300$ MeV by analyzing a single correlator using the sequential empirical Bayes method [4]. This result needs confirmation using a different method (for example the variational method used here) before one can claim the existence of light tetraquarks on the lattice with confidence.

We study the whole flavor pattern with $I = 0, 1/2, 1$ and our goal is to find out whether there are any tetraquark states on the lattice, which could be identified with observed resonances $\sigma(600)$, $\kappa(800)$ and $a_0(980)$. Our methodology and results are explained in more detail in [1].
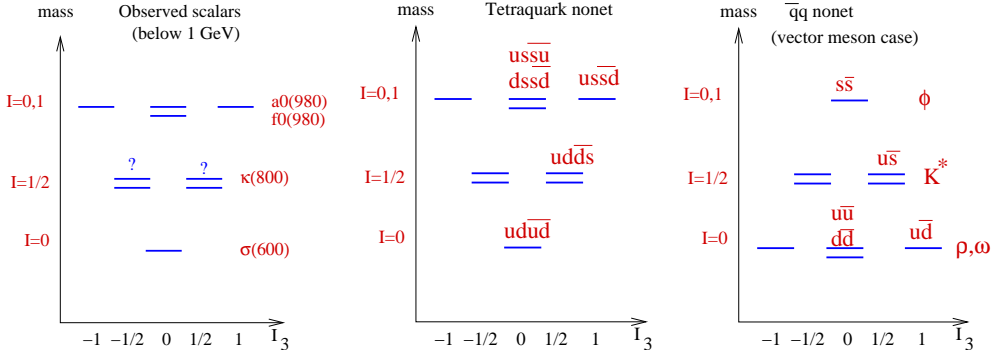

Fig.1. Schematic illustration of the observed spectrum for scalar mesons below 1 GeV (left), together with the expected mass spectrum for the nonet of scalar tetraquarks (middle), compared with a typical $\bar{q}q$ spectrum (right).

2   Lattice simulation

In our simulation, tetraquarks are created and annihilated by diquark anti-diquark interpolators

$$\mathcal{O}^{I=0} = [ud][\bar{u}\bar{d}]\,, \quad \mathcal{O}^{I=1/2} = [ud][\bar{d}\bar{s}]\,, \quad \mathcal{O}^{I=1} = [us][\bar{d}\bar{s}]\,. \tag{2}$$

In each flavor channel we use three different shapes of interpolators at the source and the sink

$$\mathcal{O}_1^I = [q_n Q_n][\bar{q}'_n \bar{Q}'_n]\,, \quad \mathcal{O}_2^I = [q_w Q_w][\bar{q}'_w \bar{Q}'_w]\,, \quad \mathcal{O}_3^I = [q_n Q_w][\bar{q}'_w \bar{Q}'_n]\,. \tag{3}$$

Here q_n and q_w denote Jacobi-smeared quarks with approximately Gaussian shape and two different widths: "narrow" (n) and "wide" (w) [8].

In order to extract energies E_n of the tetraquark system, we compute the 3×3 correlation matrix for each isospin

$$C_{ij}^I(t) = \sum_{\mathbf{x}} e^{i\mathbf{p}\mathbf{x}} \langle 0|\mathcal{O}_i^I(\mathbf{x}, t)\mathcal{O}_j^{I\dagger}(\mathbf{0}, 0)|0\rangle_{\mathbf{p}=0}$$
$$= \sum_n \langle 0|\mathcal{O}_i^I|n\rangle\langle n|\mathcal{O}_j^{I\dagger}|0\rangle\, e^{-E_n t} = \sum_n w_n^{ij} e^{-E_n t}\,.$$

Like all previous tetraquark simulations, we use the quenched approximation and discard the disconnected quark contractions. These two approximations

allow a definite quark assignment to the states and discard $[\bar{q}\bar{q}][qq] \leftrightarrow \bar{q}q \leftrightarrow vac$ mixing, so there is even a good excuse to use them in these pioneering studies. We work on two volumes $V = L^3 \times T = 16^3 \times 32$ and $12^3 \times 24$ at the same lattice spacing $a = 0.148$ fm [8]. The quark propagators are computed from the Chirally Improved Dirac operator [7]. We use $m_l a = m_{u,d} a = 0.02, 0.04$ and 0.06 corresponding to $m_\pi = 344, 475$ and 576 MeV, respectively. The strange quark mass is $m_s a = 0.08$. The analysis requires the knowledge of the kaon masses, which are 528, 576, 620 MeV for $m_l a = 0.02, 0.04, 0.06$.

The extraction of the energies from the correlation functions using a multi-exponential fit $C_{ij} = \sum_n w_n^{ij} e^{-E_n t}$ is unstable. A powerful method to extract excited state energies is the variational method, so we determine the eigenvalues and eigenvectors from the hermitian 3×3 matrix $C(t)$

$$C(t)\boldsymbol{v}_n(t) = \lambda_n(t)\boldsymbol{v}_n(t) . \tag{4}$$

The resulting large-time dependence of the eigenvalues

$$\lambda_n(t) = w_n e^{-E_n t} [1 + \mathcal{O}(e^{-\Delta_n t})] \tag{5}$$

allows a determination of energies $E_{0,1,2}$ and spectral weights $w_{0,1,2}$. The eigenvectors $\boldsymbol{v}_n(t)$ are orthogonal and represent the components of physical states in terms of variational basis (3).
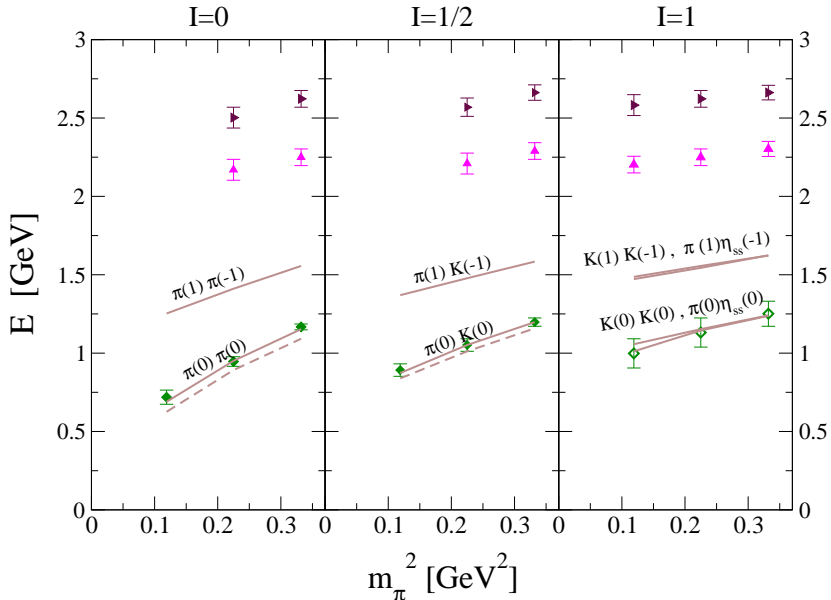

Fig.2. The symbols present the three lowest energy levels from tetraquark correlators in $I = 0, 1/2, 1$ channels at lattice volume $16^3 \times 32$. The lines give analytic energy levels for scattering states: full lines present non-interacting energies (6), while dashed lines take into account tree-level energy shifts.

3   Results

Our interpolators couple to the tetraquarks, if these exist, but they also unavoid-ably couple to the scattering states $\pi\pi$ (I = 0), $K\pi$ (I = 1/2) and $K\bar{K}$, $\pi\eta_{ss}$ (I = 1) as well as to the heavier states with the same quantum numbers. The lowest few energy levels of the scattering states $P_1(\mathbf{k})P_2(-\mathbf{k})$

$$E^{P_1(\mathbf{j})P_2(-\mathbf{j})} \simeq m_{P1} + m_{P2}, \; \ldots \; , \sqrt{m_{P1}^2 + \left(\frac{2\pi\mathbf{j}}{L}\right)^2} + \sqrt{m_{P2}^2 + \left(\frac{2\pi\mathbf{j}}{L}\right)^2}, \ldots \quad (6)$$

are well separated for our L and we have to identify them before attributing any energy levels $E \simeq m_{\sigma,\kappa,a_0}$ to the tetraquarks.

Our main result is presented in Fig. 2, where the energy levels of the tetraquark system for all isospin channels are shown. These energy levels $E_{0,1,2}$ are extracted from $\lambda_{0,1,2}(t)$ with fitting details[1] given in [1].

The *ground state* energies in I = 0, 1/2 and 1 channels are close to $2m_\pi$, $m_\pi + m_K$ and $2m_K$, $m_\pi + m_{\eta_{ss}}$, respectively, which indicates that all ground states correspond to the scattering states $P_1(\mathbf{0})P_2(\mathbf{0})$. Another indication in favor of this interpretation comes from the study of the volume dependence of the spectral weights w, defined in (5). For the ground state we get $w_0(L = 12)/w_0(L = 16) \simeq 16^3/12^3$, as shown in Fig. 3. This agrees with the expected dependence $w_0 \propto 1/L^3$ for scattering states [4], which follows from the integral over the loop momenta $\int \frac{d\mathbf{k}}{(2\pi)^3}f(\mathbf{k},t) \to \frac{1}{L^3}\sum_{\mathbf{k}}f(\mathbf{k},t)$ with $dk_i = 2\pi/L$.
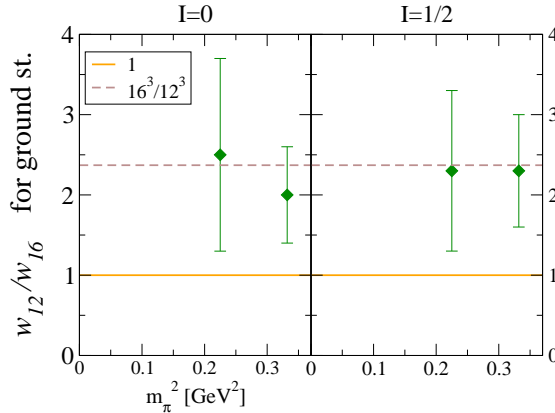

Fig.3. The ratio of spectral weights $w_0(L = 12)/w_0(L = 16)$ for I = 0, 1/2 as computed from the ground state eigenvalues for two volumes L^3.

The most important feature of the spectrum in Fig. 2 is a large gap above the ground state: *the first and the second excited states* appear only at energies above

---

[1] We observed a non-conventional time dependence of $\lambda_0(t)$ near $t \simeq T/2$, which is dis-cussed in detail in [1].

2 GeV. Whatever the nature of these two excited states are, they are much too heavy to correspond to $\sigma(600)$, $\kappa(800)$ or $a_0(980)$, which are the light tetraquark candidates we are after. The two excited states may correspond to $P_1(\mathbf{k})P_2(-\mathbf{k})$ with higher $\mathbf{k}$ or to some other energetic state. We refrain from identifying the excited states with certain physical objects as such massive states are not a focus of our present study.

At first sight it is surprising that there are no states close to the energies of $P_1(1)P_2(-1)$ with $|\mathbf{k}| = 2\pi/L$ in the spectrum of Fig. 2. In [1] we argue that this is due to the fact that our basis (3) does not decouple the few lowest scattering states to separate eigenvalues. Our data supports the hypothesis that the few lowest scattering states contribute to the ground state eigenvalue.

4   Conclusions and outlook

We find no indication for light tetraquarks at our range of pion masses $344 - 576$ MeV. However, one should not give up hopes for finding these interesting objects on the lattice. Indeed, our simulation does not exclude the possibility of finding tetraquarks for lighter $m_{u,d}$ or for a larger (different) interpolator basis. A stimulating lattice indication for σ as a tetraquark state at $m_\pi = 182 - 300$ MeV has already been presented in [4].

The present and past pioneering quenched tetraquark simulations, which discard disconnected diagrams, provide valuable information on the states with a definite quark assignment. The final conclusions will have to await dynamical simulations incorporating both disconnected quark diagrams and the $\bar{q}\bar{q}qq \leftrightarrow \bar{q}q \leftrightarrow vac$ mixing.

Acknowledgments

References

1. S. Prelovsek and D. Mohler, *A lattice study of light scalar tetraquarks*, arXiv:0810.1759 [hep-lat]; S. Prelovsek, *A lattice study of light scalar tetraquarks with isospins 0, 1/2 and 1*, presented at "Lattice 2008", to be published in PoS, arXiv:0809.5134 [hep-lat].
2. R. L. Jaffe, Phys. Rev. D 15 (1977) 267 and 281; R. L. Jaffe, *Exotica*, hep-ph/0409065; L. Maiani, F. Piccinini, A. Polosa and V. Riquer, Phys. Rev. Lett. 94 (2004) 212002.
3. M. Alford and R. Jaffe, Nucl. Phys. B 578 (200) 367, hep-lat/0001023.
4. N. Mathur *et al.*, Phys. Rev. D76 (2007) 114505, hep-ph/0607110.
5. H. Suganuma *et al.*, Prog. Theor. Phys. Suppl. 168 (2007) 168, arXiv:0707.3309.
6. M. Loan, Z.-H. Luo and Y. Y. Lam, Eur. Phys. J. C 57 (2008), arXiv: 0809.5121.
7. C. Gattringer, Phys. Rev. D 63 (2001) 114501; C. Gattringer, I. Hip and C. Lang, Nucl. Phys. B 597 (2001) 451.
8. T. Burch, C. Gattringer, L. Glozman, C. Hagen, C. Lang, and A. Schäfer, Phys. Rev. D 73 (2006) 094505.

Imitating continuum in lattice models [*]

Mitja Rosina[a,b] and Borut Tone Oblak[c]

[a] Faculty of Mathematics and Physics, University of Ljubljana, Jadranska 19, P.O. Box 2964, 1001 Ljubljana, Slovenia
[b] J. Stefan Institute, 1000 Ljubljana, Slovenia
[c] National Institute of Chemistry, Hajdrihova 19, 1000 Ljubljana, Slovenia

Abstract. Lattice models as well as few-body models with a finite Hilbert space do not provide a continuum description of the two-body decay channel. Instead, the diagonalization of the Hamiltonian yields a discrete spectrum which hides, however, a lot of information about the relevant continuum. We show a method which extracts the effective pion-pion potential and applies it to the pion-pion scattering amplitude.

As a toy model to study the relation between continuum and discrete spectrum we are using a schematic quasispin model inspired by the Nambu – Jona-Lasinio model but restricted to a finite number of quarks occupying a finite number of states in the Dirac sea and in the valence space.

1 Introduction

The diagonalization of the Hamiltonian in few-body models with a finite Hilbert space yields a discrete spectrum. There is, however, a lot of hidden information about the continuum and we have to develop a reliable method how to extract it. For this purpose we show a possible method how to extract the effective pion-pion potential and the pion-pion scattering amplitude from the discrete spectrum. The method relies on the first order Born approximation or on its suitable generalization. The Luescher formula [1] known in the literature, for example, is a special case of the (generalized) first order Born approximation.

The simplest two-level model of chiral symmetry breaking is a schematic quasispin model similar to the Nambu – Jona-Lasinio model and it is developed in the spirit of the Lipkin model [2] known from nuclear physics as a test different approximate approaches. Our model is characterized by a finite number of quarks occupying a finite number of states in the Dirac sea and in the valence space (due to a sharp momentum cutoff and periodic boundary condition). This allows us to use the first quantization and an explicit wavefunction.

Most low-lying states in the excitation spectrum can be interpreted as multi-pion states and one can deduce the effective pion-pion interaction and scattering length. However, the intruder states can be recognized as sigma-meson excitations or their admixtures to multi-pion states.

---

[*] Talk delivered by M. Rosina

The lesson learned from the toy model can be useful in a similar problem in lattice calculations – how to extract effective potential and scattering amplitudes from the discrete excitation spectrum.

2   The two-level quasispin model

In this section we repeat some properties of the two-level quasispin model which we have presented in previous Bled Workshops [3,4]. We partially use those results and partially add some new ones (arguments using N-dependence of spectra) in order to discuss the relation between the discrete spectrum and the continuum in the two-body channel.

We are aiming at a finite-dimensional N-body Hilbert space, therefore we enclose $N = \mathcal{N}$ quarks in a periodic box $\mathcal{V}$ and use a sharp momentum cutoff Λ, leading to a finite number $\mathcal{N} = \mathcal{N}_x N_s N_c N_f$ of states in the Dirac sea and the same number of states in the valence "shell". Here $\mathcal{N}_x = \mathcal{V} 4\pi\Lambda^3/(3\,(2\pi)^3)$ is the number of spacial states in each "shell", we have $N_s = 2$ helicities, $N_c = 3$ colours and we restrict the simple model to $N_f = 1$ flavour. Then $N = \mathcal{N} = 6\mathcal{N}_x = \mathcal{V}\Lambda^3/\pi^2$.

Furthermore, we take all quark kinetic energies equal to $\frac{3}{4}\Lambda$ and neglect the interaction terms which change the individual quark momenta:

$$H = \sum_{k=1}^{N} \left(\gamma_5(k)h(k)\,\tfrac{3}{4}\Lambda + m_0\beta(k) \right) - \tfrac{2G}{\mathcal{V}} \sum_{k,l=1}^{N} \left(\beta(k)\beta(l) + i\beta(k)\gamma_5(k)\cdot i\beta(l)\gamma_5(l) \right)$$

Here $h = \boldsymbol{\sigma}\cdot\mathbf{p}/p$ is helicity and γ_5 and β are Dirac matrices. We use the popular model parameters close to [5,6], $\Lambda = 648$ MeV, $G = 40.6$ MeV fm, $m_0 = 4.58$ MeV, which yield the phenomenological values of quark constituent mass, quark condensate and pion mass both in full Nambu – Jona-Lasinio model as well as in our quasispin model (using in both cases the Hartree-Fock + RPA approximations). It has been shown in [3] that in the large N limit the exact results of our quasispin model tend in fact to the Hartree-Fock + RPA values.

It is usually overlooked that the following operators obey (quasi)spin commutation relations $j_x = \frac{1}{2}\beta$, $j_y = \frac{1}{2}i\beta\gamma_5$, $j_z = \frac{1}{2}\gamma_5$. The (quasi)spin commutation relations are also obeyed by separate sums over quarks with right and left helicity as well as by the total sum ($\alpha = x, y, z$)

$$R_\alpha = \sum_{k=1}^{N} \frac{1 + h(k)}{2} j_\alpha(k) , \quad L_\alpha = \sum_{k=1}^{N} \frac{1 - h(k)}{2} j_\alpha(k) , \quad J_\alpha = R_\alpha + L_\alpha = \sum_{k=1}^{N} j_\alpha(k) .$$

The model Hamiltonian can then be written as

$$H = 2P(R_z - L_z) + 2m_0 J_x - 2g(J_x^2 + J_y^2) . \tag{1}$$

It commutes with R^2 and L^2 but not with R_z and L_z. Nevertheless, it is convenient to work in the basis $| R, L, R_z, L_z \rangle$. The Hamiltonian matrix elements can be easily calculated using the angular momentum algebra. By diagonalisation we then obtain the energy spectrum of the system.

Table 1. The spectrum of the quasispin model with N = 144 and N = 192, and the ground state quantum numbers R + L = N/4

n	Parity	$(E-E_0)$[MeV] N=144	$(E-E_0)$[MeV] N=192	$\bar{V}$[MeV] N=144	$\bar{V}$[MeV] N=192
10	+	932	(942)	-9.5	(-5.4)
9	−	803	(805)	-11.7	(-7.2)
8	+	771	861	-11.3	-8.3
7	−	767	802	-8.8	-7.3
6	+	**646**	709	-11.4	-7.3
6	+	634	**655**	-12.2	-10.9
5	−	580	611	-10.0	-7.2
4	+	482	503	-10.5	-7.1
3	−	378	388	-10.1	-7.1
2	+	261	266	-10.3	-7.1
1	−	136	137		
0	+	0	0		

3   Extraction of pion-pion interaction

The average effective pion-pion potential $\bar{V}$ given in Table 1 has been extracted from the energy levels of n-pion states

$$E_{n\pi} = n\, m_\pi + \frac{n(n-1)}{2}\bar{V}.$$

An important test to distinguish one-pion and two-pion properties is the volume-dependence (N-dependence). In a larger volume, pions are more dilute pions leading to a proportionally smaller $\bar{V}$. In fact, the ratio of $\bar{V}$ in Table 1 for N = 144 and N = 192 is 10.3/7.1 = 1.45, close to 192/144 = 1.33. (The small discrepancy does indicate that we are not yet quite in the large-N limit and further corrections might be needed).

We calculate the s-state scattering length in the first-order Born approximation ("Lüscher formula" [1])

$$a_0 = \frac{m_\pi/2}{2\pi}\int V(\mathbf{r})\,d^3r = \frac{m_\pi}{4\pi}\bar{V}\mathcal{V}. \tag{2}$$

In our example for N = 192 we have $\bar{V} = -7.1$ MeV and $\mathcal{V} = \pi^2 N/\Lambda^3 = 53\,\text{fm}^3$. This gives

$$a_0\, m_\pi = \frac{m_\pi^2}{4\pi}\bar{V}\mathcal{V} = -0.077. \tag{3}$$

Since there are no experiments with one-flavour pions it is tempting to compare with the two-flavour value (I = 2). The chiral perturbation theory (soft pions) suggests in leading order $a_0^{I=2}\, m_\pi = -m_\pi^2/16\pi f_\pi^2 = -0.0445$. Our almost twice larger value might be due to the artifact that we made up for the second flavour by replacing G with 2G. Further investigation is in progress.

4   The intruder state - the sigma meson

In the spectrum in Table 1 one can clearly distinguish the presence of the sigma meson by noticing the doubling of the positive parity states at 634 and 646 MeV for N = 144 (655 and 709 MeV for N = 192). Moreover, the states at 646 MeV (655 MeV)indicated in boldface have strong one-body transition matrix elements from the ground state. Note that going from N=144 to 192 the ordering of the two positive parity states ("σ" and "6π") has reversed because for larger N the six pions are more dilute and the energy is less depressed by attractive effective interactions between pions.

5   Relation to lattice calculations

The discrete single-particle space in our model is analogous to a lattice. The model assumption $0 \leq |\mathbf{p_i}| \leq \Lambda$ corresponds to the cell size (resolution)

$$a = \sqrt[3]{\frac{\mathcal{V}}{\mathcal{N}_x}} = \frac{\sqrt[3]{6\pi^2}}{\Lambda} = 1.2 \,\text{fm} \,.$$

Here $\mathcal{V}/\mathcal{N}_x = \mathcal{V}/(N/6)$ is the "land" available per particle in case of 2 helicities, 3 colours and one flavour.

The periodic boundary condition in $\mathcal{V}$ corresponds to the block size

$$L = \sqrt[3]{\mathcal{V}} = \frac{\sqrt[3]{6\pi^2 \mathcal{N}_x}}{\Lambda} = 3.7 \,\text{fm} \approx 3a.$$

It is surprising that such a poor resolution and block size yields excellent results. One reason is that the model interaction is not very sensitive to the number of dimensions, there are no spacial correlations. In one dimension, the ratio between the block size and the cell size $\mathcal{N}_x = 32$ is much larger than $\sqrt[3]{\mathcal{N}_x} \approx 3$ but the structure of results is the same. This is a general feature of Nambu – Jona-Lasinio models.

Furthermore, we were dealing with soft pion excitations and we get an impression that in this case a high resolution is not crucial.

References

1. M. Lüscher, Commun. Math. Phys. **104**, 177 (1986); **105**, 153 (1986); Nucl. Phys. **B354**, 531 (1991).
2. D. Agassi, H. J. Lipkin, N. Meshkov, Nucl. Phys. **86**, 321 (1966).
3. M. Rosina and B. T. Oblak, Bled Workshops in Physics **7**, No.1, 92 (2006); also available at http://www-f1.ijs.si/BledPub.
4. M. Rosina and B. T. Oblak, Bled Workshops in Physics **8**, No.1, 66 (2007); also available at http://www-f1.ijs.si/BledPub.
5. M. Fiolhais, J. da Providência, M. Rosina and C. A. de Sousa, Phys. Rev. C **56**, 3311 (1997).
6. M. Buballa, Phys. Reports **407**, 205 (2005).

Pion electro-production in the first and second resonance regions

S. Širca

Faculty of Mathematics and Physics, University of Ljubljana, 1000 Ljubljana, Slovenia
Jožef Stefan Institute, 1000 Ljubljana, Slovenia

Abstract. Many pion photo- and electro-production experiments in the energy region of the $\Delta(1232)$ resonance have been performed in the past decade, and the multipole structure of the N-Δ transition is becoming increasingly well known at least at low values of momentum transfer. In contrast, the Roper resonance, while firmly established and seen in many pion-nucleon scattering observables, it resists a clear identification and characterization by the electro-magnetic probe. I will discuss some of the outstanding theoretical and experimental issues concerning the Roper and possible means to join them fruitfully.

1 Introduction and motivation

The primary motivation to study pion electro-production in the energy region reaching to about 700 MeV above the pion production threshold is to better understand the qualitative and quantitative features of the excited baryon spectrum, and to relate the structure of baryon resonances to the mechanism of confinement and to the chiral symmetry of QCD. In addition, the results of experimental studies of nucleon resonances represent an important testing ground of theoretical models, offering in particular a way to separate the effects of resonance structure from those related to the reaction mechanism.

2 The P$_{33}$(1232) resonance

After an initial set of precision pion photo- and electro-production studies in the 1990s, mostly at energies close to threshold and only partly devoted to the N-Δ program, the more recent experiments on the N-Δ transition have completed their second stage. We have witnessed great progress and a substantial accumulation of data at many Q^2 on both unpolarized and polarized observables. The most frequently utilized quantities, used as cross-over points of experiment and theory, are the EMR and CMR ratios

$$\text{EMR} = \text{Re}\left(E_{1+}^{(3/2)}/M_{1+}^{(3/2)}\right) , \qquad \text{CMR} = \text{Re}\left(S_{1+}^{(3/2)}/M_{1+}^{(3/2)}\right)$$

which quantify the strength of the electric and Coulomb quadrupole amplitudes E_{1+} (or E2) and S_{1+} (or C2) for the N $\rightarrow$ Δ transition in the isospin-3/2 channel relative to the dominant spin-isospin-flip transition amplitude M_{1+} (or M1).

The E2 and EMR are more difficult to isolate in pion electro-production than C2 and CMR because the transverse parts of the cross-section are dominated by the $|M_{1+}|^2$ term which is absent in the longitudinal parts.

The EMR and CMR ratios have been measured in a series of experiments ranging from very low Q^2 (pion cloud physics), mostly performed at Mainz [1], through moderate to high Q^2, mostly performed at Jefferson Lab [2]. In spite of these multivariate efforts, the experimental situation at both low and high Q^2 is unsatisfactory. There are disagreements between the data, at least some of which can be attributed to the *model* dependence of the experimental extraction of the amplitudes, and/or to the truncation of the partial-wave series. At very high Q^2, where a particular scaling of the EMR and CMR ratios is expected [3], there are no data, and it remains an immense experimental challenge to reach that region. Moreover, lattice calculations of the Δ [4], although reaching high levels of sophistication, are in their infancy and are burdened with large uncertainties, and no definitive conclusions can be reached from the comparisons.

3   The $P_{11}(1440)$ and $S_{11}(1535)$ resonances

The situation for the $P_{11}(1440)$ and $S_{11}(1535)$ resonances is even less clear. The $P_{11}(1440)$ (the Roper resonance) has an unusually large width and an atypical behaviour of the πN scattering amplitudes. The masses and the widths of the Roper as obtained in different phenomenological analyses differ [5].

The $S_{11}(1535)$ resonance has an intimate connection to the Roper, in particular from the viewpoint of the lattice calculations. In the chiral limit, the first radial excitation is expected to come below the first orbital excitation in the energy spectrum, while in the heavy-quark limit, the situation should be reverse. In the past few years, there have been several attempts by various groups to observe this level ordering (parity inversion), so far with no conclusive evidence that upon chiral extrapolation, such an effect is indeed seen [6,7]. On the other hand, lattice calculations do seem to support the simple picture of the Roper, i.e. that most of its essential physics is captured by using light quarks (i.e. no quark-antiquark pairs [6].

Lattice findings are in stark contrast to two recent calculations which include also quark-antiquark components in the Roper wave-function. These studies were motivated by the failure to understand relatively large $S_{11}(1535) \to \phi N$ couplings in near-threshold $pp \to pp\phi$ and $\pi^- p \to n\phi$ processes, as well as large $S_{11}(1535) \to \Lambda K$ couplings in $\Psi \to p\bar{p}$ [8] and $\Psi \to \bar{p}\Lambda K^+$ decays [9], all of which are hard to reconcile in the 3q picture due to the OZI rule. Li and Riska [10] find that an $\approx 30\%$ admixture of the $qqqq\bar{q}$ components in the Roper reproduces the measured total width. An and Zou [11] found that the lowest 5q configuration in the $S_{11}(1535)$ resonance is $qqqs\bar{s}$; that correct $P_{11}(1440)$ vs. $S_{11}(1535)$ level ordering can thus be achieved; and that large $S_{11}(1535) \to \phi N, \Lambda K$ couplings can be understood without violating the OZI rule. Recent measurements of double-polarized asymmetries in eta electro-production at the $S_{11}(1535)$ resonance at MAMI/A1 also yielded interesting results which can only be explained by a phase rotation between the E_{0+} and $E_{2-} + M_{2-}$ multipoles [12].

4   Helicity amplitudes

Helicity amplitudes represent the strengths of the electro-magnetic vertex of the pion electro-production process. The $Q^2 \to 0$ limit of the amplitudes are the helicity couplings. The most comprehensive analysis of the couplings for all nucleon resonances below $W \sim 1.8\,\mathrm{GeV}$ are being performed at Jefferson Lab [13], and are fed by the multitude of data from single- and double-pion electro-production experiments of Hall B at that laboratory. It is the complete angular distribution that makes these data so powerful.

A coherent picture has started to emerge for the $A_{1/2}$ and $S_{1/2}$ helicity amplitudes for the $P_{11}(1440)$. A zero crossing of the $A_{1/2}$ at $Q^2 \approx 0.5\,\mathrm{GeV}^2$ is now firmly established. The Q^2-dependence of the $A_{1/2}$ rules out hybrid q^3g models of the Roper [14] which predict no zero crossing and a rapid decrease of the amplitude to zero. Moreover, the $S_{1/2}$ should vanish in the q^3g configuration, while the experimental data exhibit a large $S_{1/2}$ with a strong Q^2-dependence.

The $A_{1/2}$ helicity amplitude for the $S_{11}(1535)$ has recently been obtained with much greater precision and in a much larger Q^2-range than previously [15]. The $S_{1/2}$ has been measured for the first time in pion electro-production. The $A_{1/2}$, $A_{3/2}$ and $S_{1/2}$ for $D_{13}(1520)$ have also been obtained from the dispersion-relation analysis of all available data.

5   Experimental proposal for the $P_{11}(1440)$

In spite of all recent measurements of single- and double-pion electro-production, double-polarized experiments beyond the $\Delta(1232)$ region are rare birds. Measuring double-polarization observables allows one to access excitation amplitudes (or their bilinear forms, or interferences) much more selectively, with much greater predictive and interpretive power. Unfortunately, double-polarized measurements typically suffer from low yields and/or figures of merit and are notoriously hard to perform in the region of higher nucleon resonances where the reaction rates are small. Nevertheless, the tremendous lever arm one obtains by measuring carefully selected highly sensitive observables far outweighs the difficulties.

At MAMI, the A1 Collaboration presently pursues a feasibility study to measure recoil polarization components of protons ejected in the $p(e, e'\mathbf{p})\pi^0$ process at the Roper resonance. The experiment would be devised in analogy to the well-established procedure from the $\Delta(1232)$ case.

Ideally, one would access the polarization components in parallel (or anti-parallel) kinematics for the *pion* (i.e. $\cos\theta = \pm 1$). In this case, they can be expressed in terms of three structure functions:

$$\sigma_0(P'_x/P_e) = \pm\sqrt{2\varepsilon_L^\star(1-\varepsilon)}\, R_{LT'}^t \,,$$

$$\sigma_0 P_y = -\sqrt{2\varepsilon_L^\star(1+\varepsilon)}\, R_{LT}^n \,,$$

$$\sigma_0(P'_z/P_e) = \mp\sqrt{1-\varepsilon^2}\, R_{TT'}^l \,.$$

where P_e is the electron polarization. The multipole decomposition of $R^t_{LT'}$ up to p-waves is

$$
\begin{aligned}
R^t_{LT'} = \mathrm{Re}\{\, & L^*_{0+}(2M_{1+} + M_{1-}) + (2L^*_{1+} - L^*_{1-})E_{0+} \\
& - \cos\theta\,(\, L^*_{0+}E_{0+} - 2L^*_{1+}(3E_{1+} + 7M_{1+} + 2M_{1-}) \\
& \quad\quad + L^*_{1-}(3E_{1+} + 7M_{1+} + 2M_{1-})\,) \\
& - \cos^2\theta\,(\, 3L^*_{0+}(E_{1+} + M_{1+}) + 6L^*_{1+}E_{0+}\,) \\
& - \cos^3\theta\,(\, 18L^*_{1+}(E_{1+} + M_{1+})\,)\,\}
\end{aligned}
\tag{1}
$$

(note that the scalar and longitudinal multipoles are connected through $L \equiv (\omega/q)S$). In anti-parallel kinematics, the $R^t_{LT'}$ and R^n_{LT} measure the real and the imaginary parts respectively of the same combination of interference terms given by (1), up to a sign:

$$
\begin{aligned}
P'_x \sim R^t_{LT'} = \mathrm{Re}\{\, & L^*_{0+}E_{0+} \\
& + (L^*_{0+} - 4L^*_{1+} - L^*_{1-})M_{1-} + L^*_{1-}(M_{1+} - E_{0+} + 3E_{1+}) \\
& - L^*_{0+}(3E_{1+} + M_{1+}) + L^*_{1+}(4M_{1+} - E_{0+}) + 12L^*_{1+}E_{1+}\,, \\
P_y \sim R^n_{LT} = & -\mathrm{Im}\{\cdots\}
\end{aligned}
$$

In the case of the Roper resonance, the "M1-dominance" approximation applicable in the Δ region can not be used as many multipoles are comparable in size. With model guidance (MAID), we can estimate the role of individual terms in the expansion. The $L^*_{0+}E_{0+}$ interference is relatively large and prominent in all kinematics. The combinations $L^*_{1-}(-E_{0+} + 3E_{1+})$ and $(-4L^*_{1+} - L^*_{1-})M_{1-}$ involving M_{1-} and/or L_{1-} are either relatively small or cancel substantially. The terms largest in magnitude and sensitivity are the $L^*_{0+}M_{1-}$ and the $L^*_{1-}M_{1+}$ each involving one of the relevant Roper multipoles linearly. The contributions of the M_{1-} and S_{1-} multipoles to P'_x and P_y depend strongly on Q^2 and W, so a measurement of P'_x and P_y in a broad range of Q^2 and W would allow us to quantify these dependencies.

The expansion of the $R^l_{TT'}$ response (or P'_z) in anti-parallel kinematics is

$$
\begin{aligned}
P'_z \sim R^l_{TT'} = \mathrm{Re}\{\, & E^*_{0+}(3E_{1+} + M_{1+} + 2M_{1-})\} \\
& + |E_{0+}|^2 + 9\,|E_{1+}|^2 + |M_{1+}|^2 + |M_{1-}|^2 \\
& - 6\,\mathrm{Re}E^*_{1+}M_{1+} - 2\,\mathrm{Re}M^*_{1+}M_{1-} - 3\,\mathrm{Re}E^*_{0+}(3E_{1+} + M_{1+})\,.
\end{aligned}
$$

This response is dominated by E_{0+} and M_{1+} multipoles and is therefore less sensitive to the Roper, but it would still be important as a benchmark measurement and for calibration purposes. Most of our attention will be devoted to P'_x and P_y.

Unfortunately, due to instrumental or kinematics constraints, the measurements can only be performed at an angle near $90°$. Even at this angle, all polarization components exhibit tremendous sensitivities to the inclusion or exclusion of the Roper, as predicted by both the unitary isobar model MAID and the DMT dynamical model; see Figs. 1 and 2. These are state-of-the-art calculations which predict very different Q^2- and θ-, and W-) dependencies, mostly because resonances are treated in distinct way in the two approaches. MAID works with

dressed resonances (in terms of effective Lagrangians); DMT incorporates bare
resonances which are dressed dynamically through generation of pion loops.

From the experimental standpoint, the polarization components (the magni-
tudes of which roughly correspond to the sizes of the measured raw asymmetries)
are very large, on the scale not typically seen in other resonances. Given sufficient
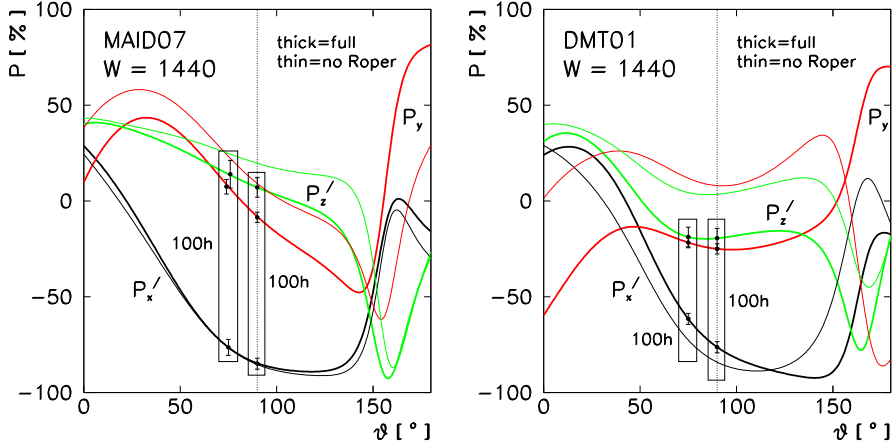beam time and a careful selection of kinematics, our measurements could help
distinguish between the methods.

Fig.1. Recoil polarization components of protons ejected in the $p(e, e'p)\pi^0$ process as a
function of the CM emission angle. Calculations are in the MAID2007 unitary isobar model
and the DMT2001 dynamical model. Shown is the effects of switching the Roper on or
off. The rectangles show possible kinematical regions where measurement appear to be
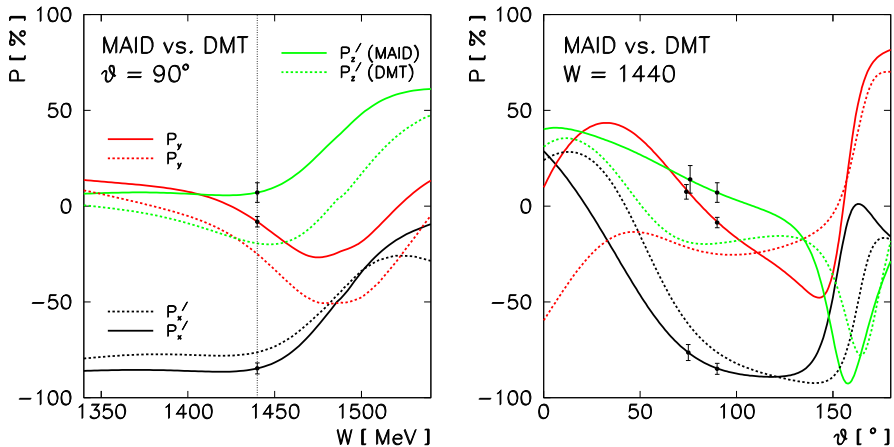feasible and would have a significant impact.

Fig.2. Recoil polarization components of protons ejected in the $p(e, e'p)\pi^0$ process as a
function of the invariant mass R and of the CM emission angle. Shown is the comparison
of MAID2007 and DMT2001 models. Projected error bars are as mentioned in Fig. 1.

References

1. N. F. Sparveris et al. (A1 Collaboration), Phys. Rev. C. **78** (2008) 018201; S. Stave et al. (A1 Collaboration), Phys. Rev. C **78** (2008) 025209; N. F. Sparveris et al. (A1 Collaboration), Phys. Lett. B **651** (2007) 102.
2. J. J. Kelly et al. (Hall A Collaboration), Phys. Rev. Lett. **95** (2005) 102001; M. Ungaro et al. (Hall B Collaboration), Phys. Rev. Lett. **97** (2006) 112003.
3. C. E. Carlson, N. C. Mukhopadhyay, Phys. Rev. Lett. **81** (1998) 2646.
4. C. Alexandrou et al., Phys. Rev. D **77** (2008) 085012.
5. R. Arndt et al., Phys. Rev. C **52** (1995) 2120; R. Arndt et al., Phys. Rev. C **69** (2004) 035213.
6. N. Mathur et al., Phys. Lett. B **605** (2005) 137; see also `hep-lat/0405001`.
7. T. Burch et al., Phys. Rev. D **70** (2004) 054502.
8. Xie et al., Phys. Rev. C **77** (2008) 015206.
9. Liu et al., Phys. Rev. Lett. **96** (2006) 042202.
10. Q. B. Li, D. O. Riska, Phys. Rev. C **74** (2006) 015202.
11. C. S. An, B. S. Zou, `arXiv:0802.3996`.
12. H. Merkel et al. (A1 Collaboration), Phys. Rev. Lett. **99** (2007) 132301.
13. I. Aznauryan, Phys. Rev. C **76** (2007) 025212.
14. Z. Li, V. Burkert, Z. Li, Phys. Rev. D **46** (1992) 70.
15. M. Dugger et al. (Hall B Collaboration), Phys. Rev. C **76** (2007) 025211.